NASA CR-120847

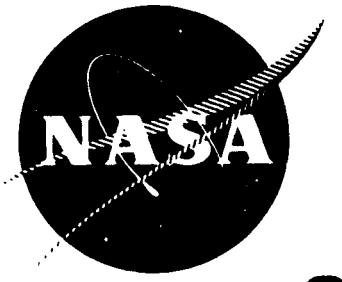

ANNUAL REPORT

AN EXPERIMENTAL INVESTIGATION OF A HOLLOW CATHODE DISCHARGE

by

PAUL J. WILBUR

under

GRANT NO. NGR-06-002-112

LEWIS RESEARCH CENTER

CLEVELAND, OHIO

DEPARTMENT OF MECHANICAL ENGINEERING

COLORADO STATE UNIVERSITY

FORT COLLINS, COLORADO

DECEMBER 1971

1. Report No.	2. Government Accession No.	3. Recipient's Catalog No.
NASA CR-120847		

4. Title and Subtitle	5. Report Date
AN EXPERIMENTAL INVESTIGATION OF A HOLLOW CATHODE DISCHARGE	December 1971
	6. Performing Organization Code
7. Author(s)	8. Performing Organization Report No.
P. J. Wilbur	
	10. Work Unit No.
9. Performing Organization Name and Address	11. Contract or Grant No.
Colorado State University Department of Mechanical Engineering Fort Collins, Colorado 80521	NGR-06-002-112
	13. Type of Report and Period Covered
12. Sponsoring Agency Name and Address	Contractor Report
National Aeronautics and Space Administration Washington, D. C. 20546	14. Sponsoring Agency Code

15. Supplementary Notes

Grant Monitor, William Kerslake, Electric Propulsion Division, NASA Lewis Research Center, Cleveland, Ohio

16. Abstract

An experimental study of the effects of various modifications to the hollow cathode discharge region of a 20 cm electron bombardment ion thruster is presented. The introduction of electrical insulation between the main and cathode discharge regions is shown to have no significant effect on thruster performance. Adjustment of both the diameter and length of the cathode discharge region from the design condition are examined and the reduced sizes are shown to effect large improvements in propellant utilization (~15%) when the thruster is operating at about 30% of the design thrust level. Performance improvements are shown to be less significant at higher thrust levels. The feasibility of using a high voltage tickler electrode to initiate the cathode-keeper discharge is considered and results obtained suggest this mode of startup is unsatisfactory.

17. Key Words (Suggested by Author(s))	18. Distribution Statement
Hollow Cathode Ion Thruster	Unclassified - unlimited

19. Security Classif. (of this report)	20. Security Classif. (of this page)	21. No. of Pages	22. Price*
Unclassified	Unclassified	77	$3.00

* For sale by the National Technical Information Service, Springfield, Virginia 22151

TABLE OF CONTENTS

	Page
Abstract	i
Introduction	1
Hollow Cathode Discharge Studies	2
Facility and Apparatus	2
Electrical Isolation of the Main and Cathode Discharges	9
Variation in Cathode Discharge Region Dimensions	13
Simultaneous Flow Distribution and Cathode Region Dimensional Adjustments	18
The Nature of the Arc Current Transition	39
High Voltage Startup Studies	51
Thermal Flow Meter	55
References	61
Appendix A - Interpretation of Langmuir Probe Data	63
Appendix B - Ion Beam Flatness Parameter	67
Appendix C - Effect of Cathode Discharge Size on Ion Losses to Cathode Region Walls	69

LIST OF FIGURES

Figure		Page
1	Schematic Diagram of Power Supply and Measurement System	3
2	Thruster Schematic	4
3	Langmuir Probe System Circuitry	7
4	Ion Beam Current Density Profile Probe and Circuitry	8
5	Main-Cathode Discharge Isolation Test Configurations	10
6	Effect of Insulating Surfaces on Performance (High Flow Condition)	11
7	Effect of Insulating Surfaces on Performance (Low Flow Condition)	12
8	Cathode Discharge Region Configurations	14
9	Typical Performance Variations with Cathode Discharge Size	16
10	Effect of Cathode Discharge Region Diameter & Length on Discharge Losses	17
11	Effect of Cathode Flow Rate	19
12	Arc Current - Voltage Characteristics	20
13	Effect of Low Cathode Flow - Small Cathode Discharge (Throttled Flow)	21
14	Arc Current-Voltage Characteristics - Small Cathode Discharge (Throttled Total Flow)	23
15	Effect of Low Cathode Flow - Small Cathode Discharge (High Total Flow)	24
16	Arc Current-Voltage Characteristics - Small Cathode Discharge (High Total Flow)	25
17	Cathode Flow and Discharge Loss Variations with Cathode Discharge Size (High Total Flow)	27

Figure		Page
18	Cathode Flow and Discharge Loss Variations with Cathode Discharge Size (Throttled Total Flow)	28
19	Cathode Discharge Plasma Properties (High Total Flow)	29
20	Cathode Discharge Plasma Properties (Throttled Total Flow)	30
21	Effect of Cathode Sleeve on Beam Profile	32
22	Effect of a Cathode Magnetic Field on Ion Beam Profile	33
23	Effect of 3.5 cm Diameter Pole Piece on Beam Profile .	34
24	Effect of Pole Piece-Sleeve Substitution on Performance	36
25	Effect of Pole Piece-Sleeve Substitution on Arc Current Voltage Characteristics	37
26 & 27	Cathode Tip Temperature vs. Arc Current	38
28	Effect of Keeper Current at Various Cathode Flows . .	40
29	Effect of Cathode Flow on Keeper Voltage	43
30	Effect of Mode Change on Cathode Region Electron Density	44
31	Effect of Mode Change on Cathode Region Electron Temperature	45
32	Effect of Mode Change on Cathode Power Losses	47
33	Effect of Mode Change on Primary Electron Energy . . .	48
34	Effect of Mode Change on Main Region Electron Density Ratio and Temperature	49
35	High Voltage Startup Schematic	52
36	Enclosed Keeper Configuration	52
37	H.V. Start Test Schematic	54

Figure		Page
38	Effect of Tickler Voltage on Cathode Temperature at H.V. Discharge	54
39	Thermal Flowmeter	57
40	Thermal Flowmeter Output	58
41	Thermal Flowmeter Calibration Curves	59
A-1	Typical Langmuir Probe Data	64
A-2	Typical Semi-Log Plot of Cathode Data	64
A-3	Langmuir Probe Trace Construction	65
A-4	Main Discharge Maxwellian Electron Plot	65
C-1	Effect of Cathode Region Dimensions on Electron Density	70
C-2	Effect of Cathode Discharge Size on Discharge Losses due to Ion Flux to Confining Walls (Fixed Cathode Flow)	72
C-3	Effect of Cathode Discharge Size on Discharge Losses due to Ion Flux to Confining Walls (Variable Cathode Flow)	73

INTRODUCTION

The hollow cathode is widely used to generate electrons in an electron bombardment ion thruster because it exhibits long life characteristics and can be ground tested before it is used on a flight mission. The introduction of the hollow cathode in place of the oxide cathodes resulted, however, in increased thruster complexity, both in terms of required support systems and thruster discharge phenomena. Increased support systems complexity arises because of the addition of the cathode mercury feed system, cathode heater system and keeper system. The discharge phenomena are more complex in hollow cathode thrusters because two distinct discharges are present (cathode and main discharge) and because the detailed mechanism of hollow cathode operation is not understood.

The focus of the research effort described herein is the hollow cathode discharge and the effect of variations in cathode discharge dimensions, cathode mercury flow rate and cathode pole piece wall conductivity on thruster performance variables and main and cathode discharge plasma properties. These studies are directed at reducing discharge losses, increasing propellant utilization, flattening the ion beam profile and understanding the mechanism by which these quantities change through analysis of measured variations in plasma properties. The studies have been carried out at two total propellant flow conditions corresponding to 30% and 60% of full thrust.

The startup characteristic of hollow cathode discharges, which involves heating the cathode to thermionic emission temperatures with a resistance heater, has been somewhat unpredictable[1]. Additional studies reported herein have been centered on the use of a high voltage discharge to the cathode as a means of assuring reliable startup. The ultimate objective of such an effort is the elimination of the cathode heater in favor of high voltage discharge heating and startup. This mode of startup could then be compared to the resistance heating mode in terms of reliability and weight.

HOLLOW CATHODE DISCHARGE STUDIES

Facility and Apparatus

The tests were performed in the Colorado State University 1.2 m dia. x 4.6 m long ion thruster test facility. The pressure in the tank was maintained at less than 4×10^{-5} torr during operation. The thruster was fired into a radiation cooled stainless steel target located about 4 m from the thruster.

Power is supplied to the thruster systems from the power supplies shown schematically on Figure 1. As suggested by this schematic, the cathode and main feed systems float at the thruster potential rather than being held at ground potential through an isolator. A neutralizer has not been used in these tests so beam neutralization has been achieved by electrons from the vacuum tank walls.

A 20 cm dia. hollow cathode, bombardment thruster obtained from the Jet Propulsion Laboratory was employed[2,3]. This thruster utilizes a single reverse main feed entry into the main discharge region. The thruster schematic is Figure 2. Two noteworthy changes have been incorporated into the basic thruster since tests began. They are: 1) the removal of the screen grid braces discussed in Reference 3 and 2) increasing the grid separation distance above the values used by JPL. Both changes were incorporated to prevent arcing between the grids at high arc power conditions. Arcing, which was observed during early testing when arc power was raised to high values probably because of expansion of the screen grid braces, was eliminated when the braces were removed. The increased grid separation distance resulted in an increase in arc discharge losses over losses observed with lesser separations, but this distance was held constant throughout the tests to facilitate comparative interpretation of the data. The cathode used in the tests was 0.32 cm dia., and it had a 0.063 cm dia. orifice in it.

Measurement of arc voltage, arc current, beam current, and keeper voltage were obtained from digital voltmeters sensing the voltage across the load or a shunt and the values are considered accurate to within ± 1/2%. Other currents and voltages were read on panel meters (±1%).

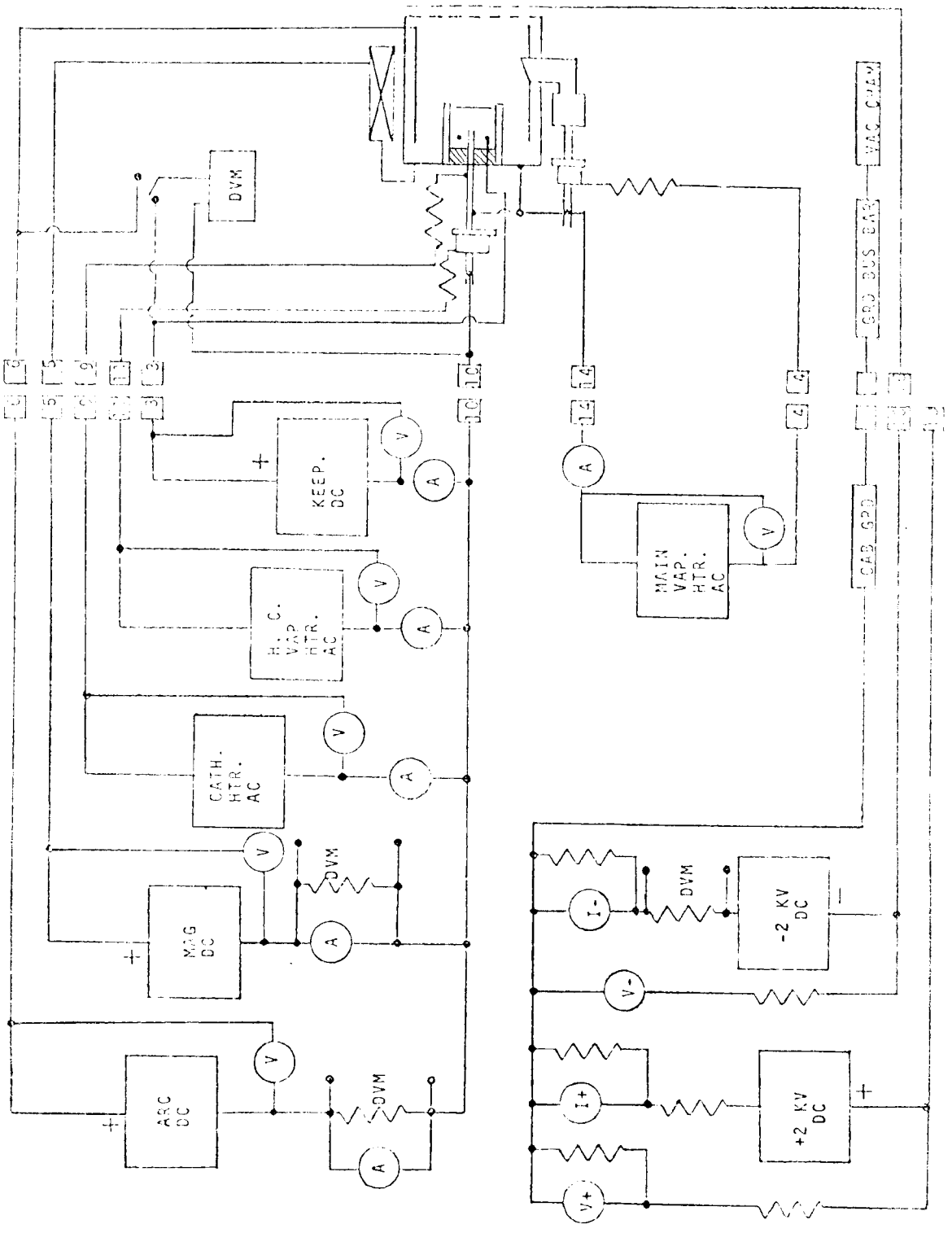
DVM
KEEP. DC
MAIN VAP. HTR. AC
CATH. HTR. AC
MAG DC
ARC DC
-2 KV DC
+2 KV DC
I-
I+
V-
V+
V
A

FIGURE

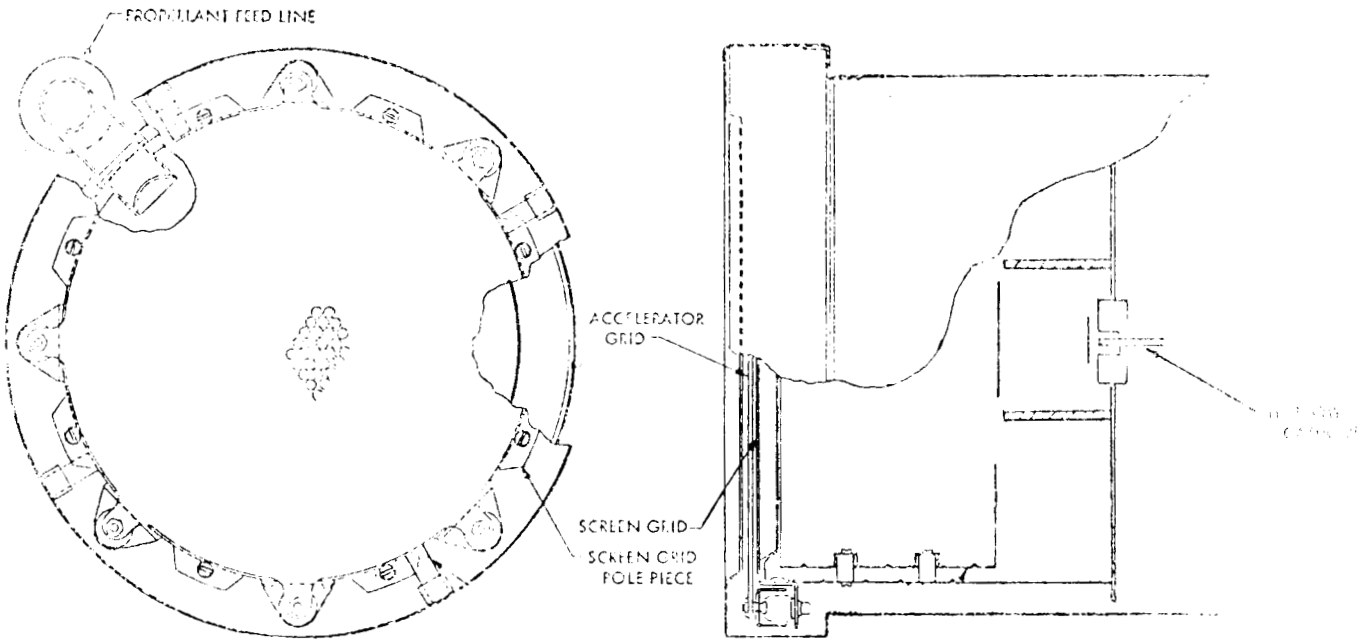

BEAM DIA.-20 CM.
THRUSTER LENGTH-18 CM.
ANODE LENGTH-12.7 CM.

GRIDS - APERTURE DIA.-0.462 CM.
SCREEN THICKNESS-0.076 CM.
GRID SEPN.-0.178 CM.
OPEN AREA-72%

CATH. POLE PIECE-6.35 CM. DIA. X 5.33 CM.
BAFFLE DIA.-5.4 CM.

THRUSTER SCHEMATIC

FIGURE 2

Mercury flow rates were obtained by measuring the time required for a mercury column to fall through two scribe marks on 0.9 mm bore glass tubes. Initial calibration of these tubes was accomplished by measuring the mass of mercury between the marks with an analytical balance. Mercury flow rates were considered accurate to within 1%, so data could be recorded, when the following conditions were met:

1) Two consecutive measurements yielded flow rate values within 1% of each other.
2) No significant variations in thruster operating conditions were observed during the two measurements.
3) No significant variations in mercury vaporizer temperatures were detected during the measurements (thermocouple meter accuracy about ± 1°C).

Tests were conducted at two total flow conditions namely: 825 ma equiv. ± 1% which produces a maximum beam current near the allowable maximum of the available high voltage power supply, and 465 ma equiv. ± 1% which resulted in about half of the beam current observed at the high flow. JPL has reported satisfactory operation up to a beam current level of 1.3 a with a similar thruster (total flow ~ 1.4 a)[3] so the thruster was operating near 60% and 30% of the maximum thrust level during these tests.

The general procedure used to obtain data involved thruster stabilization and flow rate measurement over a period of approximately one hour at the following conditions:

Arc Voltage	=	37 v
Keeper Current	=	0.5 a
Magnet Current	=	1.7 a
High Voltages	=	± 2 kv
Cathode Heater Current	=	0 a

Langmuir probe and ion beam current density profile data were taken at these conditions. The arc voltage was next varied and arc, beam, keeper and impingement data were gathered as quickly as possible in the following arc voltage sequence: 37 v, 40 v, 45 v, 50 v, 55 v, 37 v, ~ 30 v, 37 v. The data collection over the variable arc voltage sequence generally

required about two minutes, and the mercury flow into the thruster was affected during this period to an extent which depended on the variation in arc current that occurred. The extent and effect of variations in flows can be determined in the data presented in this report by considering the variation in data obtained at the beginning, middle and end of the sequence at 37 v. Data obtained at 37 v arc voltage are identified on performance curves as solid symbols and three such points will be indicated if significant variations were observed. When Langmuir probe, beam profile and more accurate performance data were desired over a range of arc voltage conditions, stabilized thruster operation and flow rate consistency was established at each arc voltage.

Plasma properties were sensed by two Langmuir probes, one located at a radius of 5 cm at the baffle plane in the main discharge and the other located at a radius of 1 cm, 0.75 cm aft of the cathode in the cathode discharge region. The probes were made of 0.074 cm dia. tantalum wire extending 0.127 cm beyond the end of the aluminum oxide insulating wire containment tube. The aluminum oxide tubes were replaced after about 20 hours of operation to prevent the formation of a conducting layer on their surface. Probes were held at a voltage of +60 to +90 v for a period of several seconds just prior to data collection to burn off probe surface contamination[4]. Langmuir probe data were recorded through the circuitry shown in Figure 3 on an 11 in. x 14 in. plotting surface x-y plotter. The method of interpretation of raw Langmuir probe data is presented in Appendix A.

The temperature of the cathode tip was sensed by a tungsten--5% rhenium, tungsten--26% rhenium thermocouple spot welded to it at the edge of the tungsten orifice plate and connected to an API thermocouple meter.

The ion beam current density profile was sensed by a Faraday probe which could be swept through the ion beam manually during thruster operation. The basic probe design and circuitry required to effect beam probe readout are shown in Figure 4. The sensor was biased +9 v relative to tank ground to suppress error due to secondary electrons. All beam probe data were taken with the sensor located 5 cm downstream of

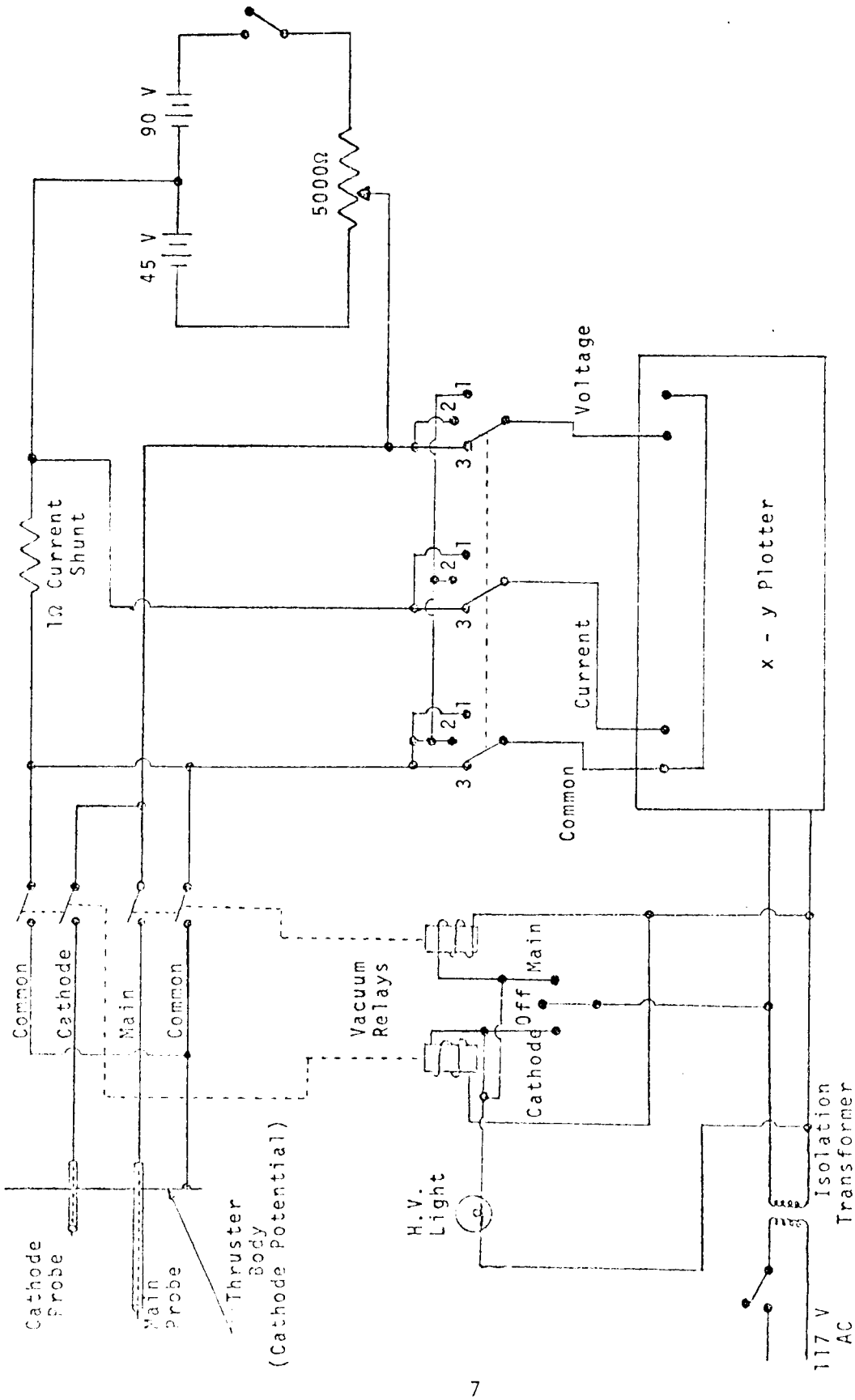

LANGMUIR PROBE SYSTEM CIRCUITRY

FIGURE 3

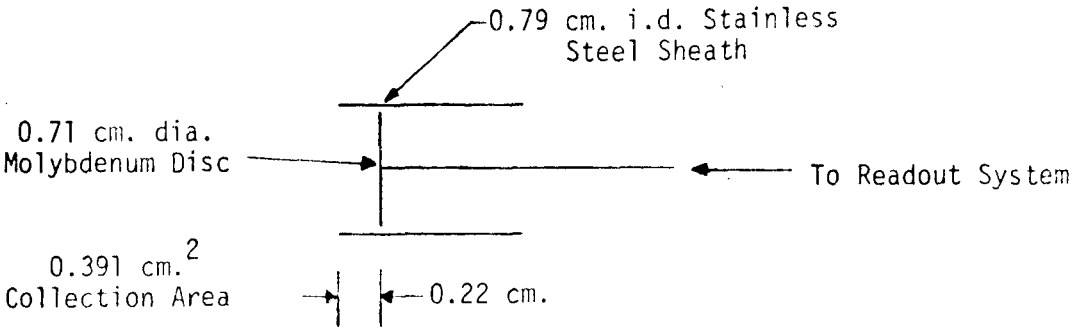

ION BEAM CURRENT DENSITY PROFILE PROBE

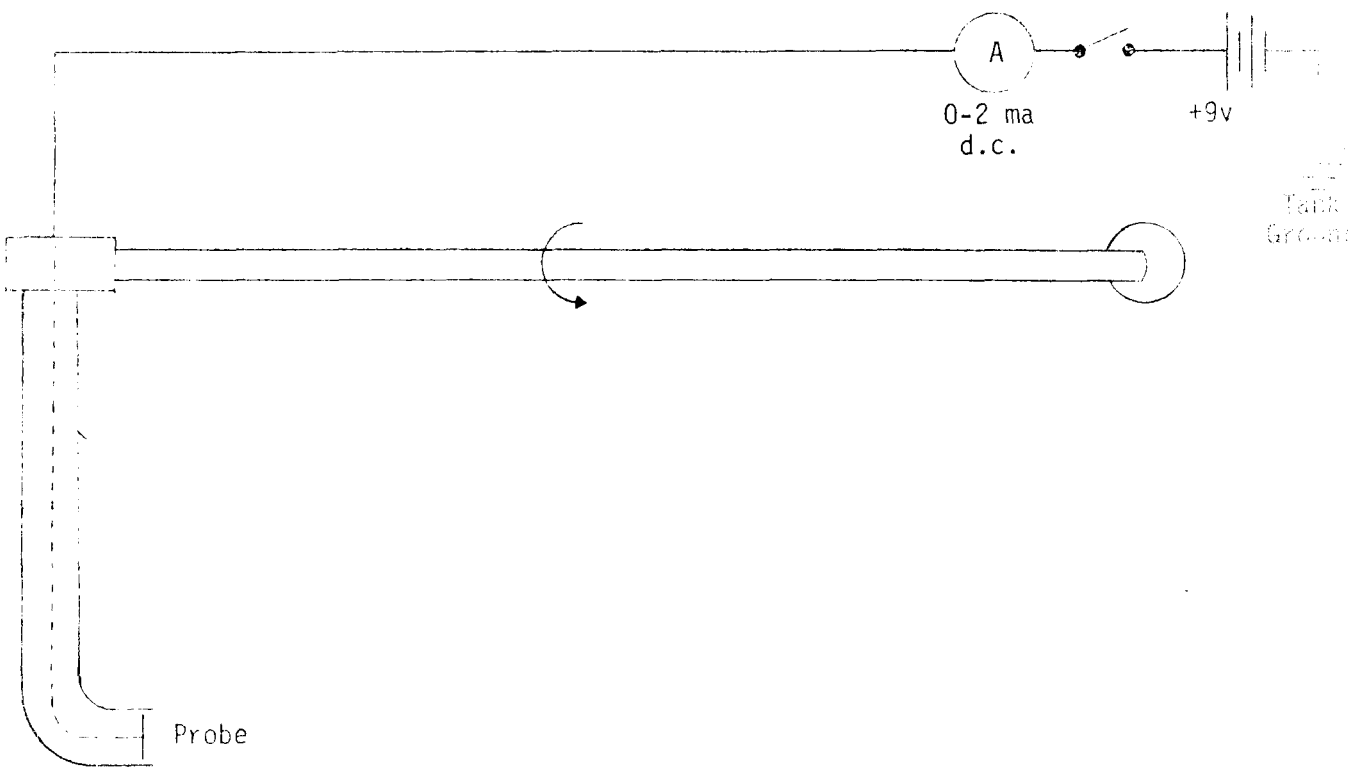

BEAM CURRENT PROBE CIRCUITRY

FIGURE 4

the accel grid. The data obtained were translated into the beam profile flatness parameter ($\mathbb{F}$) described in Appendix B. This parameter has a value of unity for a flat profile, a value of zero for a delta function profile, and it weights the radial variation in current density according to the increased beam area at greater beam radii.

Electrical Isolation of the Main and Cathode Discharges

Since the main and cathode discharge regions of the thruster sustain different plasma potentials, the possibility of introducing electrical isolation between the discharges at all locations but the baffle aperture was investigated. It was expected such isolation would reduce ion wall currents by reducing the mobility of electrical charge around and through the baffle and cathode pole piece walls and that this would in turn result in reduced arc discharge losses.

Two tests were conducted using 0.0127 cm thick Polyimide Kapton H Film fitted in the cathode pole piece region in the manner suggested in Figure 5 to effect the desired electrical isolation. Performance curves obtained with these configurations are compared to the standard uninsulated performance curves in Figures 6 and 7 which correspond to the high and throttled total flow conditions discussed previously. For the high flow case presented in Figure 6, no significant variation in performance is observed, when the Kapton is used inside the pole piece or as a baffle and pole piece cover.

Figure 7 does show about a 5% increase in utilization when the inside of the pole piece is coated with Kapton. Part of this may be accounted for in the measured 0.050 gram weight loss of the Kapton and tape used to secure it during the test. Assigning an average atomic weight of 12 to particles coming from these materials, this translates into an average flow over the duration of the test of about 10 ma equiv. which would correspond to a 2% increase in utilization. Considering this effect and experimental errors, the observed increase in utilization is not considered significant.

Langmuir probe data obtained during these tests suggest no significant

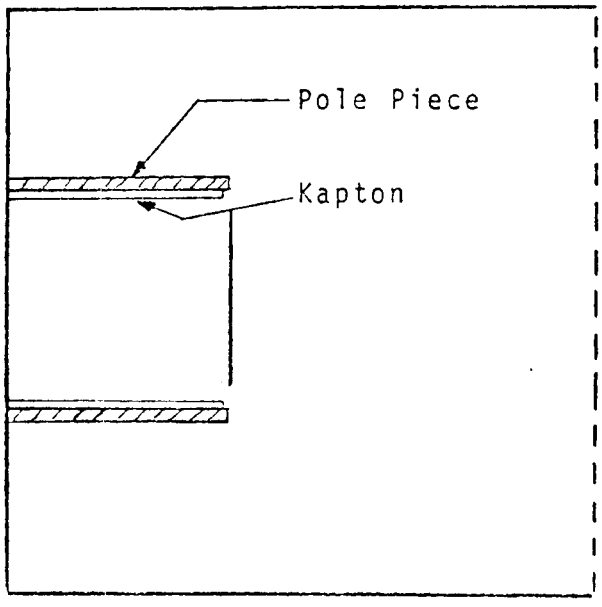

KAPTON INSIDE POLE PIECE

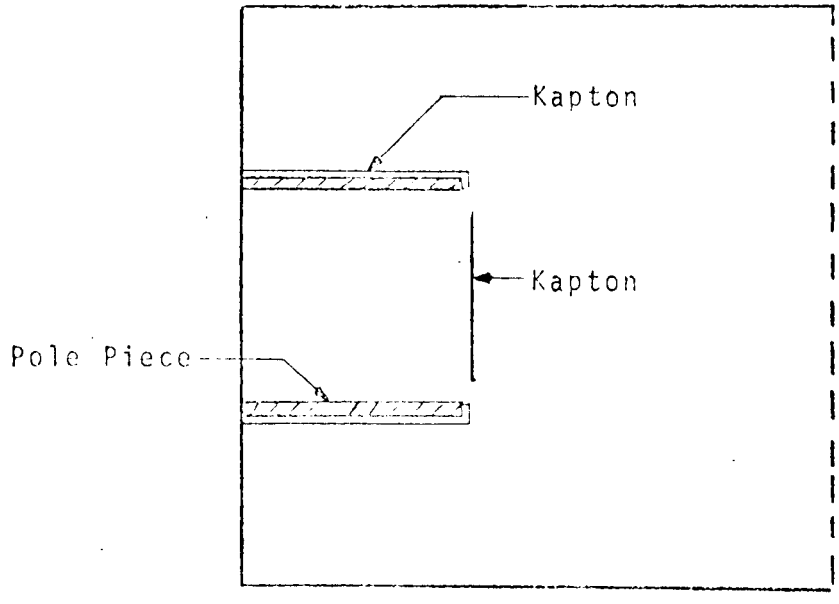

KAPTON BAFFLE & POLE PIECE COVER

MAIN - CATHODE DISCHARGE ISOLATION TEST CONFIGURATIONS

FIGURE 5

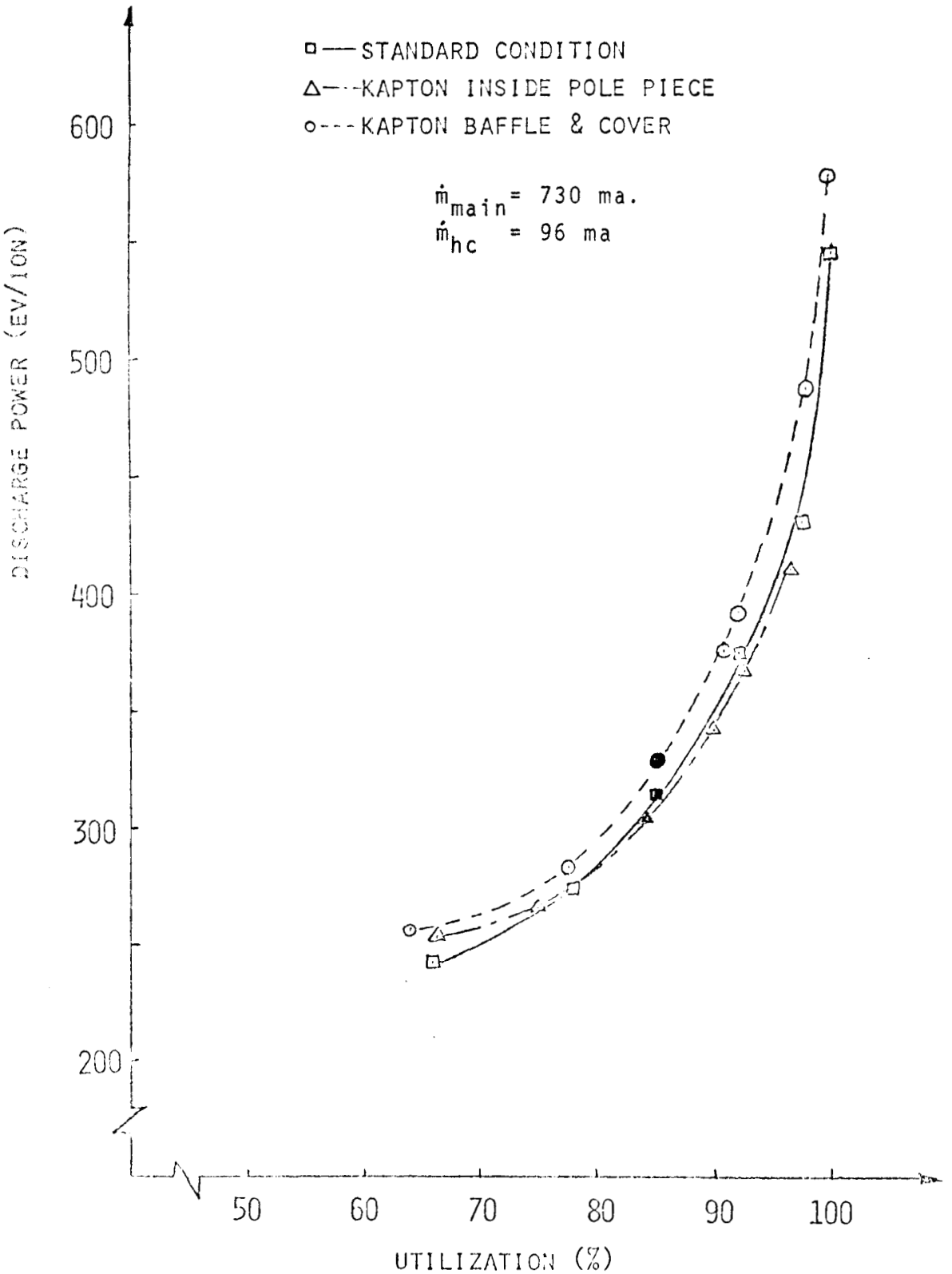

EFFECT OF INSULATING SURFACES ON PERFORMANCE
(HIGH FLOW CONDITION)

FIGURE 6

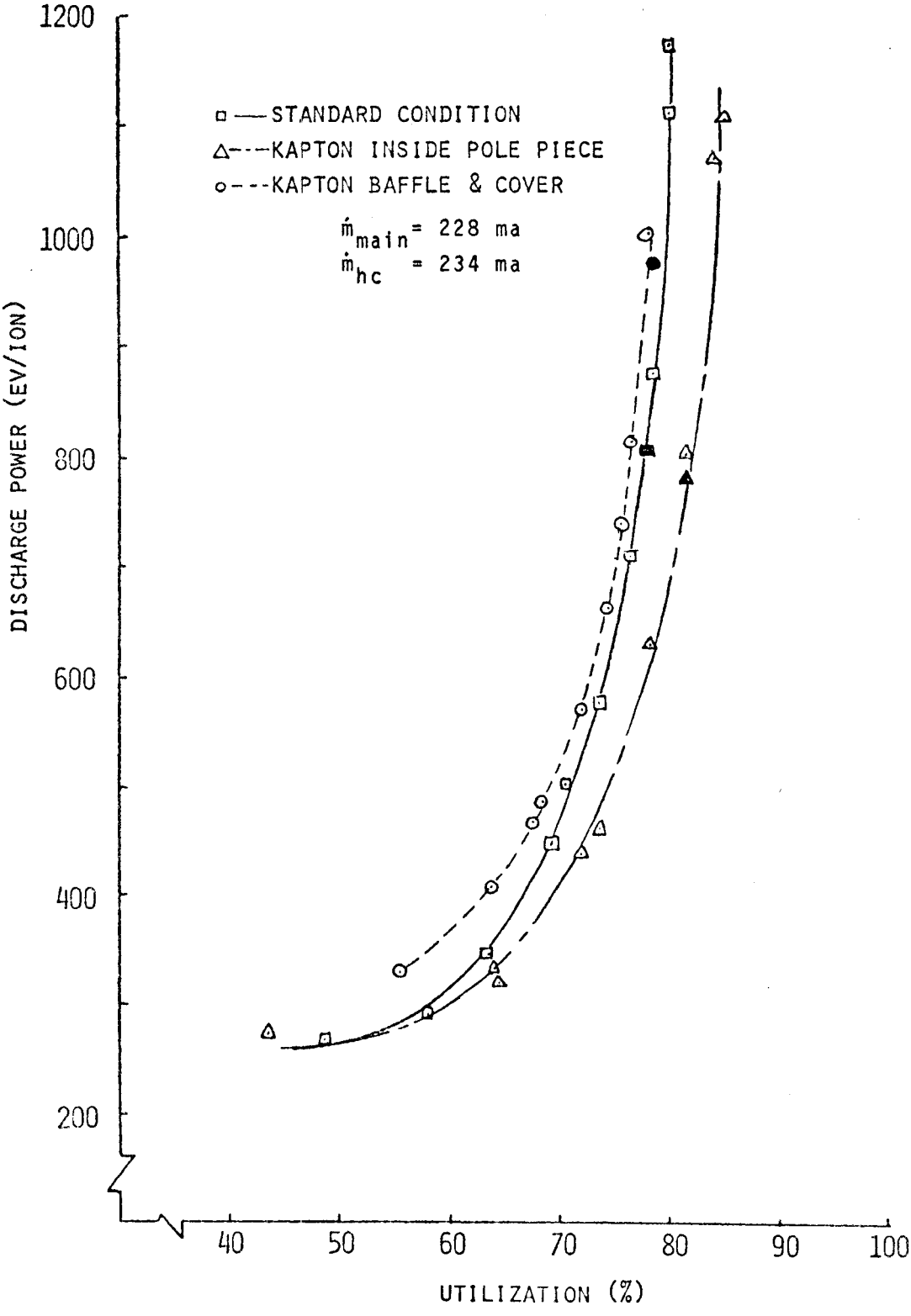

EFFECT OF INSULATING SURFACES ON PERFORMANCE
(LOW FLOW CONDITION)

FIGURE 7

variations in main and cathode plasma potentials when the insulation is installed. The Kapton films showed a slight charring when they were removed from the thruster, but the minimum surface resistance between probes separated by one inch on the film surfaces was greater than 15,000 Ω in the regions of lowest resistance.

It was concluded from these tests that electrical insulation on the cathode pole piece and baffle surfaces is not effective in reducing discharge losses. It is believed the insulation was ineffective because electrical communication between the main and cathode discharges was achieved through a high conductivity interface between the Kapton and the plasma in the operating thruster.

Variation in Cathode Discharge Region Dimensions

Preliminary investigations conducted at Colorado State University[5] suggested arc discharge losses could be reduced through adjustments in the diameter of the cathode discharge region. In order to extend this work, the thruster was modified so the cathode could be moved axially during the thruster operation within the cathode pole piece or cylindrical sleeves centered inside the pole piece in the manner suggested in Figure 8. The table presented on Figure 8 shows the cathode discharge region diameters considered in this study, together with the corresponding baffle diameters and baffle aperture areas. The length of the discharge region was variable in the range of 1.5 to 5.3 cm at each diameter. The baffle diameters used in this study were picked so the ratio of aperture area to baffle area was constant with discharge diameter variations. This criterion was used because preliminary tests showed a reduction in baffle aperture area in this ratio resulted in similar arc voltage conditions at given main and cathode flow rates. It should be noted that the use of this criterion led to about a 5 to 1 variation in baffle aperture area for the range of discharge diameters considered. The unnecessary losses associated with the baffle supports was recognized, but the supports were retained to permit comparison of data obtained throughout the test period. Performance results obtained with the

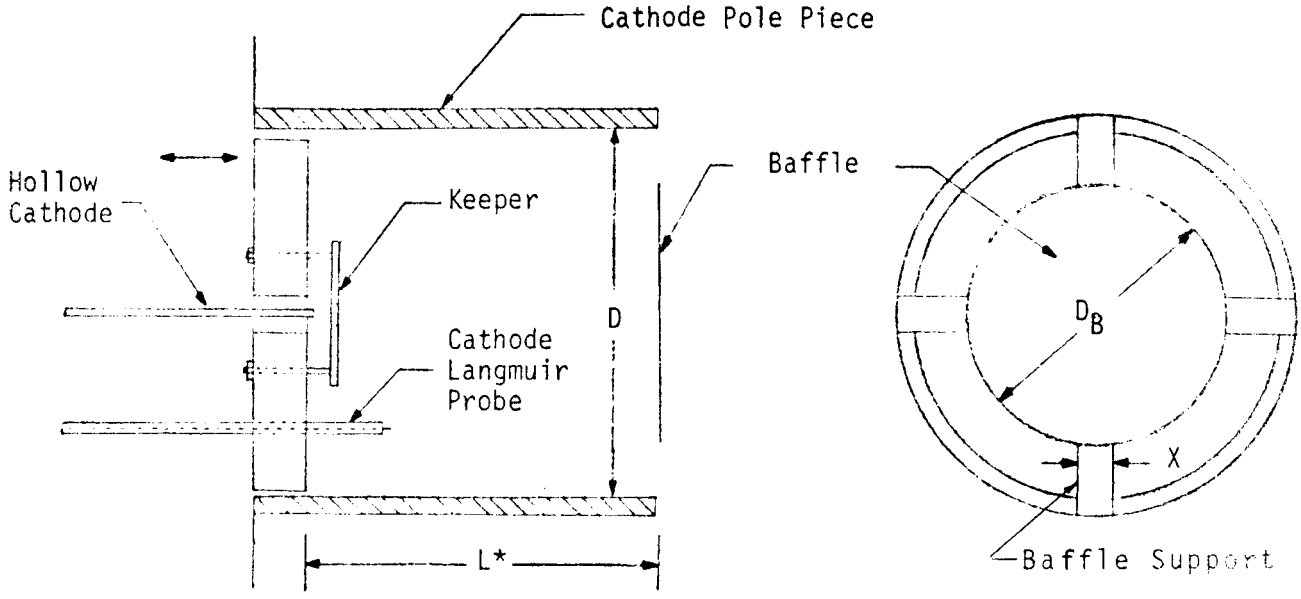

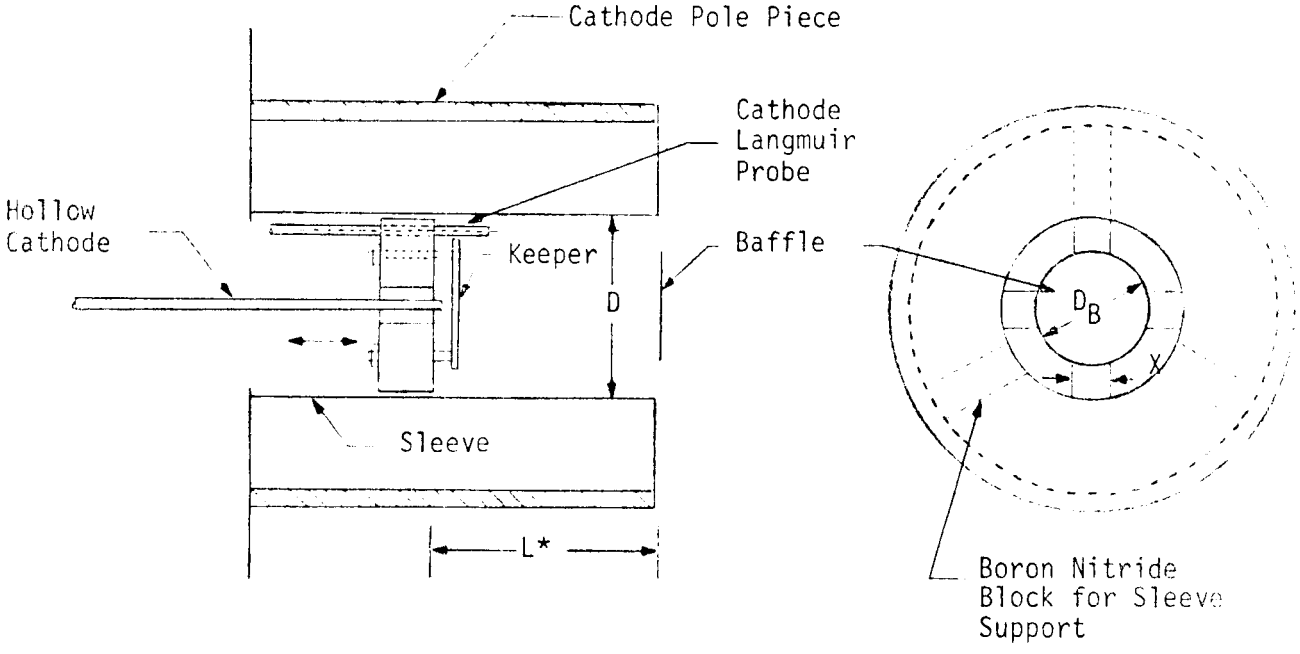

D (cm)	D_B (cm)	X (cm)	Aperture Open Area (cm^2)
6.35	5.40	0.91	5.30
4.92	4.20	0.91	3.30
3.50	2.33	0.91	0.95

*L, The discharge region length (cathode-baffle separation distance) can be adjusted during operation.

CATHODE DISCHARGE REGION CONFIGURATIONS

FIGURE 8

extremes of the cathode discharge volumes considered are presented in Figure 9 for the high and throttled flow conditions. In both cases the smaller cathode discharge volume results in a degradation in performance, but the more substantial increase in losses is exhibited under throttled flow conditions.

If one selects utilizations of 85% at high flow and 70% at throttled flow and picks off the discharge power from these and similar curves for the range of geometries studied, the results of Figure 10 are obtained. These curves show the following:

1) Reductions in diameter of the discharge region and corresponding reduction of the baffle aperture area at a fixed main-cathode flow split result in an increase in arc discharge losses. This increase is much more substantial for the case of throttled flow.
2) Reductions in cathode discharge region length produce a decrease in arc discharge losses followed by an increase. This result tends to support a similar observation reported by Pawlik and Fitzgerald at JPL[6].

An interpretation of Langmuir probe data obtained during these tests is presented in Appendix C. These data show ion recombination losses on the cathode discharge confining walls are reduced by reductions in both diameter and length of the cathode discharge region. This suggests the observed performance degradations result from conditions in the main discharge brought on by changes in the cathode discharge.

It was concluded from these tests that some improvement in performance could be achieved with the thruster operating at a fixed flow distribution between the main and cathode vaporizers if the cathode region length were cut in half. Further reductions in cathode region length and any reduction in its diameter result in a performance degradation. The effect of these dimensional changes is most significant at throttled flow conditions where cathode flow rate is higher.

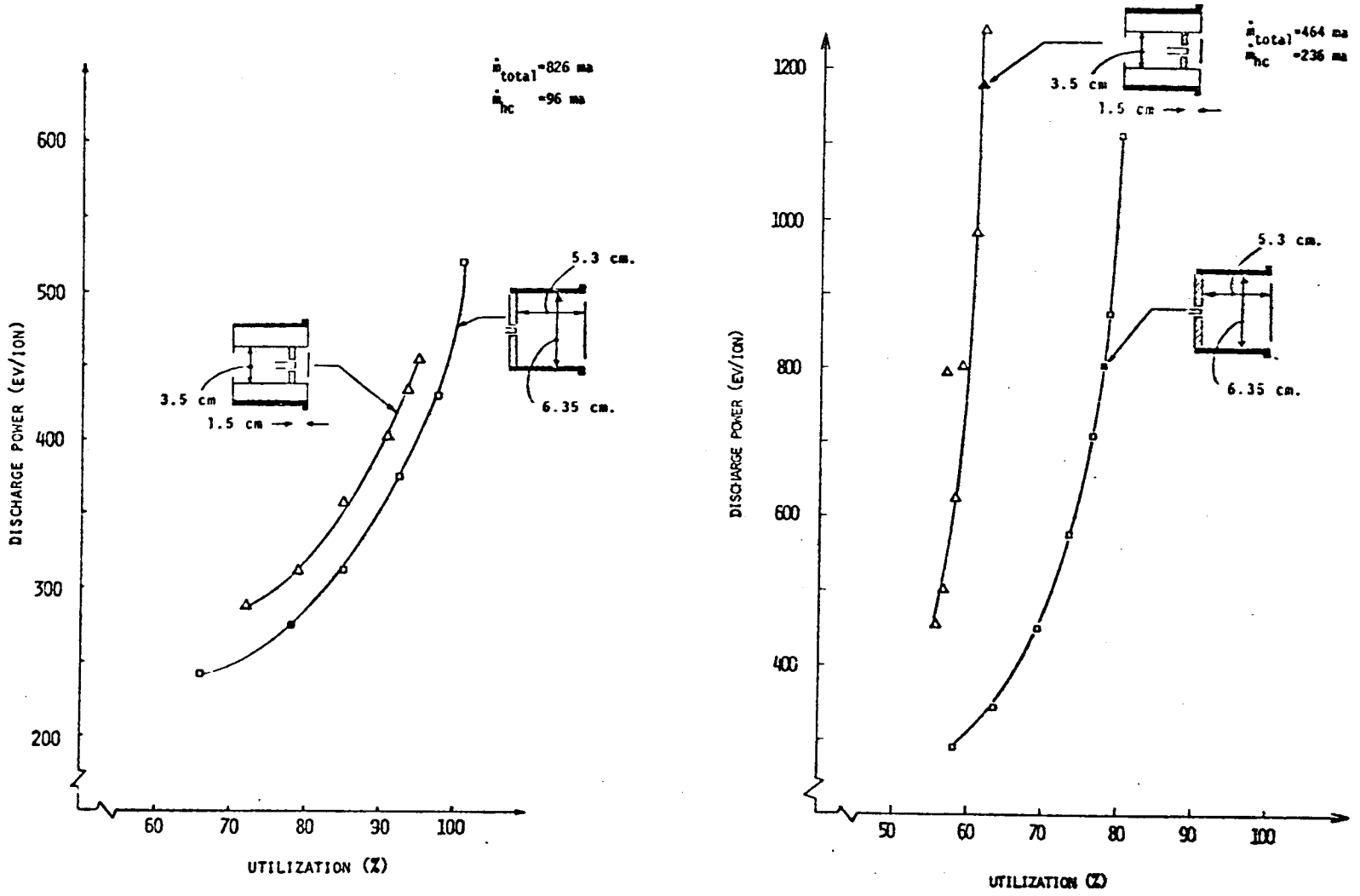

TYPICAL PERFORMANCE VARIATIONS
WITH CATHODE DISCHARGE SIZE

FIGURE 6

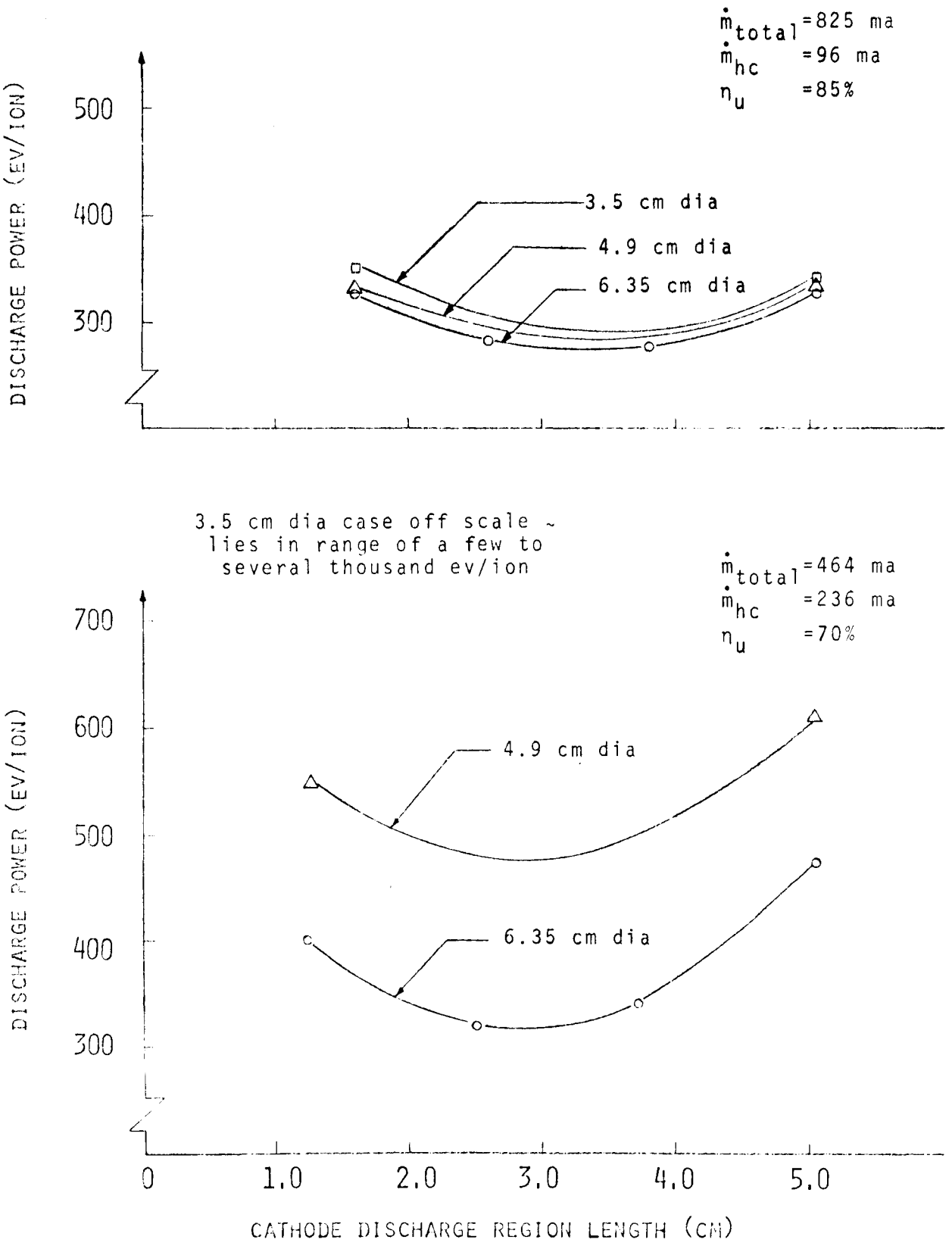

EFFECT OF CATHODE DISCHARGE REGION DIAMETER & LENGTH ON DISCHARGE LOSSES

FIGURE 10

Simultaneous Flow Distribution and Cathode Region Dimensional Adjustments

During the tests mentioned in the previous section, operation with short or small diameter cathode discharge regions was found to result in high arc currents, particularly at the throttled total flow condition. When a smaller fraction of the total flow was passed through the hollow cathode, thruster performance did improve as shown in Figure 11 (full sized cathode discharge region as indicated by sketch). Attempts to reduce the cathode flow below the 165 ma condition shown were thwarted by the occurrence of low frequency oscillations (period of the order of a few seconds) observed on arc and high voltage instrumentation which eventually resulted in arc extinction. Figure 12 shows the effect of reducing cathode flow rate (while holding total flow into the thruster constant) on the arc current-voltage curve. Simultaneous consideration of Figures 11 and 12 suggests cathode flow reductions result in increased propellant utilization and reduced arc current at a fixed arc voltage. One might conclude from this that reductions in cathode flow effect performance gains by increasing the effectiveness of ionizing electrons. This conclusion is contradicted however by a measured decrease in primary electron energy with cathode flow rate which would suggest lower ionization cross sections.

When the cathode discharge region dimensions are reduced to 3.5 cm dia. x 2.67 cm long, much lower cathode flow rates can be sustained as shown in Figure 13 where data obtained with cathode flow rates as low as 40 ma are presented. It is apparent from comparison of the 100 ma cathode flow case with the standard pole piece case (165 ma flow reproduced from Figure 11) in Figure 13 that lower cathode flows are required to achieve the same performance conditions with the smaller cathode discharge volume. It is also apparent that performance is best at a cathode flow rate near 80 ma.

During the acquisition of the data of Figure 13, a sudden transition was observed when the hollow cathode flow rate was between 100 ma and 80 ma. This transition was accompanied by a high impingement current and

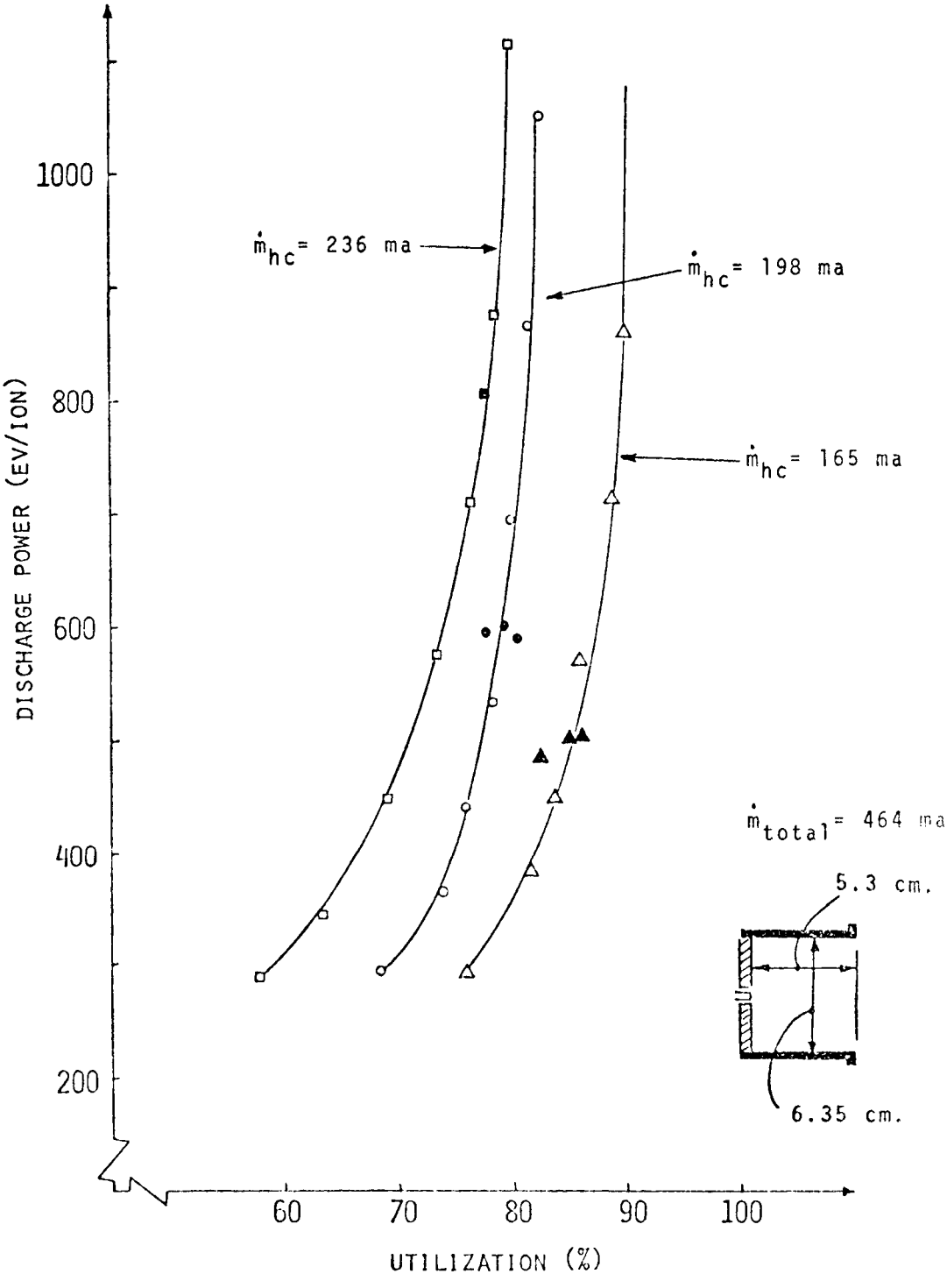

EFFECT OF CATHODE FLOW RATE

FIGURE 11

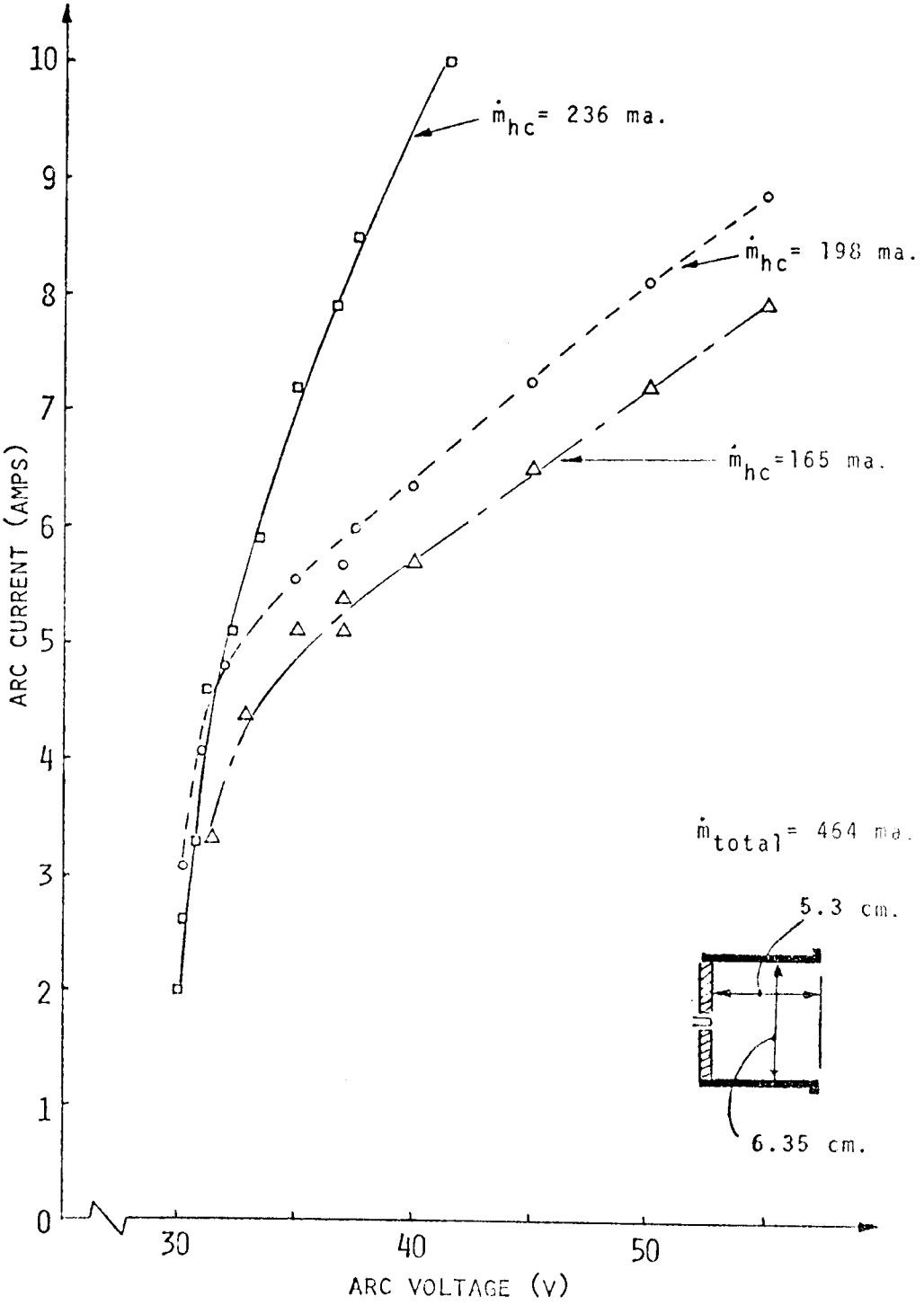

ARC CURRENT - VOLTAGE CHARACTERISTICS

FIGURE 12

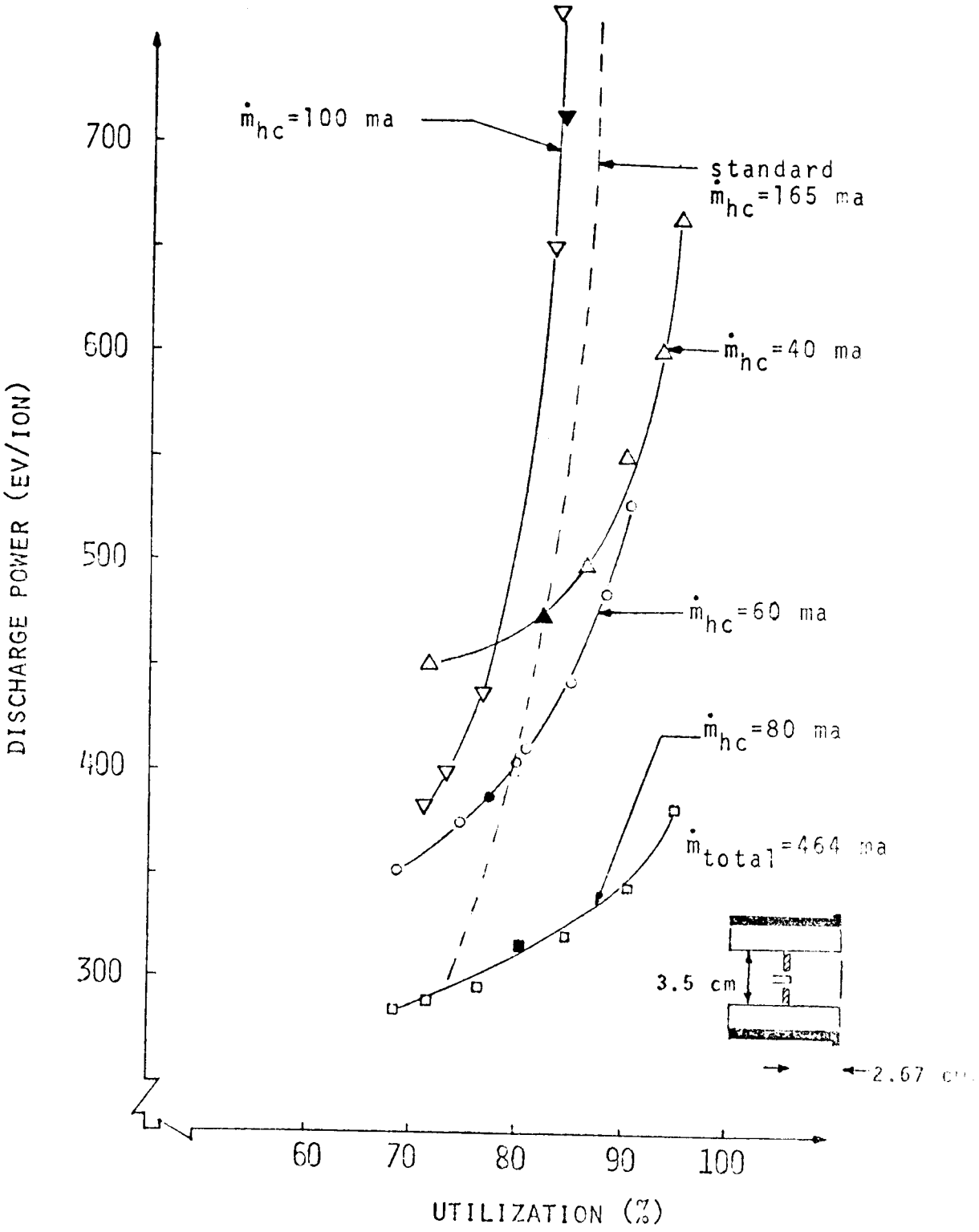

EFFECT OF LOW CATHODE FLOW - SMALL CATHODE DISCHARGE
(THROTTLED FLOW)

FIGURE 13

considerable arc noise. It can be seen from Figure 13 that optimum performance is achieved on the low flow side of the onset of this transition, and that the performance improvement is very substantial (~ 15% utilization). Even though there is arc noise and a high impingement current at the transition cathode flow rate, operation on either side of this flow is characterized by normal impingement and stability. Some insight into the nature of the transition can be gained by considering the corresponding arc current-voltage characteristic presented as Figure 14. The nearly horizontal curves corresponding to 80 ma and lower cathode flow rates suggest the transition involves a shift into an arc current limited mode of operation. As cathode flow rate is reduced below 80 ma, Figure 14 shows the characteristic remains horizontal and rises to progressively higher currents. The nature of the transition will be discussed further in a section of this report which follows.

The effect of low cathode flows and a small cathode discharge region on performance at the high total flow condition is presented in Figure 15. The standard flow curve (shown dotted) is reproduced from Figure 9 and corresponds to a 96 ma cathode flow into the 5.3 cm x 6.35 cm dia. cathode discharge region. It is also apparent from this figure that lesser cathode flow rates are required with the smaller discharge volume to achieve about the same performance conditions. Although a slight improvement in performance is observed with flow and cathode dimension reductions for this high flow case, it is not nearly as great as that observed in the throttled total flow case. In proceeding to progressively lower cathode flow rates no sudden transition in operating mode was observed. This observation is consistent with the arc current-voltage characteristics shown in Figure 16 which exhibit a gradual tendency to a current limited characteristic curve rather than the sudden jump observed at the throttled total flow operating condition.

If one selects a propellant utilization efficiency, the cathode flow rate can be adjusted to produce a desired arc voltage at that utilization, and the discharge power and cathode flow rate are thereby uniquely determined. The discharge power achieved under this condition at a given cathode discharge size can then be compared meaningfully to other sizes.

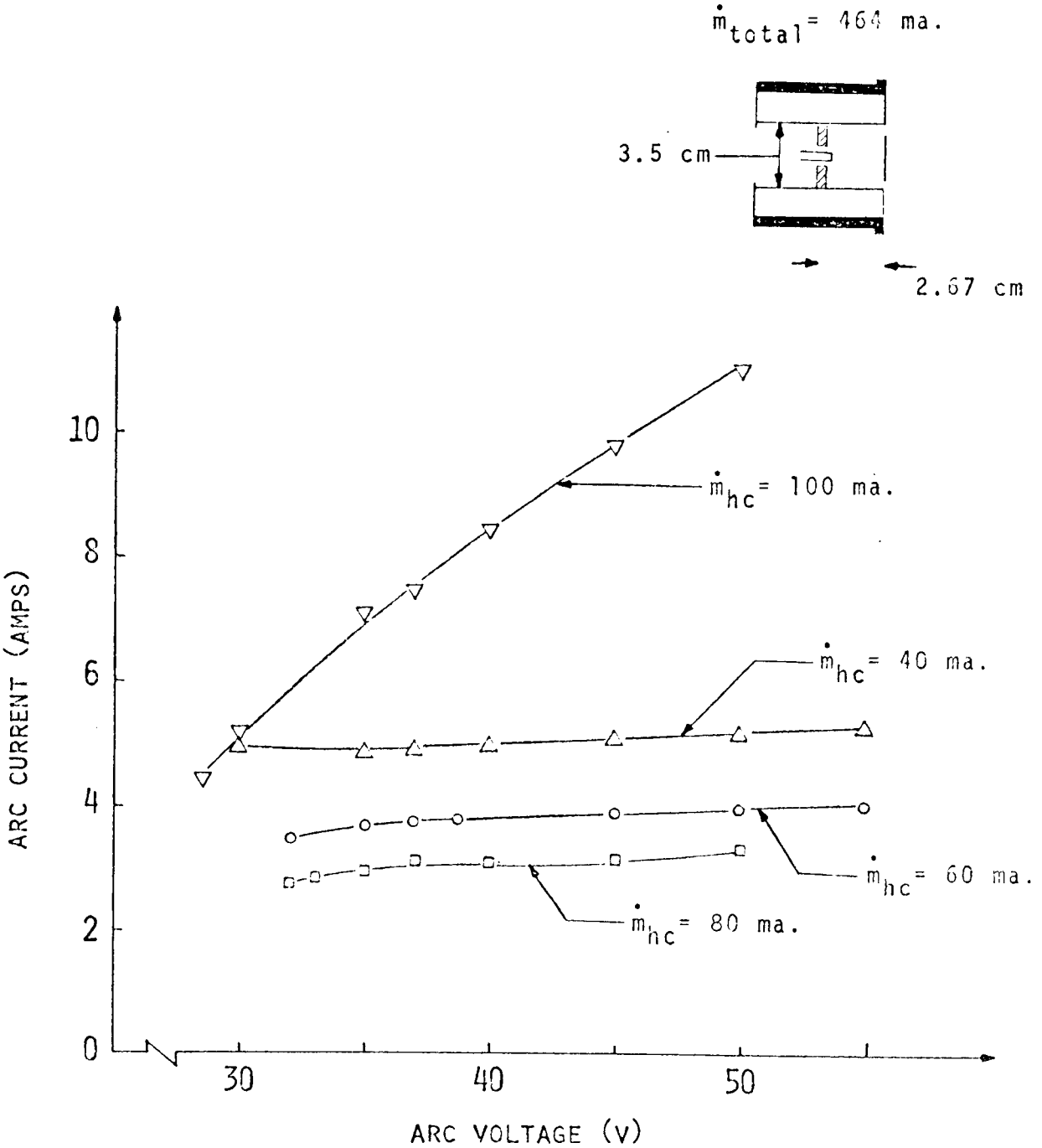

ARC CURRENT-VOLTAGE CHARACTERISTICS -
SMALL CATHODE DISCHARGE
(THROTTLED TOTAL FLOW)

FIGURE 14

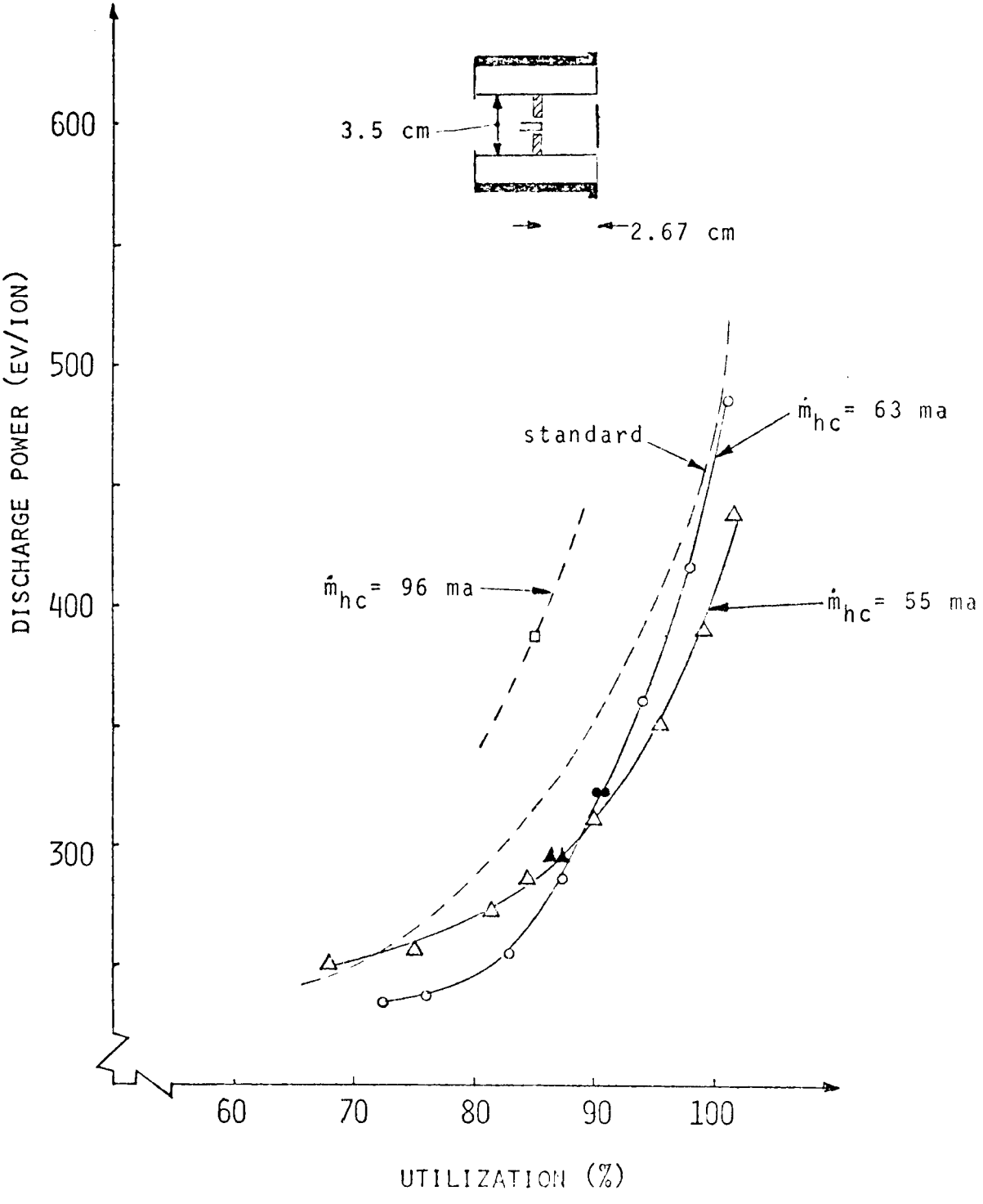

EFFECT OF LOW CATHODE FLOW - SMALL CATHODE DISCHARGE
(HIGH TOTAL FLOW)

FIGURE 15

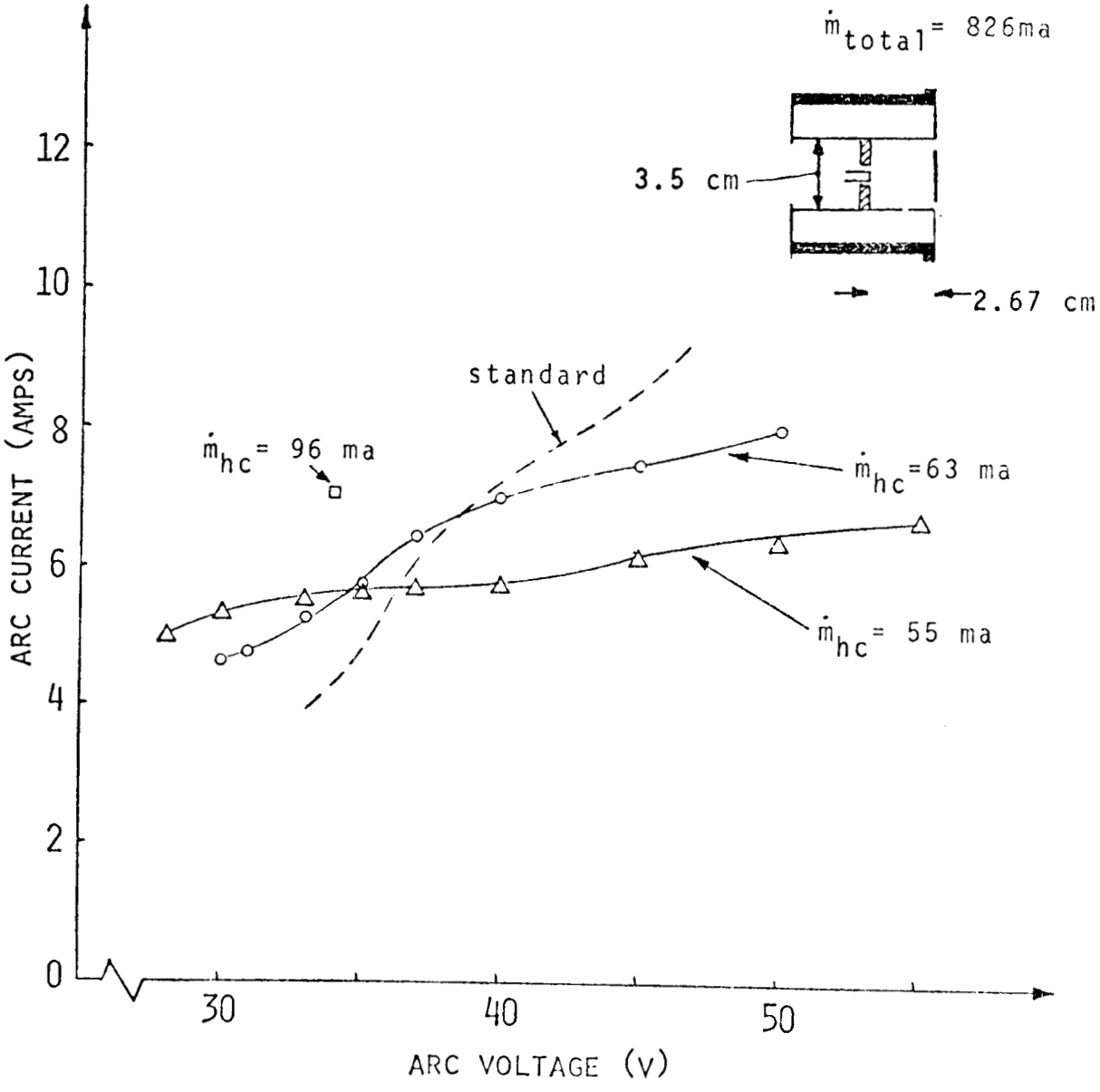

ARC CURRENT-VOLTAGE CHARACTERISTICS -
SMALL CATHODE DISCHARGE
(HIGH TOTAL FLOW)

FIGURE 16

This procedure was followed and the results presented in Figure 17 were obtained after cross-plotting for the high total flow condition. The cathode flow rates required to assure a 37 v arc voltage at 85% utilization are presented in the lower graph for the two cathode discharge diameters considered. The discharge power required at these flow rates and at 85% utilization are presented on the upper graph. These curves show that at the high total flow condition: 1) lower cathode flow rates are required with the smaller cathode discharge regions, 2) performance is not affected significantly by the reduction in cathode discharge diameter used and 3) performance is either unchanged or possibly improved slightly by reducing cathode discharge length from 5 cm to ~2 cm and is degraded by further length reductions.

Similar curves obtained under the throttled total flow conditions are presented in Figure 18 for the condition of 37 v arc voltage at 80% utilization. In this case very substantial reductions in discharge losses are achieved when either the length or diameter of the cathode discharge are reduced. The effect of reductions in discharge size on discharge losses is examined in terms of measured plasma properties in Appendix C.

Comparison of the cathode flow curves of Figures 17 and 18 shows one could select a cathode discharge size (~3.5 cm dia. x 4 cm long) which would result in the same cathode flow rate at both the high and throttled total flow conditions. This suggests a new mode of thruster control which may help reduce instabilities observed in some control systems[7]. In this scheme cathode flow rate would be held constant and main flow would be adjusted as necessary to achieve the desired beam current. Preliminary tests performed using manual control on these variables confirm the acceptability of this mode of thruster control

Figures 19 and 20 present the cathode region plasma properties corresponding to the high flow (Figure 17) and throttled flow (Figure 18) respectively. These data show in general lower electron densities, plasma potentials and electron temperatures for the larger diameter discharge, but the scatter in these data and the small sample of data makes additional interpretation inadvisable.

From the preceding discussion it is apparent that throttled thruster performance is enhanced by a reduction in the size of the cathode dis-

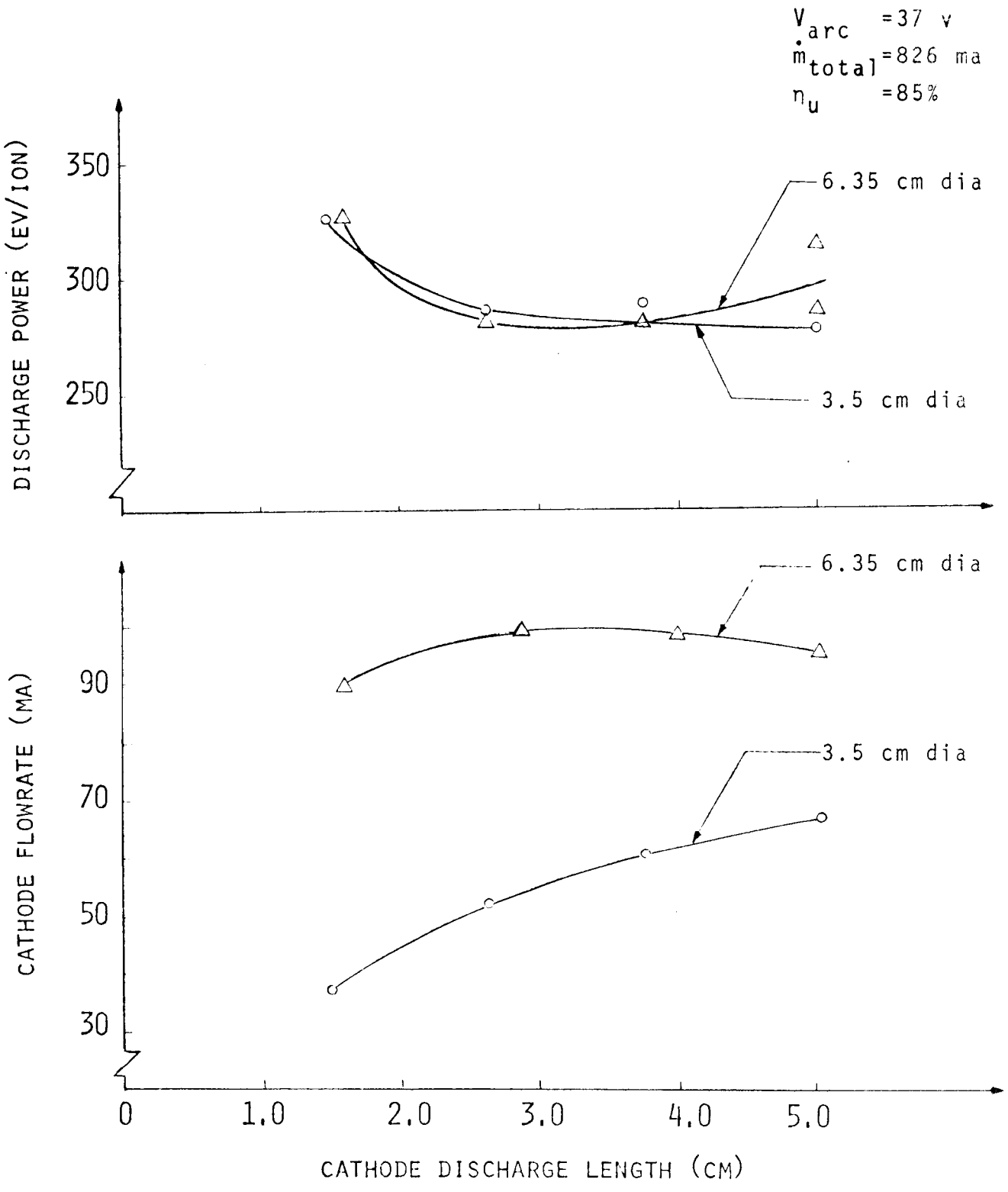

CATHODE FLOW AND DISCHARGE LOSS VARIATIONS
WITH CATHODE DISCHARGE SIZE
(HIGH TOTAL FLOW)

FIGURE 17

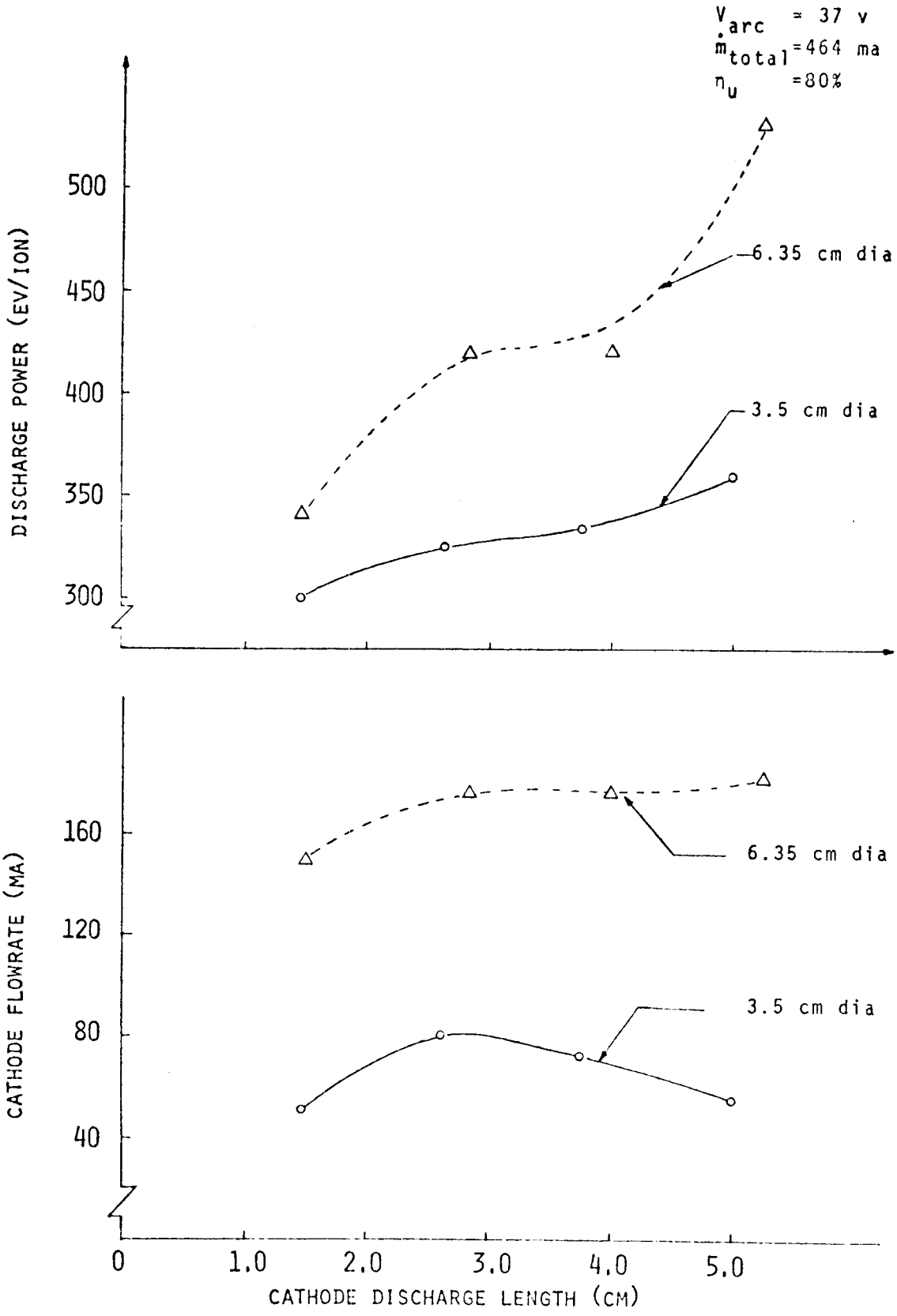

CATHODE FLOW AND DISCHARGE LOSS VARIATIONS
WITH CATHODE DISCHARGE SIZE
(THROTTLED TOTAL FLOW)

FIGURE 18

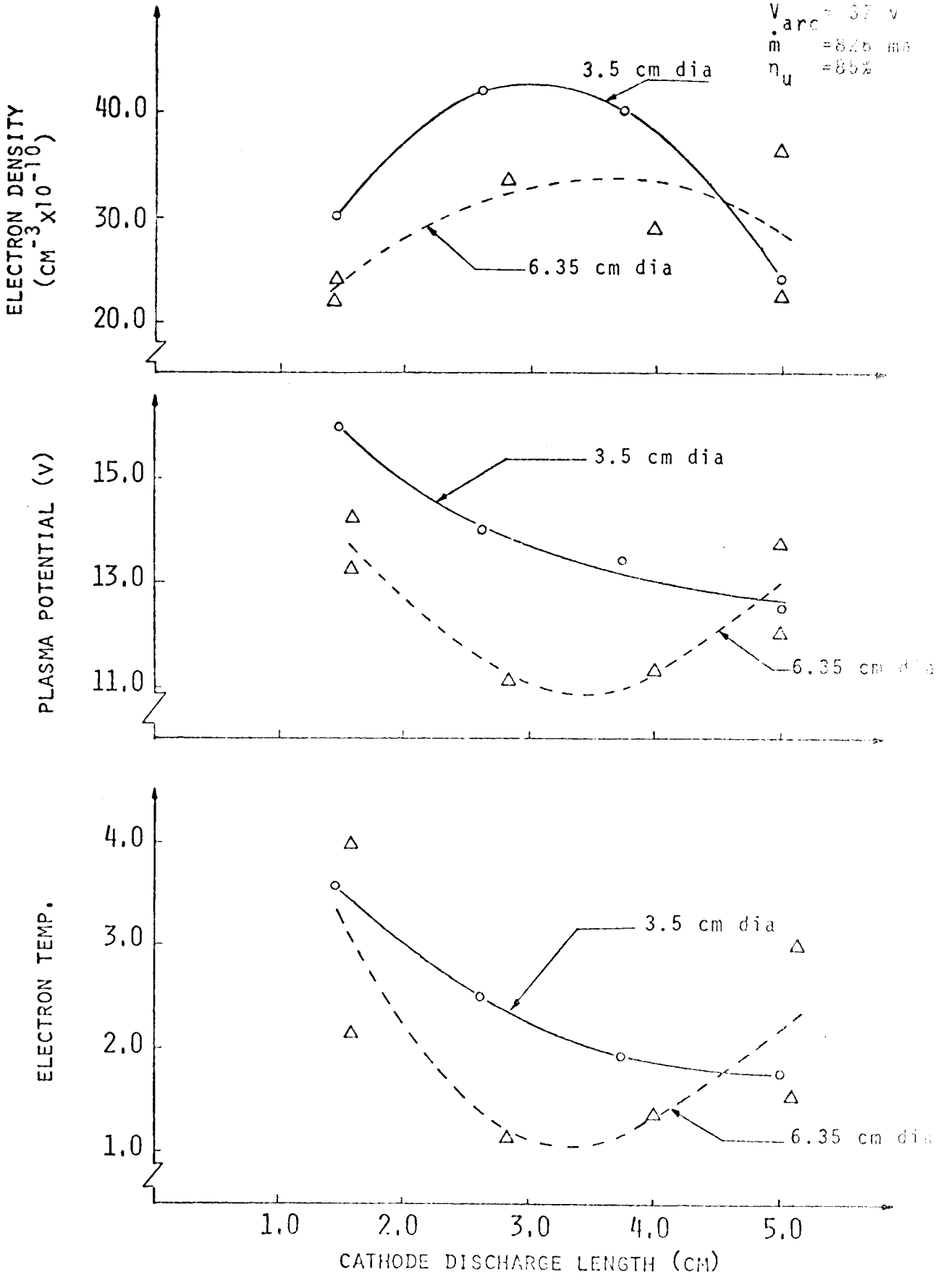

CATHODE DISCHARGE PLASMA PROPERTIES
(HIGH TOTAL FLOW)

FIGURE 19

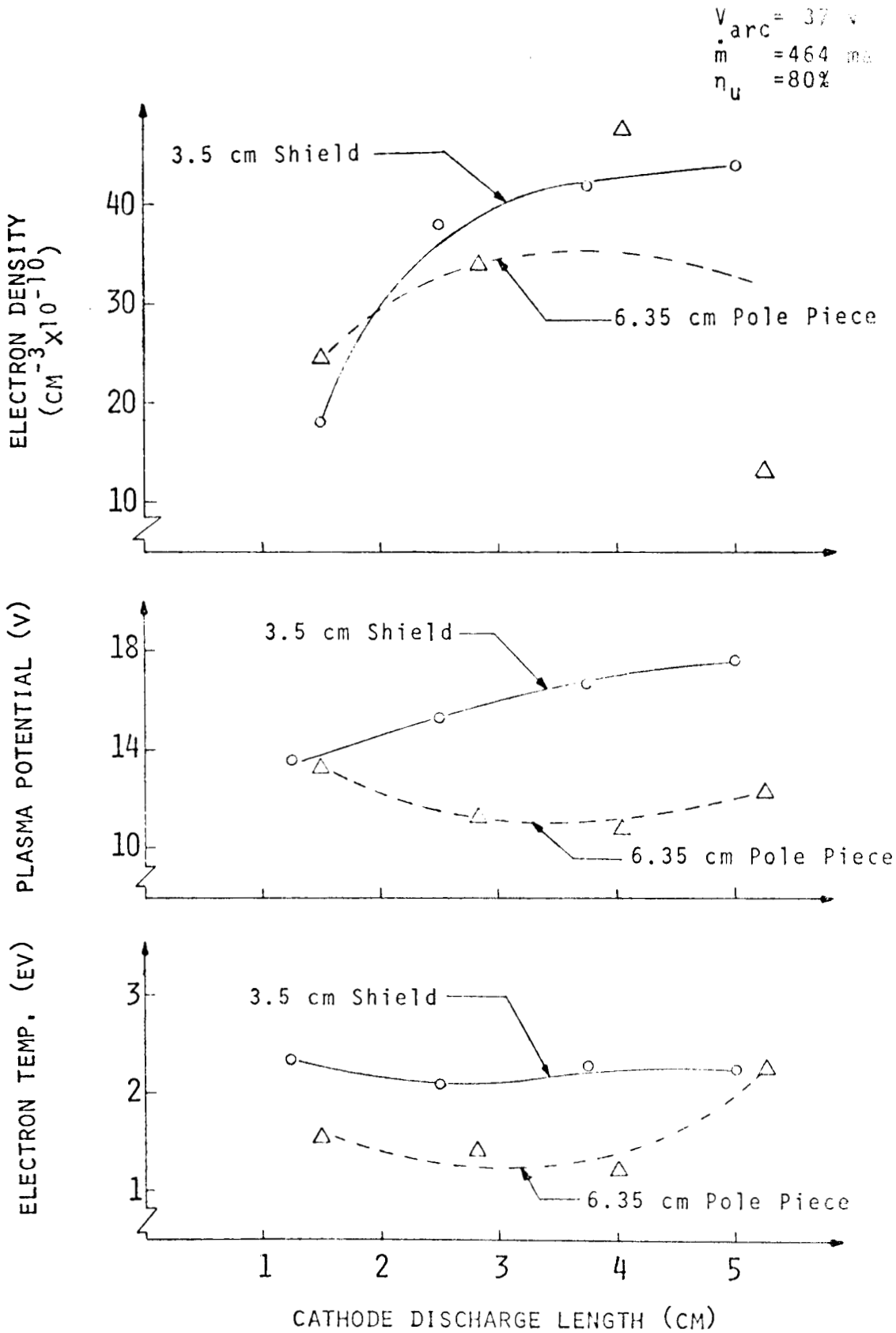

CATHODE DISCHARGE PLASMA PROPERTIES
(THROTTLED TOTAL FLOW)

FIGURE 20

charge and a corresponding reduction in cathode flow rate. The ion beam profile is however degraded when the sleeve is inserted to reduce the discharge diameter as illustrated in Figure 21. The extent of the degradation is best indicated by the change in the flatness parameter (Φ) assigned to each curve and defined in Appendix B. The greater peaking of the ion beam profile observed when the sleeve is employed to reduce the cathode discharge diameter is considered to be due to the resultant separation between the baffle aperture and the cathode pole piece. This separation causes the primary electrons to be introduced into the main discharge away from the critical field line thereby depriving plasma near the outer radius of the main discharge of these electrons.

Two approaches were considered in attempting to correct this problem. They were: 1) the use of a magnetic field within the cathode pole piece opposing the main magnetic field, and 2) the use of a 3.5 cm dia. pole piece in place of the standard one (6.35 cm dia.). The magnetic field was applied within the cathode pole piece (Approach 1) by a field coil installed in the manner suggested by the insert on Figure 22. Figure 22 shows the effect of a cathode region magnetic field opposing the main magnetic field is to flatten the ion beam profile as desired. It should be noted by comparison of Figures 21 and 22 that the cathode magnetic field does not produce a flatter profile than the one achieved with the full sized pole piece (6.35 cm). Performance curves showed lower discharge losses at low utilizations and higher discharge losses above ~ 80% utilization when the cathode field coil was operating. Because of these effects the testing was not pursued and data were not collected with the cathode magnetic field at the high flow rate condition.

When the 3.5 cm dia. pole piece was substituted for the 3.5 cm dia. sleeve within the 6.35 cm dia. pole piece, the beam profile was also flattened as shown in Figure 23 for the throttled flow case. The profile is still not as flat as the one obtained with the larger pole piece. Additional testing is required at various magnet currents to see if the ion beam profile obtained with the small pole piece can be improved.

The effect of substitution of the 3.5 cm dia. pole piece for the sleeve on thruster performance arc current-voltage characteristics is

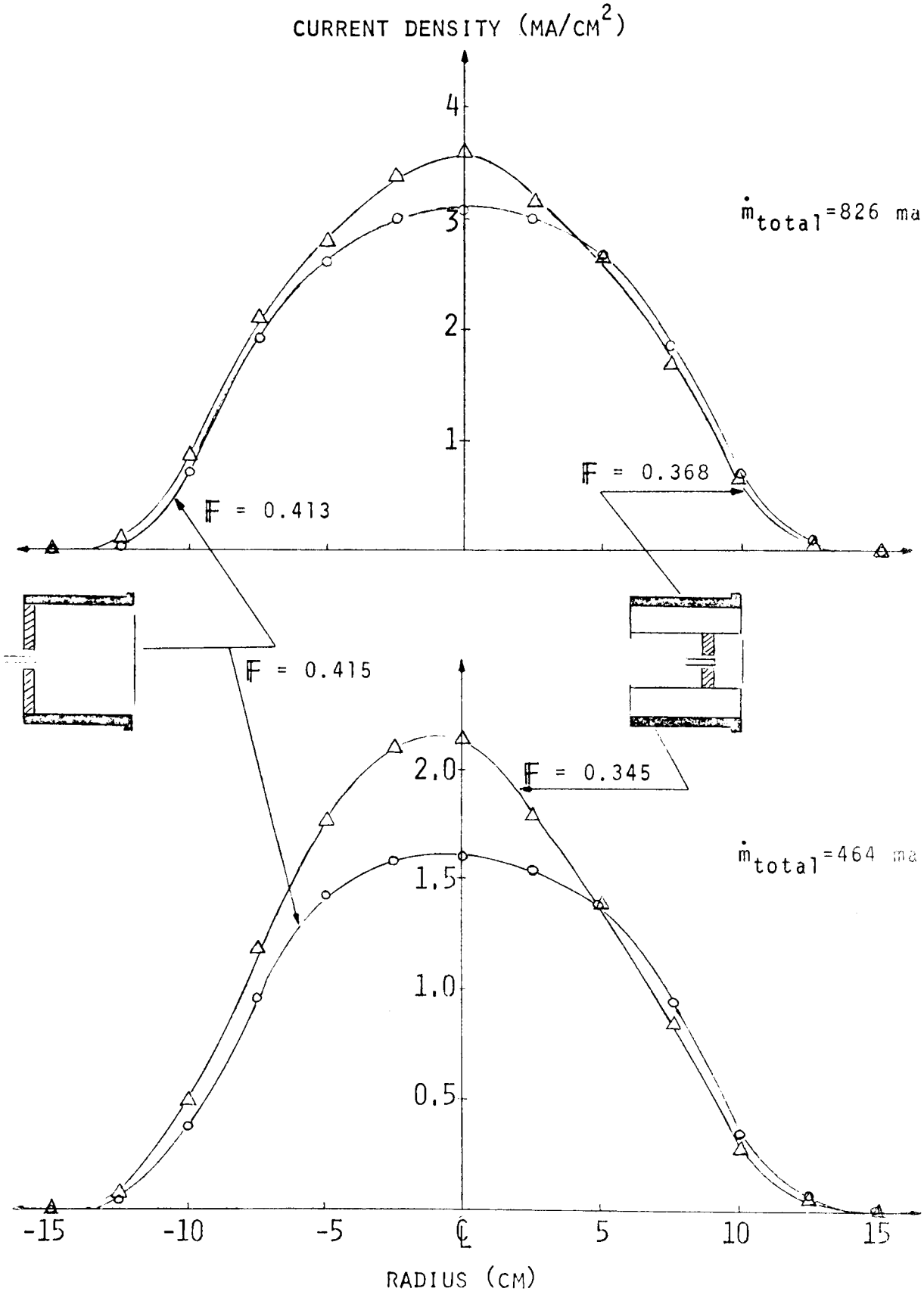

EFFECT OF CATHODE SLEEVE ON BEAM PROFILE

FIGURE 21

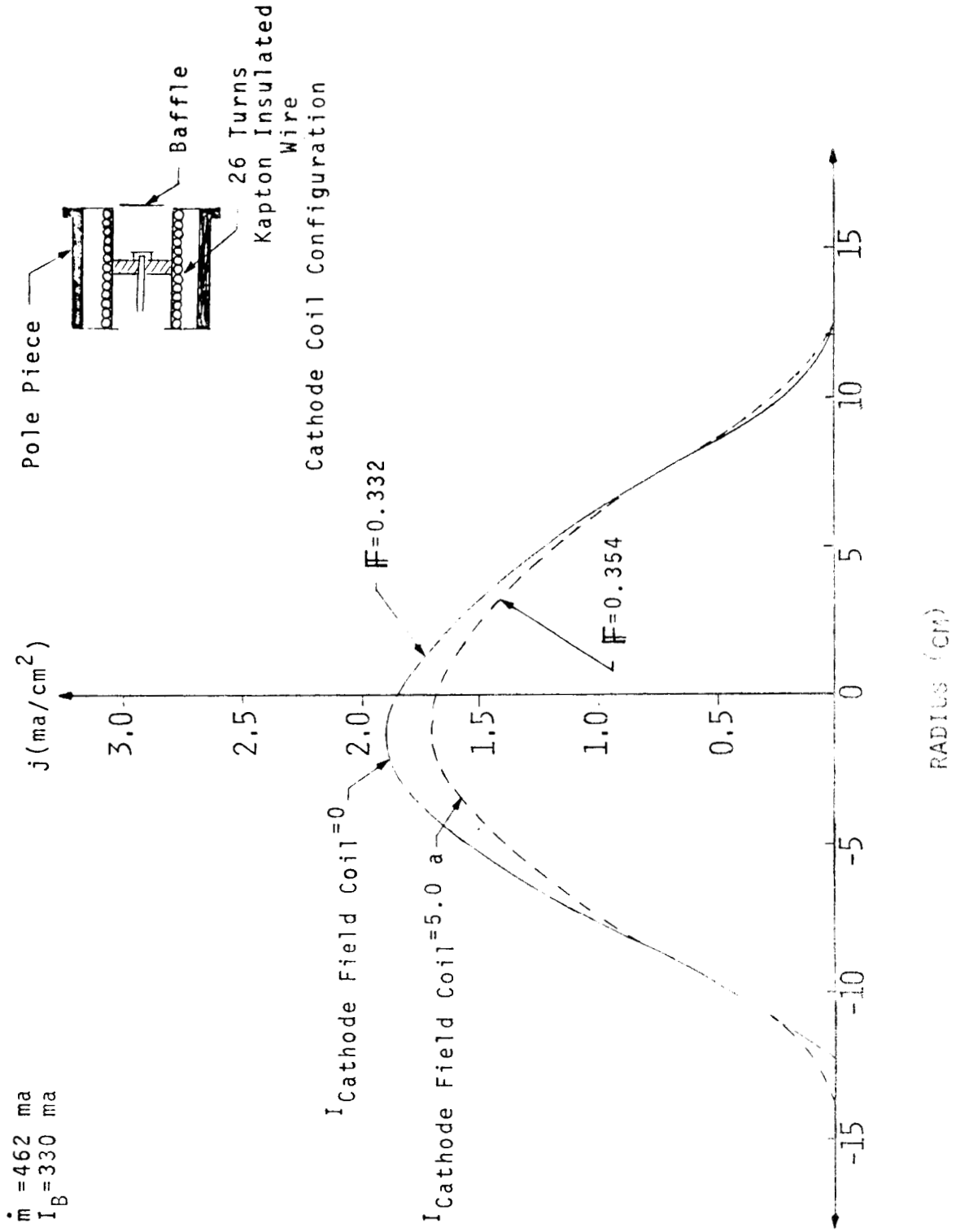

EFFECT OF A CATHODE MAGNETIC
FIELD ON ION BEAM PROFILE

FIGURE 22

$\dot{m}_{total}$=464 ma

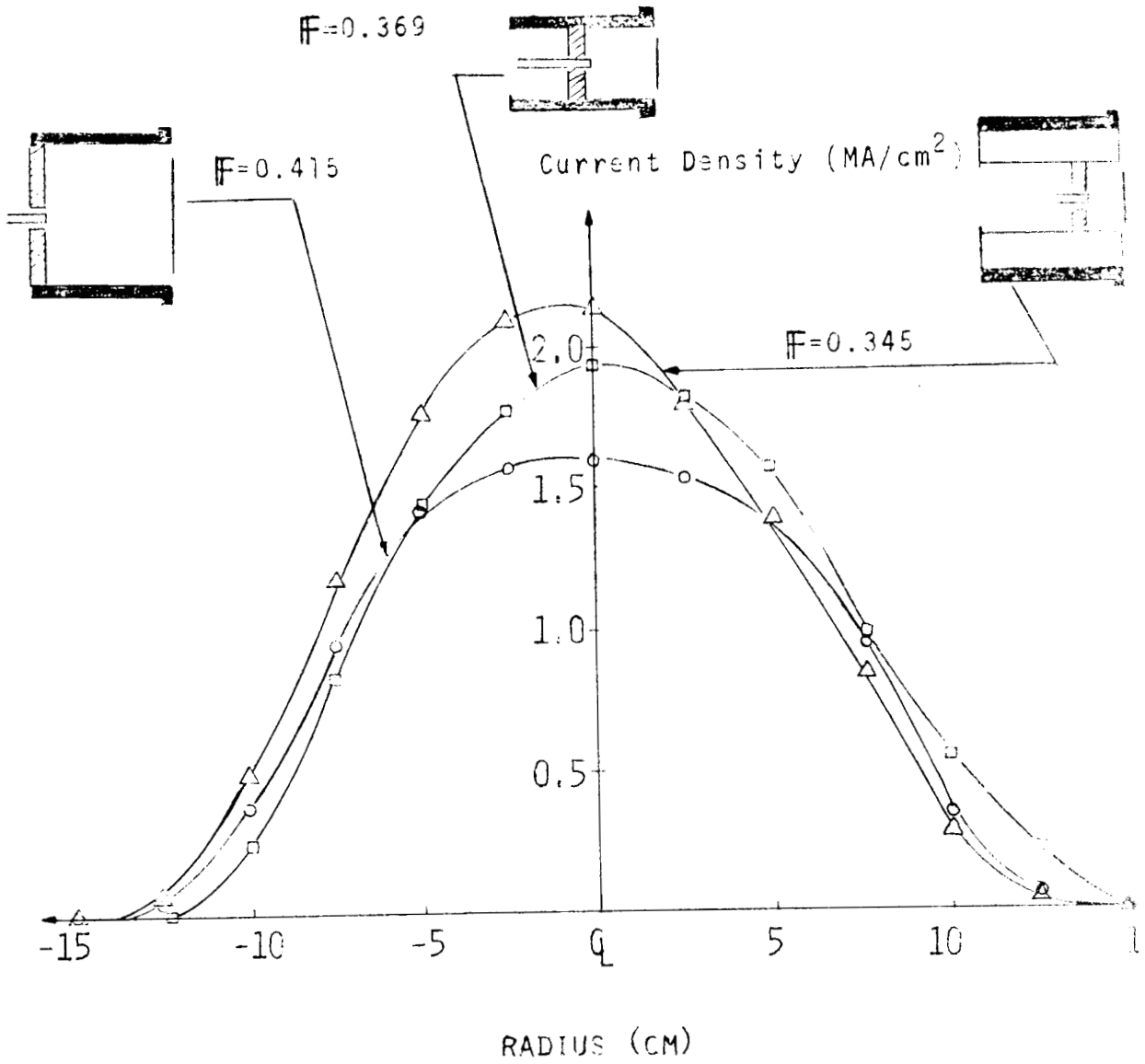

EFFECT OF 3.5 CM DIAMETER POLE PIECE ON BEAM PROFILE

FIGURE 25

presented in Figures 24 and 25. Figure 24 shows slightly better thruster performance when the pole piece is used rather than the sleeve and that the transition between the limited and variable arc current modes of operation is achieved with slightly lower cathode flows with the 3.5 cm dia. pole piece. Figure 25 shows essentially the same types of arc current-voltage characteristics are achieved with either the 3.5 cm dia. pole piece or sleeve in each operating mode.

Throughout the aforementioned tests the cathode tip temperature was monitored with a thermocouple. Figures 26 and 27 show this temperature data as a function of arc current--keeper current is fixed at 0.5 a--for the 3.5 cm and 6.35 cm dia. discharge region respectively. Figure 26 shows cathode tip temperatures rise as cathode flow is reduced until the previously mentioned arc current transition occurs. At this point the cathode temperature curve drops markedly, and then begins to rise with further reductions in cathode flow. The additional striking feature of the curves of Figure 26 is the fact that the arc current (and hence temperature) changes over the arc voltage range 30-55 v, are reduced greatly when the transition occurs (comparison of the temperature and current variations at the $\dot{m}_{hc}$ = 83 ma curve with those at lower cathode flows). Presuming lower cathode temperatures imply longer cathode life, operation at the onset of limited arc current mode of operation would yield the longest cathode lifetime. Figure 27 shows reductions in cathode flow result in increases in cathode tip temperature at both the high and throttled total flow conditions.

One can conclude from these tests that reducing the cathode discharge diameter and length enables one to operate a throttled thruster at a sufficiently low cathode flow rate to achieve an arc current limited mode of operation. In this mode propellant utilization is increased significantly (~ 15%) and cathode tip temperatures are held at low values (~ 1050°C). The ion beam profile becomes more peaked when the pole piece diameter is reduced and magnet current is not adjusted. Additional testing is required to determine if changes in magnet current can be used to flatten the profile back to that one observed with the larger pole piece.

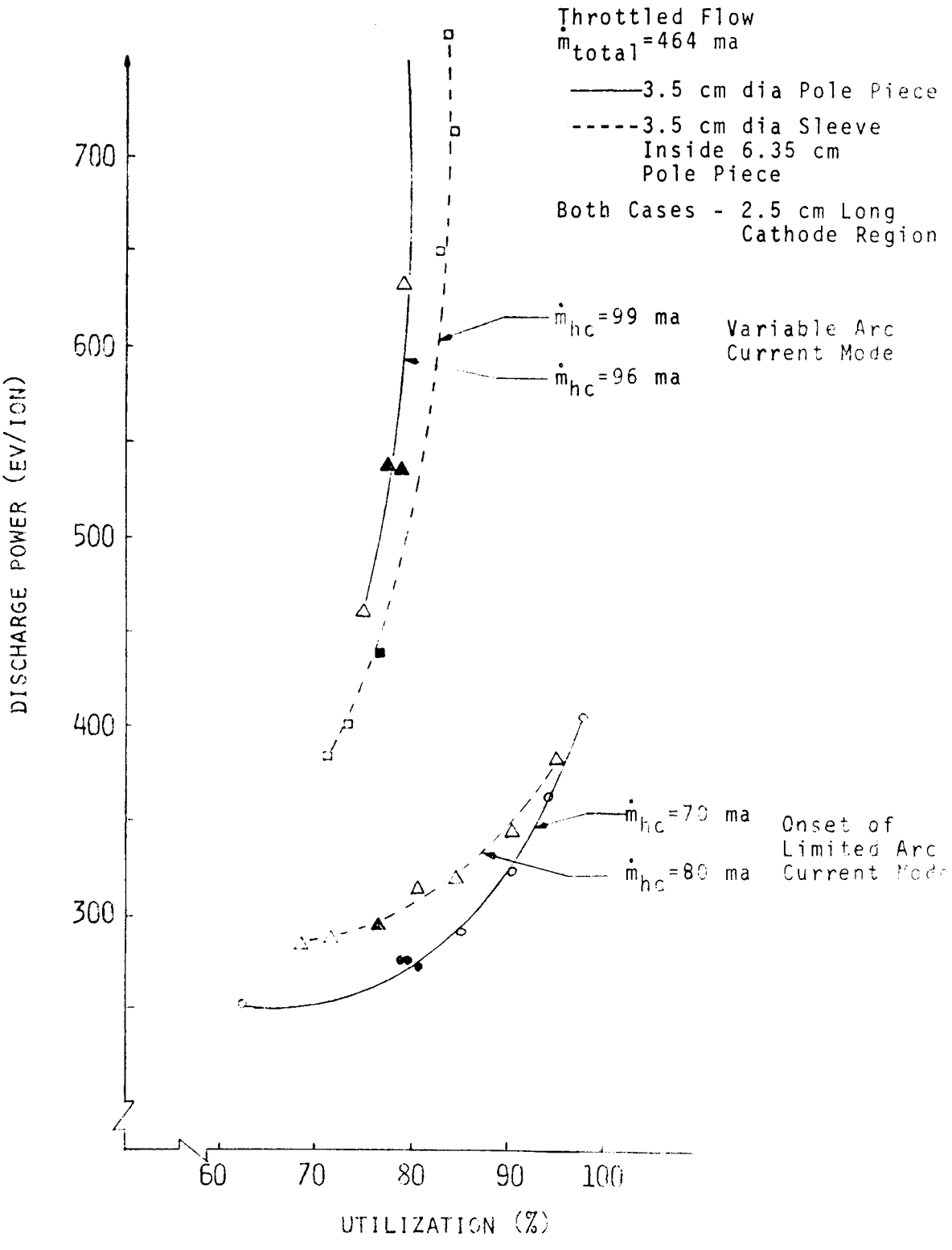

EFFECT OF POLE PIECE-SLEEVE SUBSTITUTION ON PERFORMANCE

FIGURE 24

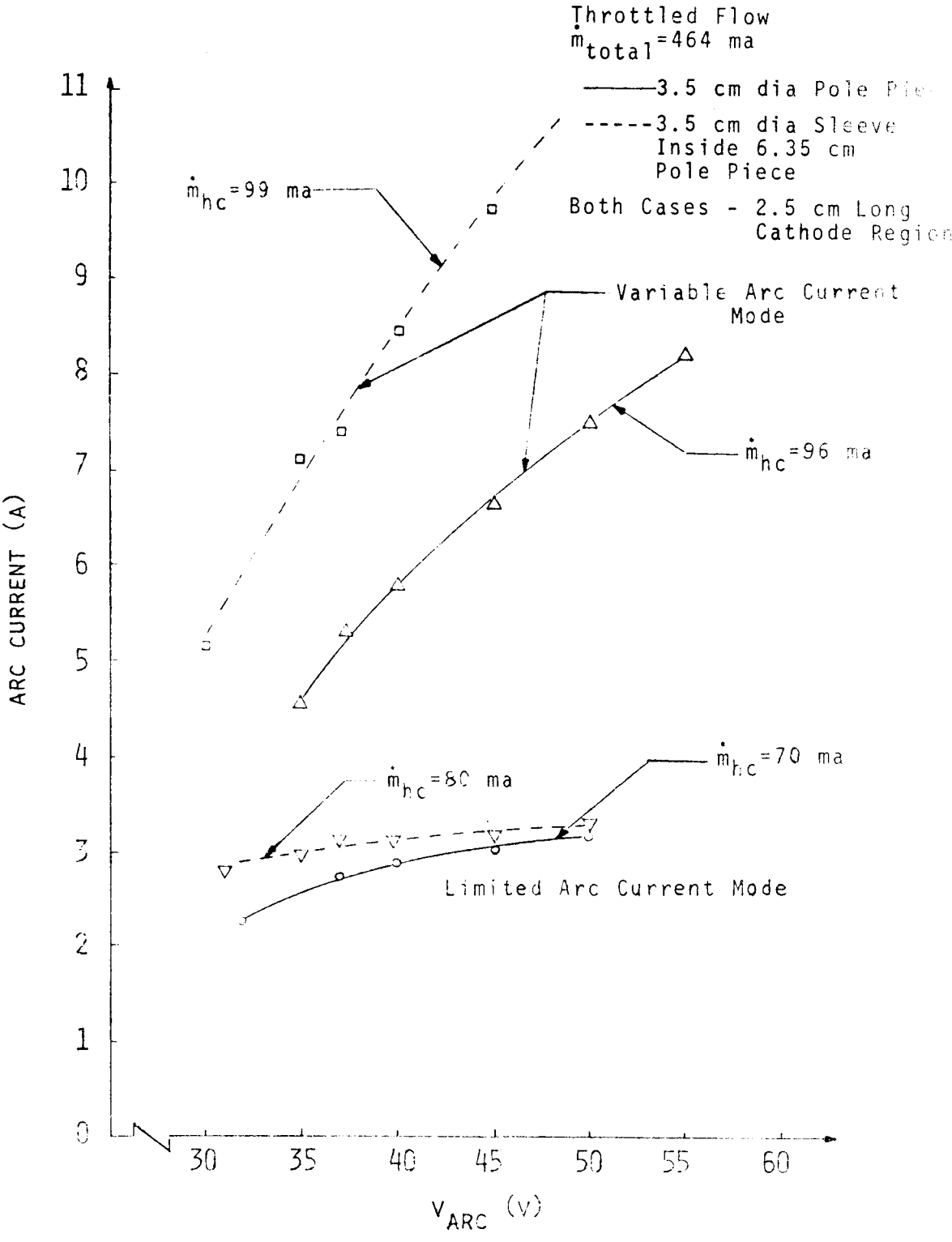

EFFECT OF POLE PIECE - SLEEVE SUBSTITUTION ON ARC CURRENT VOLTAGE CHARACTERISTICS

FIGURE 25

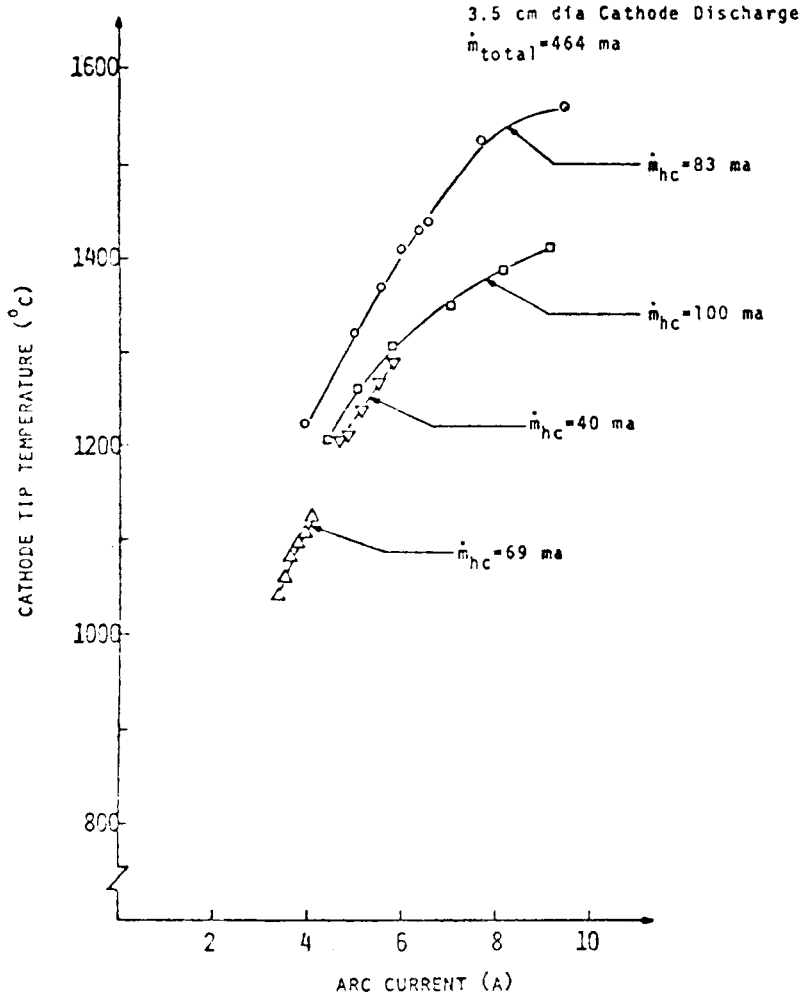

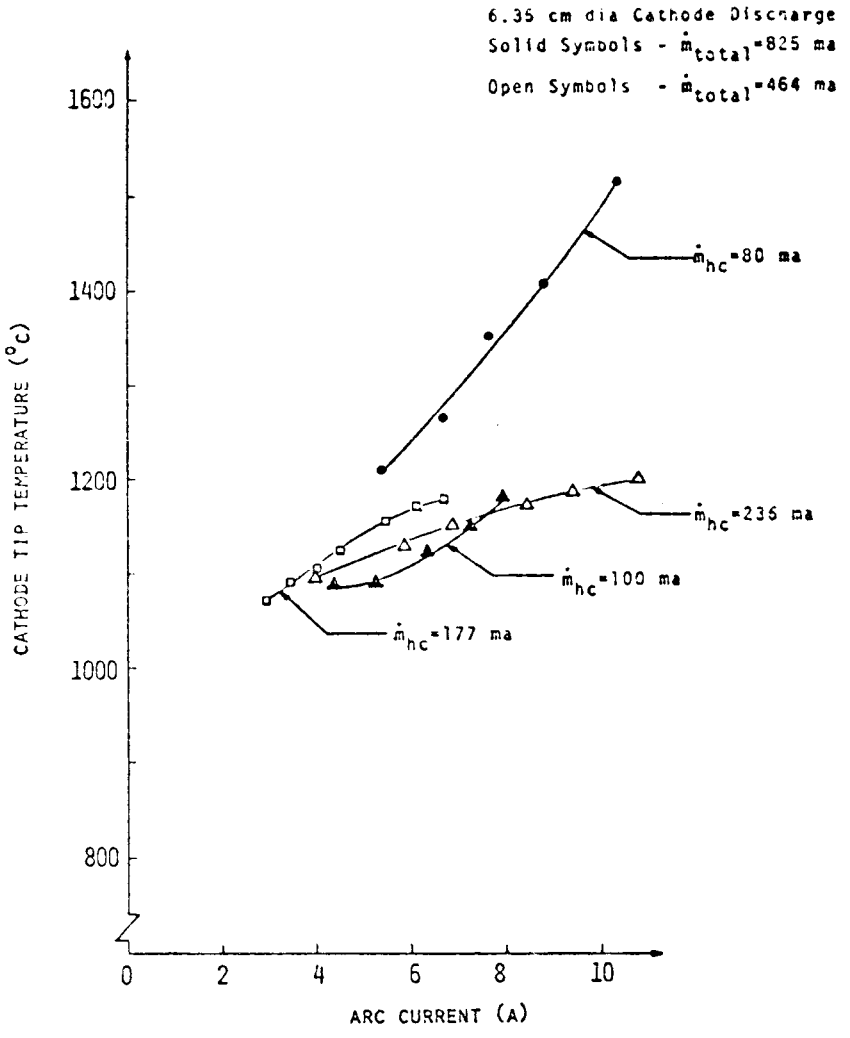

CATHODE TIP TEMPERATURE VRS ARC CURRENT

FIGURE 27

FIGURE 27

The reductions in cathode discharge dimensions and attendant reductions in cathode flow rate effect only slight improvements in thruster operation at higher total flow rates.

The Nature of the Arc Current Transition

When the thruster is operated with the 3.5 cm dia. cathode discharge at the throttled total flow condition, a sudden transition in the mode of thruster operation is observed as cathode flow rate is decreased through the 80 ma equivalent flow condition. The transition is characterized by a sudden decrease in arc current, a temporary increase in impingement current and temporary keeper, arc and impingement current oscillations. At flow rates on either side of this transition flow, thruster operation is stable. Because an optimum in thruster performance occurs on the low flow side of this transition, the mechanism of the transition is of interest. The following discussion is intended to shed some light on this mechanism.

As pointed out in the course of the discussion of Figures 13 and 14, the arc current-voltage characteristics changes from one in which arc current varies significantly with arc voltage (variable arc current mode) to one in which arc current is essentially unchanged by variations in arc voltage (limited arc current mode) as cathode flow rate is reduced to effect the transition. With further reductions in cathode flow the arc current variation is still limited but the arc current is sustained at progressively higher levels (see Figure 14).

The arc current is probably limited at low cathode flows by phenomena associated with 1) the cathode, 2) the baffle aperture or 3) the anode. The fact that the transition is brought on by reductions in cathode flow indicates however that this is not an anode phenomenon. In order to determine whether the cathode or the baffle aperture is limiting the current, the keeper current was varied from the 0.5 amp standard operating value. These data are presented in Figure 28 for three cathode flow rates, one significantly below the transition flow rate (36 ma), one near the transition cathode flow rate (80 ma) and one well above the

EFFECT OF KEEPER CURRENT AT VARIOUS CURRENT FLOWS

FIGURE 28

transition flow rate (127 ma). For the 36 ma and 127 ma cathode flow cases the arc currents are quite high and the impingement current and keeper voltage show regular variations with keeper current. At the intermediate cathode flow rate (80 ma), the arc current is much lower than the other cases and the keeper voltage, arc current and impingement current all exhibit anomalous behavior over the range of keeper currents examined. At the low and intermediate cathode flows, oscillations were observed at keeper currents greater than about 1.5 a, and for the low flow case they were so severe that the arc and keeper discharges could not be sustained. Although the arc current transition is not as dramatic as that observed when the cathode flow rate was reduced to effect the transition these tests demonstrated the transition could be effected through keeper current variations when the cathode flow rate was near the transition value. From the intermediate flow data of Figure 28 the keeper voltage is seen to reach a maximum of about 11 v as the transition begins. This is considered significant because the voltage is near the ionization potential of mercury (10.4 v).

In order to investigate the effect the keeper discharge might be having on this transition, the keeper discharge was operated without the arc discharge. In order to sustain this discharge over a range of cathode flow rates estimated to be 20 to 140 ma from cathode vaporizer temperatures a 2 a. keeper current was maintained. At high cathode flows a 0.1 v oscillation (100 hertz) was observed on an 8.6 v keeper voltage signal. As flow was reduced the noise level was unchanged and the keeper voltage rose until it reached 10.4 v at about 60 ma cathode flow. At this point the mean keeper voltage rose rapidly to about 13 v and voltage fluctuations of about 2 v amplitude at 20 hertz were superimposed on the previously observed "noise" (0.1 v, 100 hertz). Additional tests showed the noise frequencies were influenced by the keeper power supply impedance but the magnitudes and transition point were not.

The preceding data suggest the limited to variable arc current transition observed during thruster operation is a cathode-keeper phenomenon. The increase in keeper discharge noise at the mercury ionization potential must occur because of the energy sink available to electrons

falling through potentials at and greater than the ionization potential. It has been suggested the oscillations are a result of a transient ionization process in which the discharge couples somehow to acoustic waves[8].

Data accumulated from various 3.5 cm dia. cathode sleeve tests have been assembled in Figure 29 to show the effect of cathode flow rate on keeper voltage when total flow and arc voltage are fixed. All of these data were obtained at the standard keeper current indicated (0.5 a). Although they show some scatter, the qualitative behavior shown by the curve was observed several times during attempts to stabilize flow conditions, and it is considered to be accurate. This figure again suggests the keeper voltage may approach the ionization potential at the transition flow rate.

Keeper voltages at the higher flow rates and the flow rates themselves are in the range where the cathode operates in the spot mode[9,10] (i.e., the variable arc current mode corresponds to the spot mode of cathode operation). The limited arc current mode however is not so easily related to either the transition or plume modes of cathode operation. The plume mode is for example characterized by keeper voltages in the range 20 to 50 v[10], which is far above the keeper voltages in Figure 29. In the transition mode, the keeper voltage is insensitive to cathode flow and the keeper voltage vs. flow curve has a negative slope while the limited arc current mode of Figure 29 violates both of these criteria. Reference 11 points out, however, that in the plume mode a limited variation of arc current with arc voltage is observed.

Figures 30 and 31 show the cathode region electron density and temperature obtained from Langmuir probe data. The numbers presented by each data point on these curves are the cathode flow rates at which the data were obtained. These flows represent respectively the approximate minimum cathode flow at which the variable arc current mode can be sustained (dotted curve), and the approximate maximum cathode flow at which the limited arc current mode can be sustained. These data show the cathode flow needed to effect the transition decreases with increasing

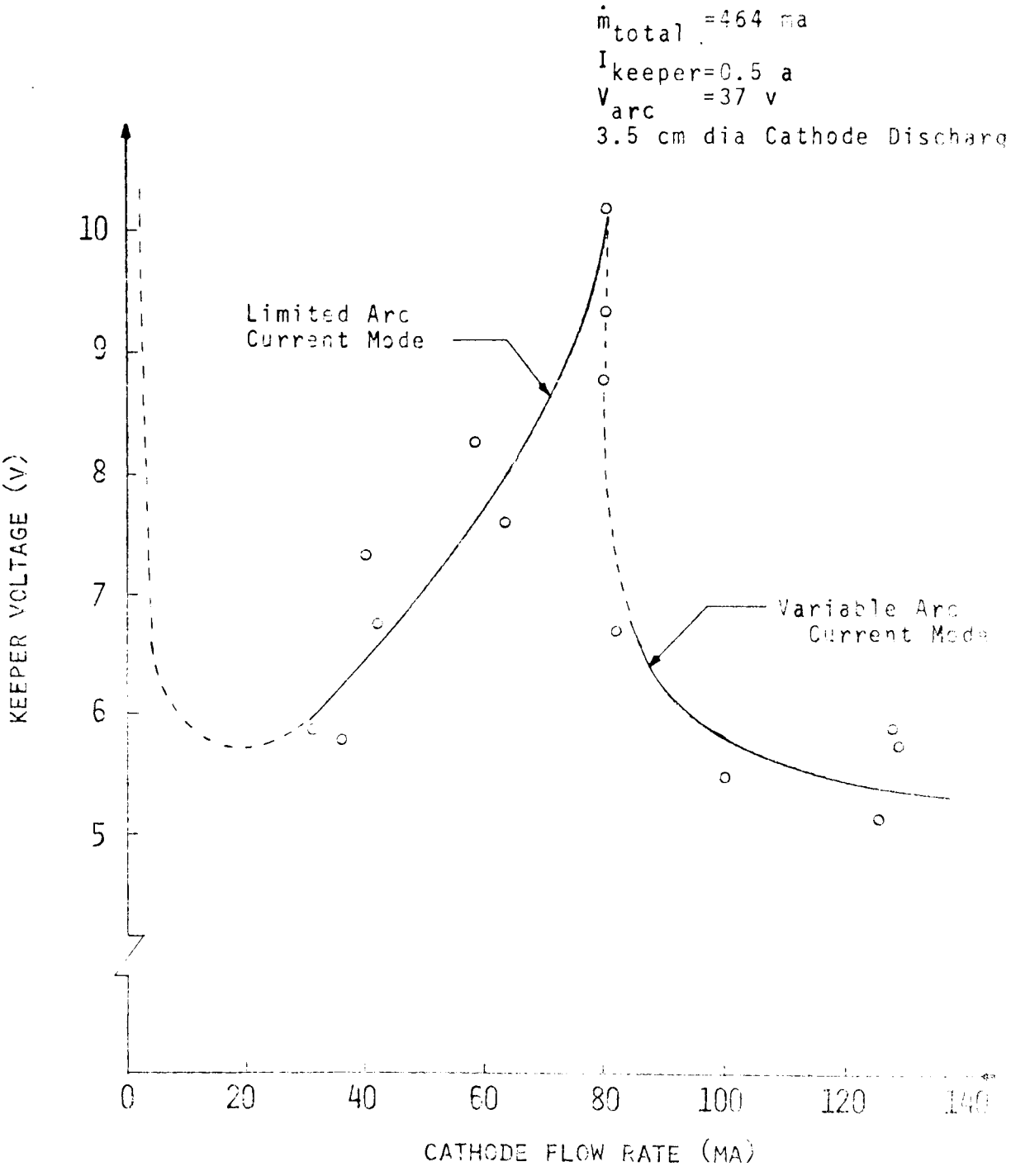

EFFECT OF CATHODE FLOW ON KEEPER VOLTAGE

FIGURE 29

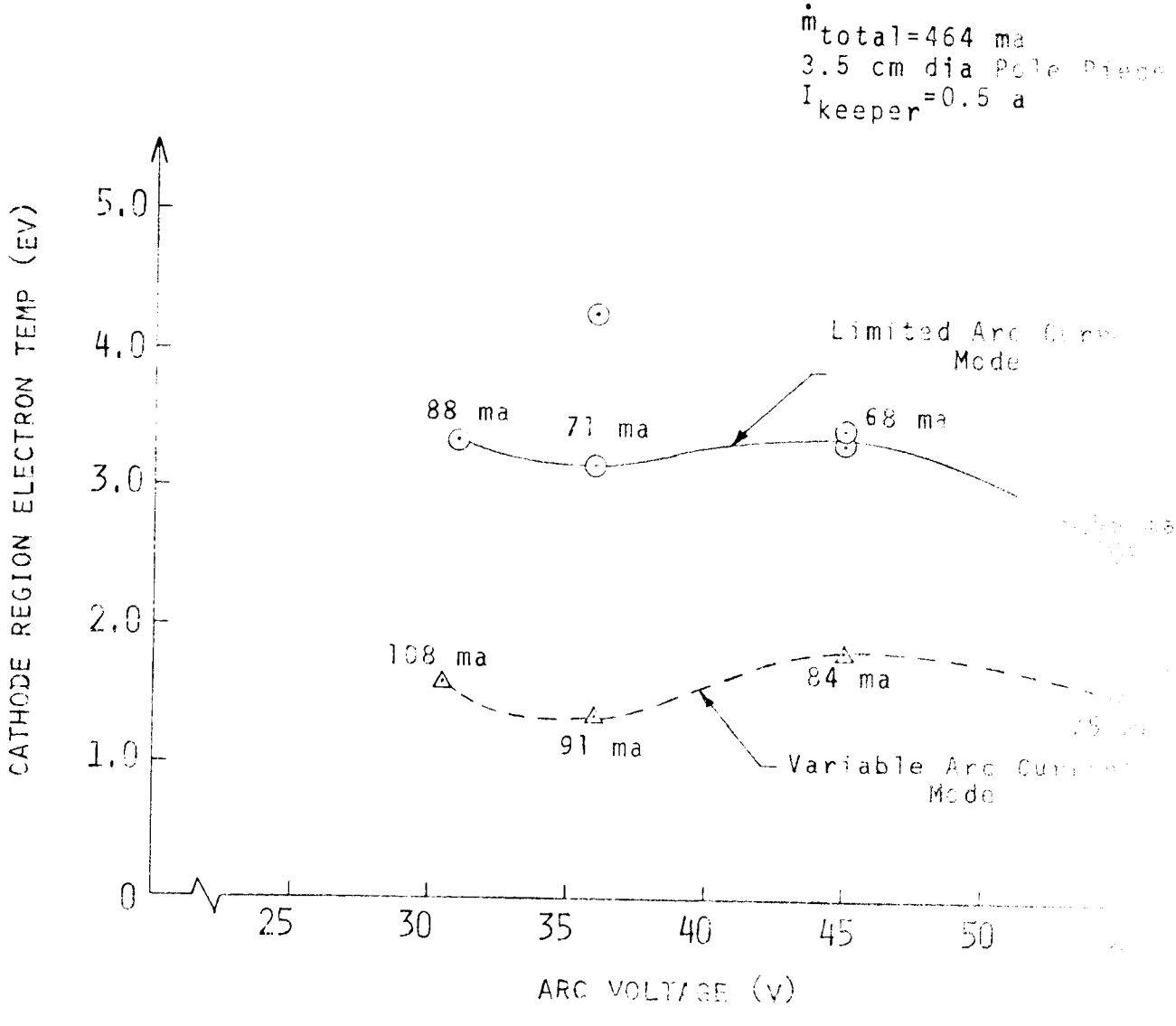

EFFECT OF MODE CHANGE ON
CATHODE REGION ELECTRON TEMPERATURE

FIGURE 31

arc voltage. Further, Figures 30 and 31 show electron density and temperature are generally higher for the limited arc current mode. If one assumes a plasma ion production cost of 70 ev/ion, these data can be used to calculate the cathode discharge region ion losses to the discharge confining walls (See Appendix C). The resultant data are presented as Figure 32, and they show cathode region ion losses are greater in the limited arc current mode.

The observed performance improvements in the limited arc current mode must be explained then in terms of the main discharge. Some insight into the mechanism by which improvements are realized can be gained by considering the following:

1. Kaufman's equation[12] for neutral density (n_o) in a thruster in terms of Maxwellian electron temperature (T_m), primary electron energy (ζ_p), the primary electron volume to surface area ratio (V_p/A_p), the ionization cross section (σ) and the ratio of primary to Maxwellian electron densities (n_p/n_m).

$$n_o = \frac{\sqrt{m_e/m_i}}{\sigma(V_p/A_p)} \sqrt{\frac{T_m}{\zeta_p}} \frac{(1 + n_p/n_m)^{3/2}}{(n_p/n_m)}$$

2. The primary electron energies for the two modes presented in Figure 33 as a function of arc voltage. These data show primary electrons have lower energies in the limited arc current mode at a given arc voltage.
3. Figure 13 which shows utilization is higher and hence neutral flow rate and neutral density are lower in the limited arc current mode at a given arc voltage.
4. The Maxwellian electron temperature (T_m) and ratio of primary to Maxwellian electron densities (n_p/n_m) for the main discharge presented in Figure 34; both are lower in the limited arc current mode.

If one assumes the plasma ion production cost is not changed by the

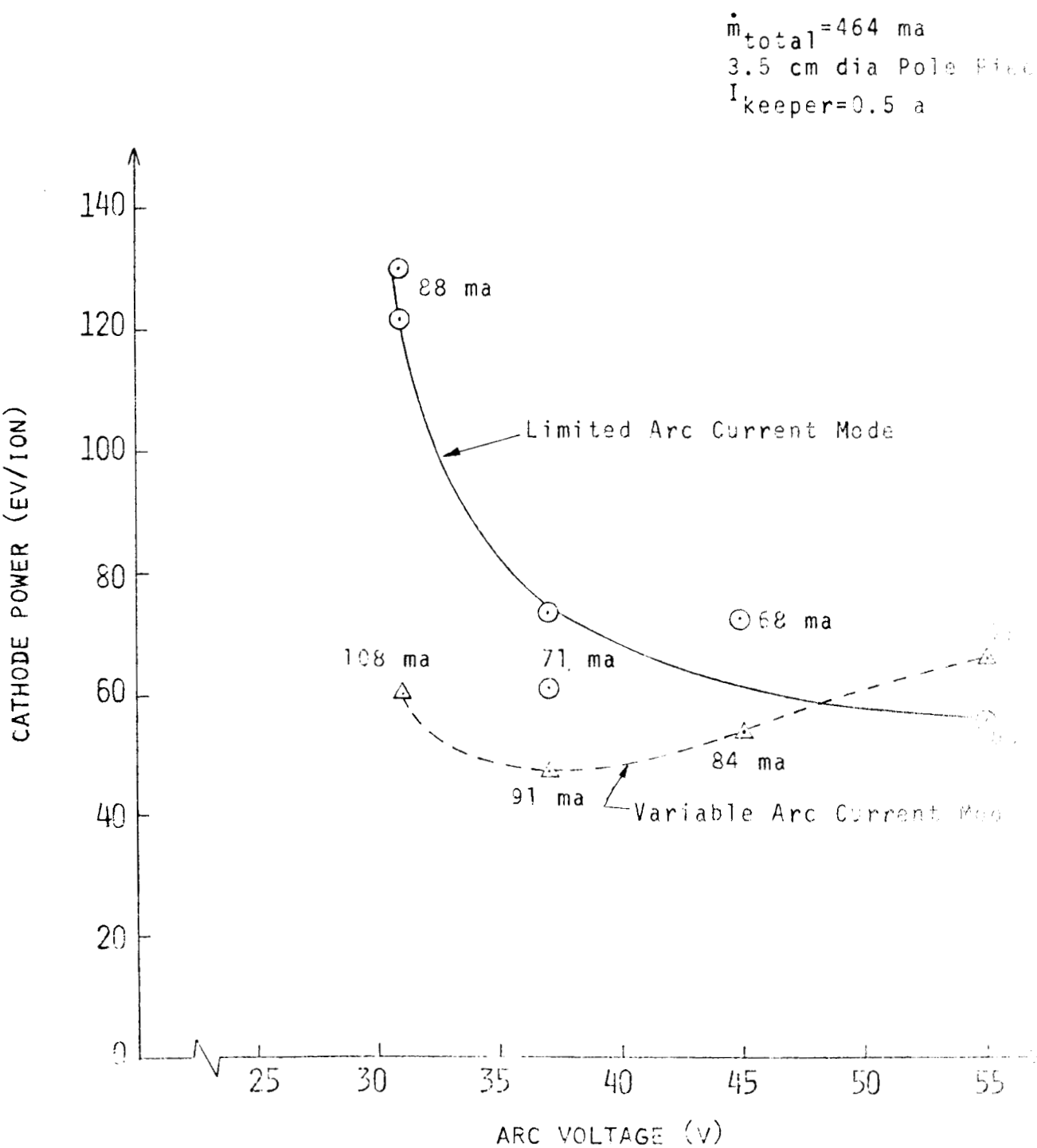

EFFECT OF MODE CHANGE ON
CATHODE POWER LOSSES

FIGURE 32

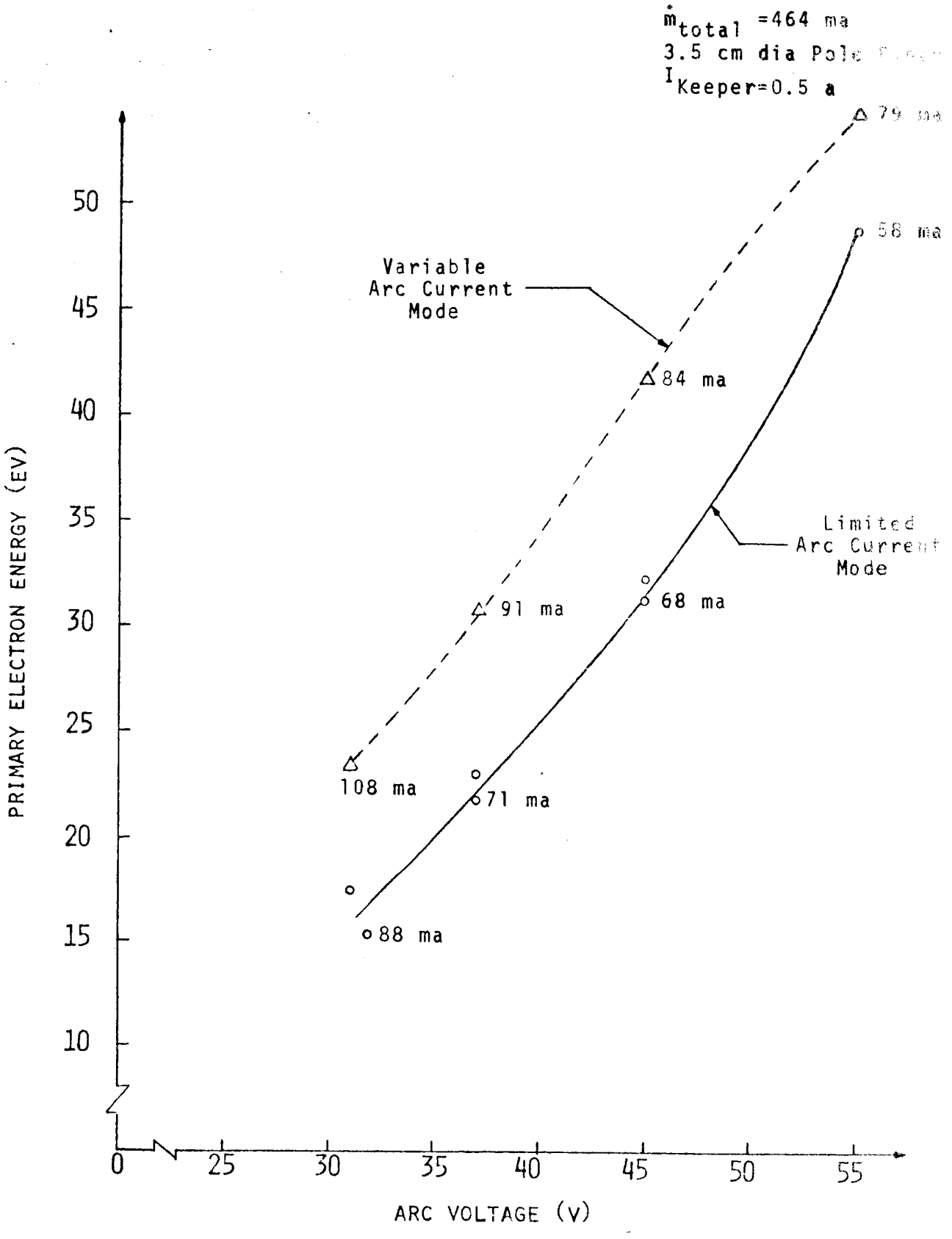

EFFECT OF MODE CHANGE ON PRIMARY ELECTRON ENERGY

FIGURE 33

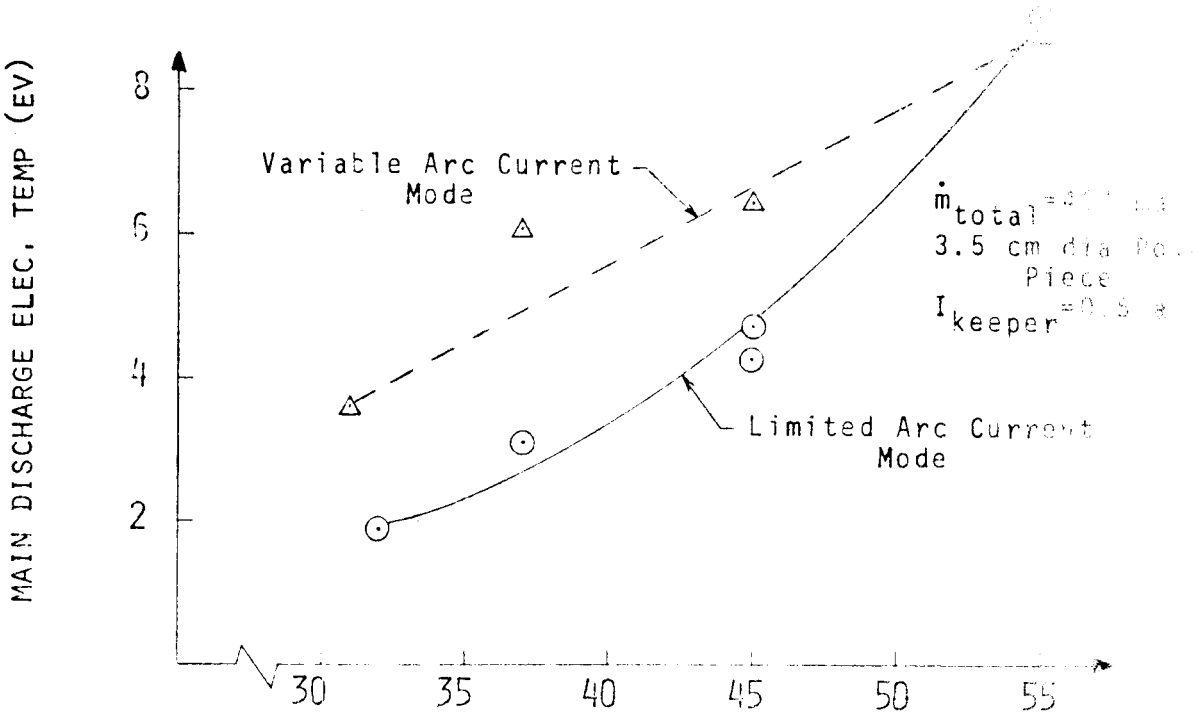

EFFECT OF MODE CHANGE ON MAIN REGION ELECTRON TEMPERATURE

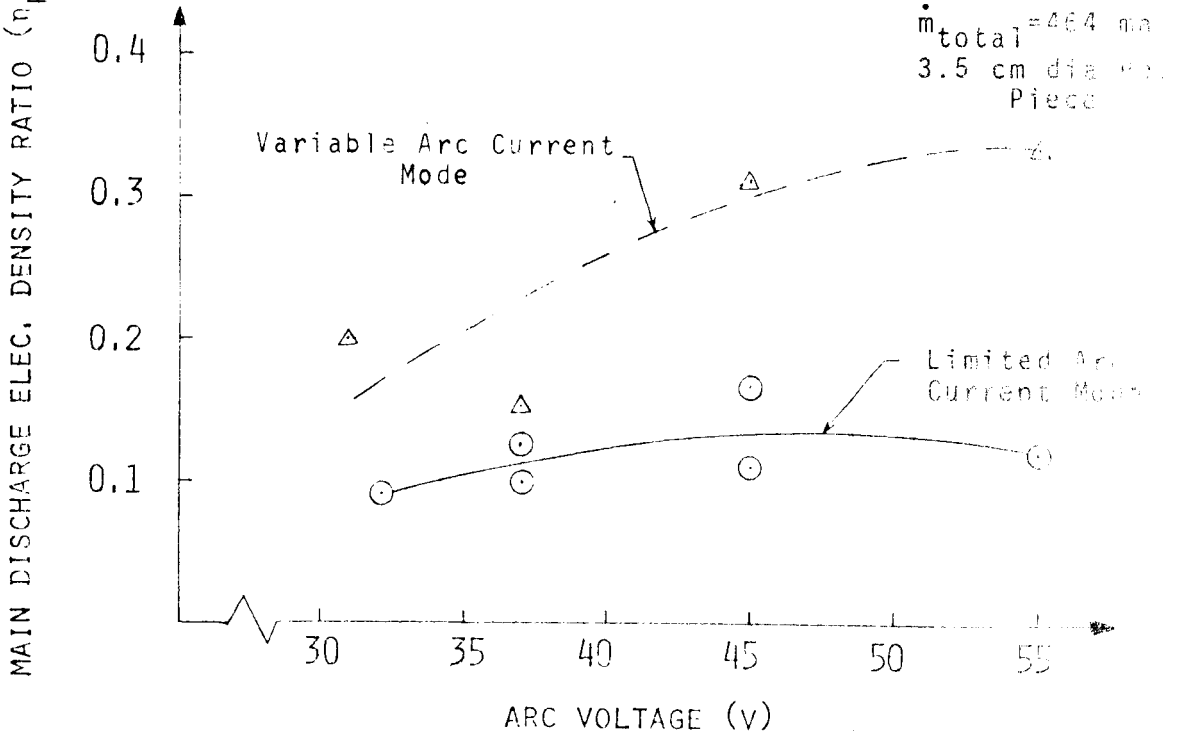

EFFECT OF MODE CHANGE ON MAIN REGION ELECTRON DENSITY RATIO

FIGURE 34

transition, collective consideration of these tendencies and their magnitude indicates the observed improvement in propellant utilization can only be explained by an increase in the primary electron region volume to surface area ratio occurring at the transition.

The primary electron energies presented in Figure 33 were obtained by taking the difference between the plasma potentials in the main and cathode discharge regions in the vicinity of the baffle aperture. It is of additional interest to note from this figure that primary electron energy is generally 5 to 15 ev below the applied arc voltage. This suggests a hollow cathode thruster should be operated at several volts higher arc voltage than was the oxide cathode thruster achieving similar performance.

HIGH VOLTAGE DISCHARGE STARTUP

The feasibility of striking an arc from a high voltage tickler electrode to the hollow cathode to heat the cathode and start the keeper discharge has been investigated. Figure 35 is a schematic of the system used in this study. Tests were conducted with a cathode-keeper-tickler assembly located within a simulated cathode pole piece, but with no additional thruster components. The test procedure involved charging the 14 μf, high voltage capacitor bank at from 500 to 1500 v, setting the keeper voltage in the range 150 to 200 v and then turning on the cathode vaporizer heater. The cathodes used in the study were a 3 mm dia. JPL cathode and later a SERT II cathode; both were supplied mercury vapor through a SERT II vaporizer.

Initial tests were unsuccessful because the high voltage discharge could not be established. In an attempt to increase the neutral mercury density in the cathode-keeper-tickler region the enclosed keeper configuration shown in Figure 36 was tried. This change made it possible to initiate the high voltage discharge. Oscillograph traces of the Rogowski coil (current) and high voltage probe outputs showed the capacitor network rang down in about four cycles (with a 40 μ sec. period). This caused a keeper discharge to be established, but it could be sustained for no more than about 20 milliseconds. It was decided that the keeper power supply was probably causing the discharge to terminate. Subsequent tests using battery power supplies and various values of capacitance (C in Figure 35) installed as near the cathode and keeper as possible resulted in no significant improvement in the duration of the keeper discharge. The resistance (R) shown in Figure 35 was adjusted over the range zero to 60 Ω to prevent the keeper-cathode discharge from drawing excessive current.

For the next series of tests the SERT II cathode was installed and the cathode heater was employed to assist in the initiation of the discharge, the enclosed keeper was removed and replaced by a tantalum wire loop keeper and the high voltage tickler was moved so it was on the cathode axis. With this arrangement the tickler could be moved axially

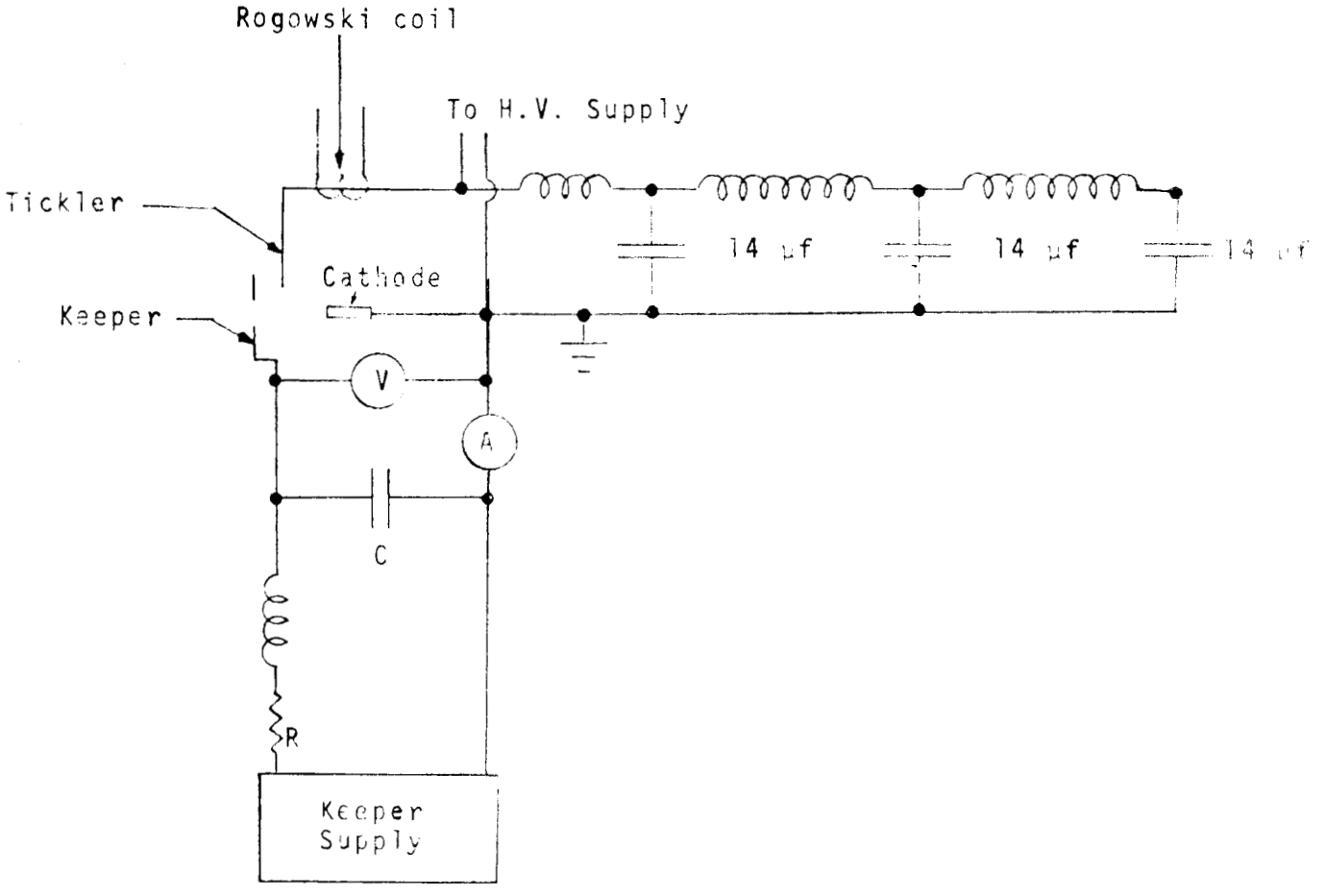

HIGH VOLTAGE STARTUP SCHEMATIC

FIGURE 2

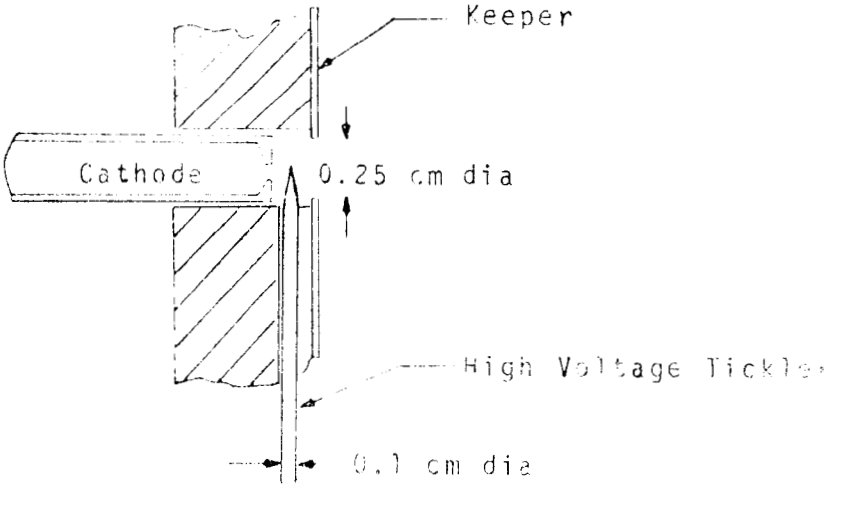

ENCLOSED KEEPER CONFIGURATION

FIGURE 3

to vary the cathode tickler distance in the manner suggested by Figure 37. The test procedure used was to set the keeper voltage at 150 v and establish a cathode flow rate corresponding to a 300°C vaporizer ($\dot{m}$ = 300 ma). The high voltage was next set at the desired level and the cathode heater current was raised in steps until the high voltage discharge occurred and keeper operation was established. Cathode tip temperatures were measured with an optical pyrometer at each step increase in cathode heater power so ignition could be correlated with this temperature. Cathode temperatures at startup determined by this means are considered accurate to within ±25°C.

Figure 38 shows the cathode temperature at which ignition occurred as a function of the voltage applied to the tickler. Two distinct sets of data present themselves; those designated by solid symbols were obtained immediately after barium carbonate had been applied to the front and interior of the cathode orifice plate; those designated by open symbols were obtained two days later after the cathode had been exposed to the atmosphere. The data suggest a slight decrease in the cathode temperature required to initiate the keeper discharge with tickler voltage, but more data are required to determine the extent of this decrease with any degree of confidence.

Data point A deserves special mention, because the high voltage tickler was charged to 1000 v when the keeper discharge started, but high voltage capacitors did not discharge in this case. The cathode-keeper-tickler assembly was observed during the tests and the startup always involved a glow discharge which persisted for of the order of a few minutes before the high voltage discharge occurred and keeper arc was established. The nature of the glow discharge was influenced by the voltage applied to the tickler. When the tickler was at a high positive potential, the glow between the cathode and tickler was a rather intense narrow column which passed through the center of the keeper. As the tickler potential was reduced the diameter of the glow column increased and its intensity decreased. A few tests conducted with the tickler negative relative to the cathode showed a diffuse glow discharge which exhibited a conical region void of visible emission in

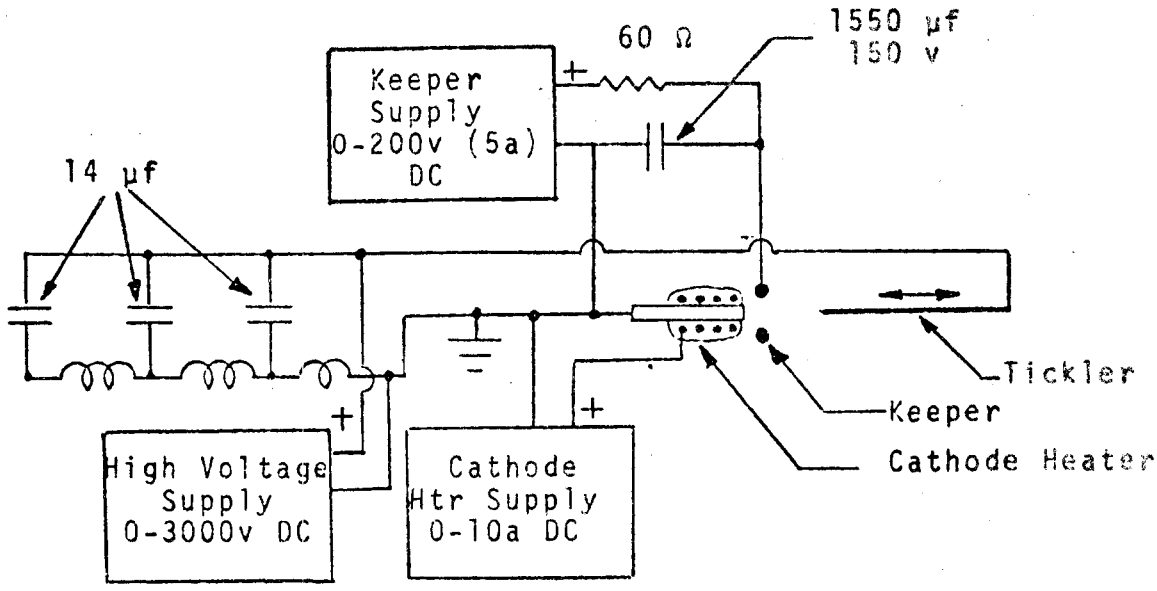

H.V. START TEST SCHEMATIC

FIGURE 37

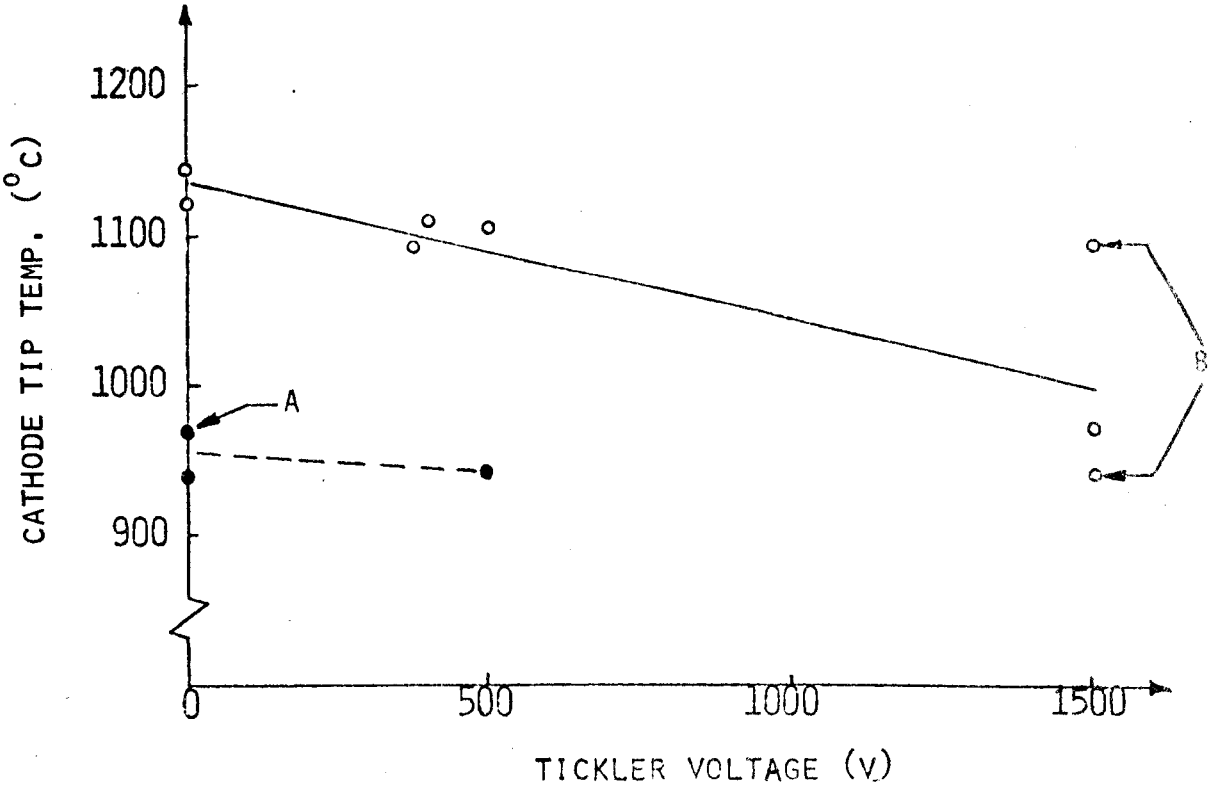

EFFECT OF TICKLER VOLTAGE ON CATHODE TEMP. AT H.V. DISCHARGE

FIGURE 38

the region around the tickler. During tests conducted with the tickler charged to a high positive voltage (1500 v-designated as points B on Figure 38) and at a position less than 1 mm from the cathode tip (plane of keeper about 1 mm away from cathode tip). The high voltage discharge was observed to occur without initiating the keeper arc discharge.

Based on these tests it has been concluded that a high voltage tickler discharge which doesn't pull the electron current across the keeper is ineffective in establishing a steady keeper discharge. Additional tests in which 1) the high voltage is applied between the keeper and the cathode and 2) the tickler is located on a line between the cathode and a part of the keeper are planned to confirm this conclusion.

THERMAL FLOW METER*

In the course of conducting experimental studies of mercury bombardment thrusters, considerable time is consumed in waiting to obtain accurate mercury flow rate information. This problem could be alleviated if a continuously indicating accurate flowmeter were available. The thermal flowmeter measuring liquid flow rate has been proposed as a possible solution. The basic concept involves the addition of heat at a rate $\dot{q}$ into a tube carrying the flowing liquid mercury. If one measures the temperature of the fluid at two locations: 1) downstream of the point of heat addition (T_{meas}), and 2) sufficiently far upstream of this point so the ambient fluid temperature (T_{ref}) is sensed, the mass flow rate ($\dot{m}$) is given by

$$\dot{m} = \frac{\dot{q}}{C(T_{meas} - T_{ref})}$$

where C is the specific heat of the flowing fluid. The device being used presently requires heat input at a fixed rate and the output of the instrument is the temperature difference ($T_{meas} - T_{ref}$) which is inversely

*Work performed by Richard Vahrenkamp, Graduate Student.

proportional to mass flow rate*.

The device designed for this particular application is shown schematically in Figure 39. The temperatures are sensed by two 1 mm dia. glass bead thermistors connected into the wheatstone bridge circuit as shown. Both thermistors are mounted so they are in contact with the mercury flowing within the 0.33 mm I.D. stainless steel flow tube. The thermistors have a resistance of about 10 kΩ at 25 ^{o}C, a time constant of about 2 seconds, and a dissipation constant of 0.7 milliwatts/^{o}C. The current through the 1Ω heater yields an input power of about 100 milliwatts. The entire flow tube-sensor assembly is enclosed in plexiglas to eliminate spurious convective heat losses.

The temperature profile between the heater and R_{ref}, neglecting heat transfer through and along the stainless steel flow tube, is given by:

$$T - T_{ref} = (T_{meas} - T_{ref}) \exp \left[- \frac{4\dot{m}xC}{k\pi d^2} \right]$$

where C and k are the specific heat and conductivity of the liquid mercury flowing at a rate $\dot{m}$. In order to assure $(T - T_{ref}) \rightarrow 0$, it was desirable to have an exponent near minus five which corresponds to an R_{ref}-heater separation distance x = 11 cm at a mercury flow rate $\dot{m}$ = 100 ma.

A tracing of a typical voltage output vs. time trace is shown as Figure 40. The currents indicated are vaporizer heater currents supplied to a SERT II vaporizer which was used to produce the desired flow rates. The initial current (1.3 amps) supplied to the vaporizer is seen to produce a negative flow rate as the mercury being heated at the vaporizer expands. When the vaporizer temperature reached 300^{o}C it was necessary to reduce the heater current to maintain this temperature and to achieve a constant flow rate corresponding to the 300^{o}C flow rate. One can see it took about an hour to achieve the steady flow condition.

Figure 41 presents preliminary attempts at the establishment of a calibration curve. Actual flow rates were measured by timing the drop

---

*This type of device can also operate so the temperature difference is held constant by adjustment of the heat flux through a feedback network. In such an instrument the power to the heater is directly proportional to the mass flow rate, and it represents the output signal.

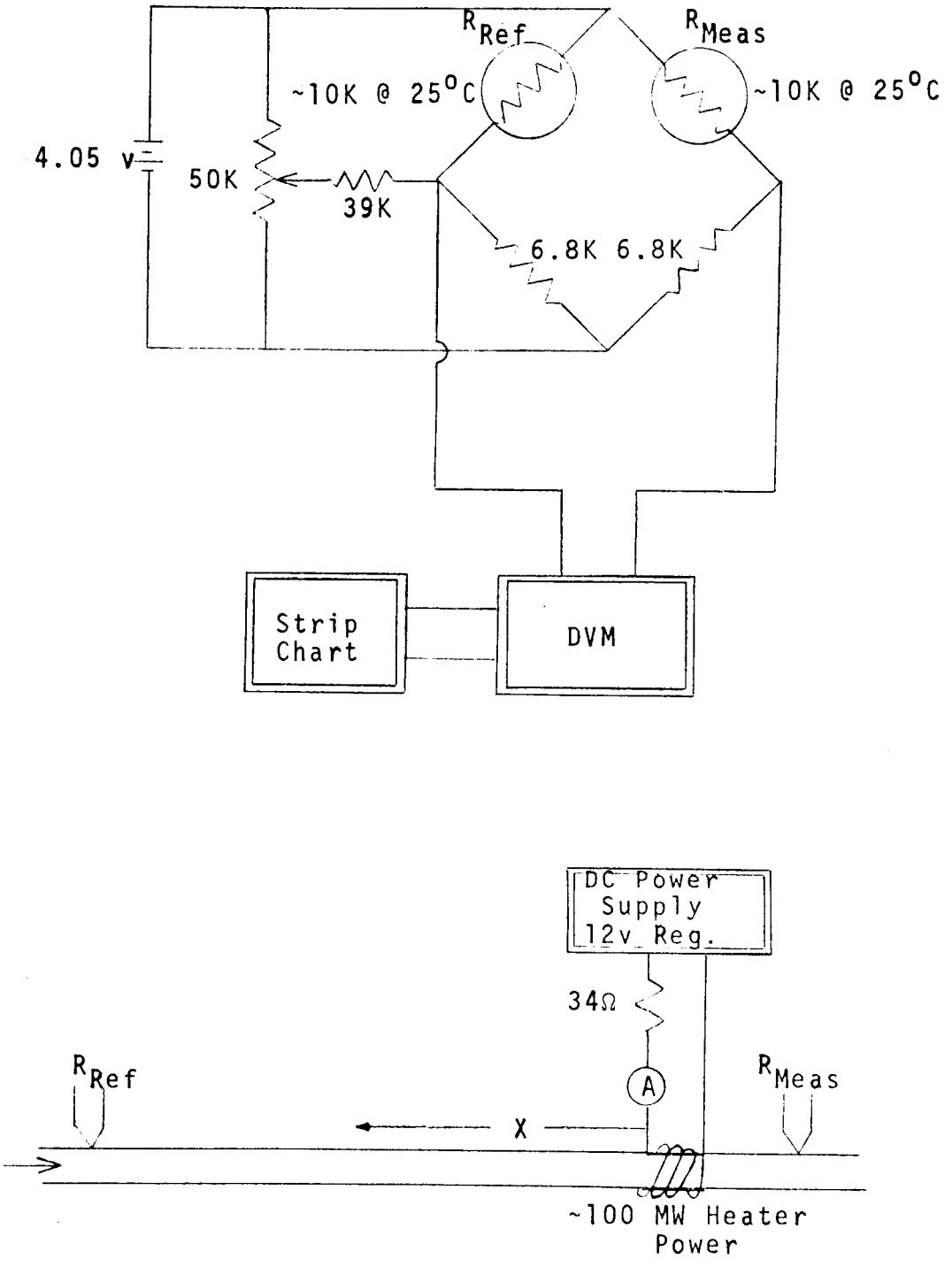

THERMAL FLOWMETER

FIGURE 39

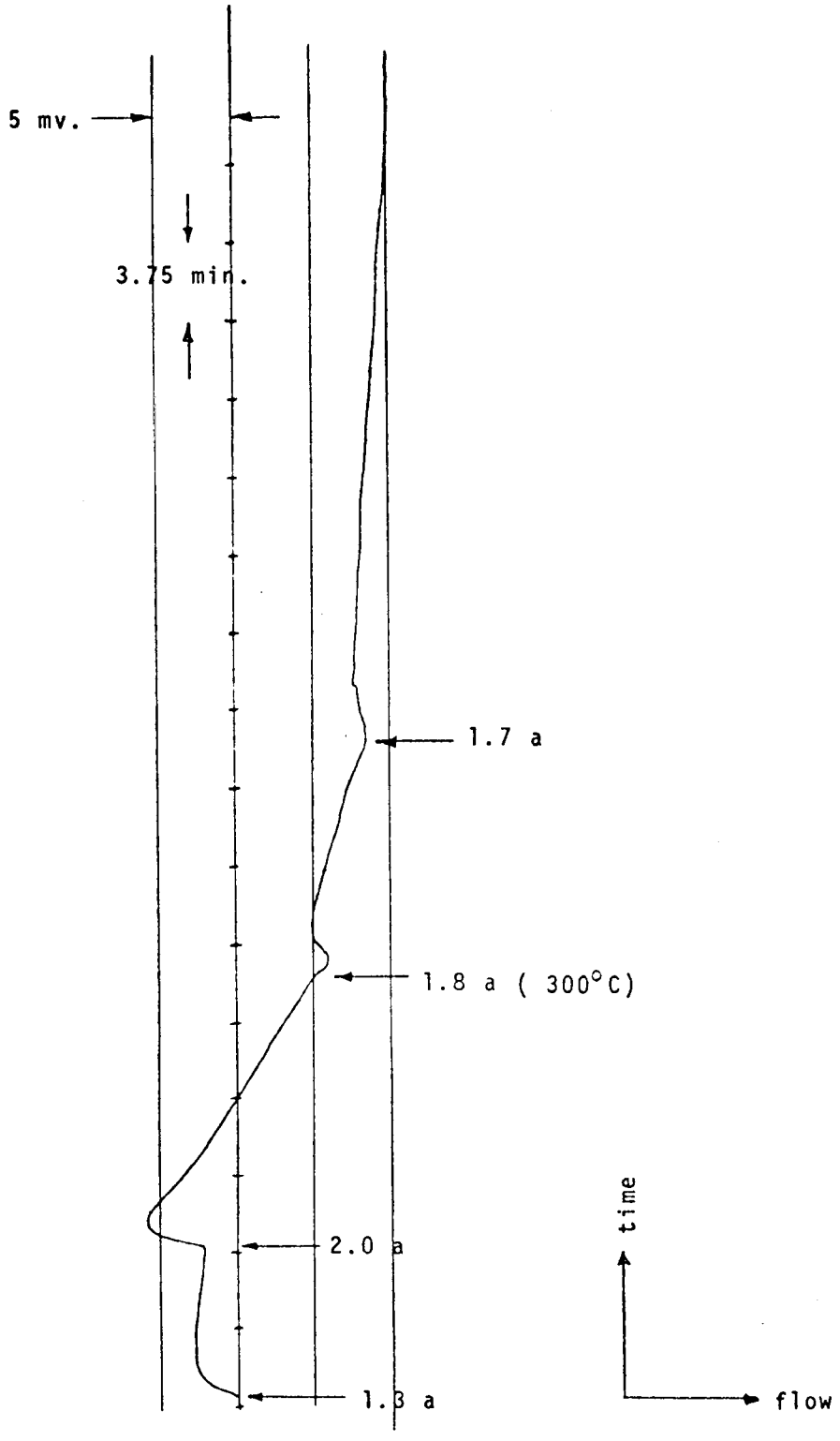

THERMAL FLOWMETER OUTPUT

FIG 40

THERMAL FLOWMETER CALIBRATION CURVES

FIGURE 41

of the mercury meniscus in a calibrated glass tube. Additional testing is required to obtain data at low flow rates, to determine reproducibility and sensitivity to ambient conditions and flow tube heater current, and to assure reliable operation on an operating thruster.

References

1) Nakaniski, S., et al., "Status of a Five-Centimeter-Diameter Ion Thruster Technology Program: AIAA Paper No. 71-690, June 1971.

2) Masek, T. D. and E. V. Pawlik, "Thrust System Technology for Solar Electric Propulsion," AIAA Paper 68-541, AIAA 6th Electric Propulsion Conference, Cleveland, Ohio.

3) Pawlik, E. V., "Performance of a 20-cm Diameter Electron Bombardment Hollow-Cathode Ion Thruster," NASA Technical Memorandum 33-468, February 15, 1971.

4) Strickfaden, W. B. and K. L. Geiler, "Probe Measurements of the Discharge in an Operating Electron Bombardment Engine," AIAA Journal, Vol. 1, No. 8, pp. 1815-1822, August 1963.

5) Palumbo, G., et al., "Effect of Geometry and Field inside the Pole Piece in an Electron Bombardment Thruster," AIAA Paper No. 70-1088, September 1970.

6) Pawlik, E. V. and D. J. Fitzgerald, "Cathode and Ion Chamber Investigations on a 20-cm Diameter Hollow Cathode Ion Thruster," AIAA Paper No. 71-158, January 25-27, 1971.

7) Pawlik, E. V., et al., "Operation of a Lightweight Power Conditioner with a Hollow-Cathode Ion Thruster," J. Spacecraft & Rockets, Vol. 8, No. 3, pp. 245-250, March 1971.

8) Granowski, W. L.,"Electric Currents in Gases," Vol. 1, pp. 443-444, Akademie-Verlag, Berlin, 1955.

9) Byers, D. C. and Aaron Snyder, "Parametric Investigation of Mercury Hollow Cathode Neutralizers," AIAA Paper No. 70-1090, Sept. 1970.

10) Rawlin, V. K. and W. R. Kerslake, "Durability of the SERT II Hollow Cathode and Future Applications of Hollow Cathodes," AIAA Paper No. 69-304, March 1969.

11) Fearn, D. G., C. M. Phillip and J. W. Pye, "The Development of Hollow Cathodes, Vaporizers and Isolators for Use in Mercury Ion Thrusters," Paper-DGLR Symposium, 22/23 June 1971, Braunschweig, W. Germany.

12) Kaufman, H. R., "Ion Thruster Propellant Utilization," Ph.D. Thesis, Colorado State University, June 1971.

13) Masek, T. D., "Plasma Properties and Performance of Mercury Ion Thrusters," AIAA Paper 69-256, March 1969.

APPENDIX A

INTERPRETATION OF LANGMUIR PROBE DATA

The Langmuir probe traces shown in Figure A-1 are typical of those obtained during this test sequence. The outputs of the probes, which sense main and cathode discharge plasma properties in the vicinity of the baffle aperture, were generally recorded within one minute of each other on the same sheet of paper as shown.

The cathode probe trace is analyzed first by plotting probe current vs. probe voltage on semi-log paper in the manner shown in Figure A-2 and interpreting the data in the usual way[4]. The plasma potential, ϕ_{cath}, is determined by the break in the curve. The electron temperature, T_e, is given in electron volts by the equation:

$$T_e = \frac{V(10I) - V(I)}{2.3}$$

where the numerator represents the voltage change over a decade change in probe current. For the Langmuir probe surface area of $3.37 \times 10^{-6} m^2$ used in these tests the electron density, n_e, (cm^{-3}) is given by:

$$n_e = 1.11 \times 10^{10} \frac{i_{sat}}{\sqrt{T_e}}$$

where i_{sat} is the saturation current (ma) identified in Figure A-2.

In order to evaluate the main discharge probe trace it is necessary to subtract of the primary electron contribution to the current[4]. Previous workers seem to have accomplished this largely by guess, but the availability of a cathode probe trace makes it possible to determine the primary electron current more accurately using the following technique.

The cathode region plasma potential is plotted on the page containing traces as a vertical dotted line in the manner shown on Figure A-3. The energy of the primary electrons should be about equal to the difference between the main and cathode discharge plasma potentials. This means the primary electron current should begin to appear on the main discharge trace at a voltage equal to ϕ_{cath}, i.e. at point A in Figure A-3 (intersection of ϕ_{cath} and the horizontal extension of the ion current

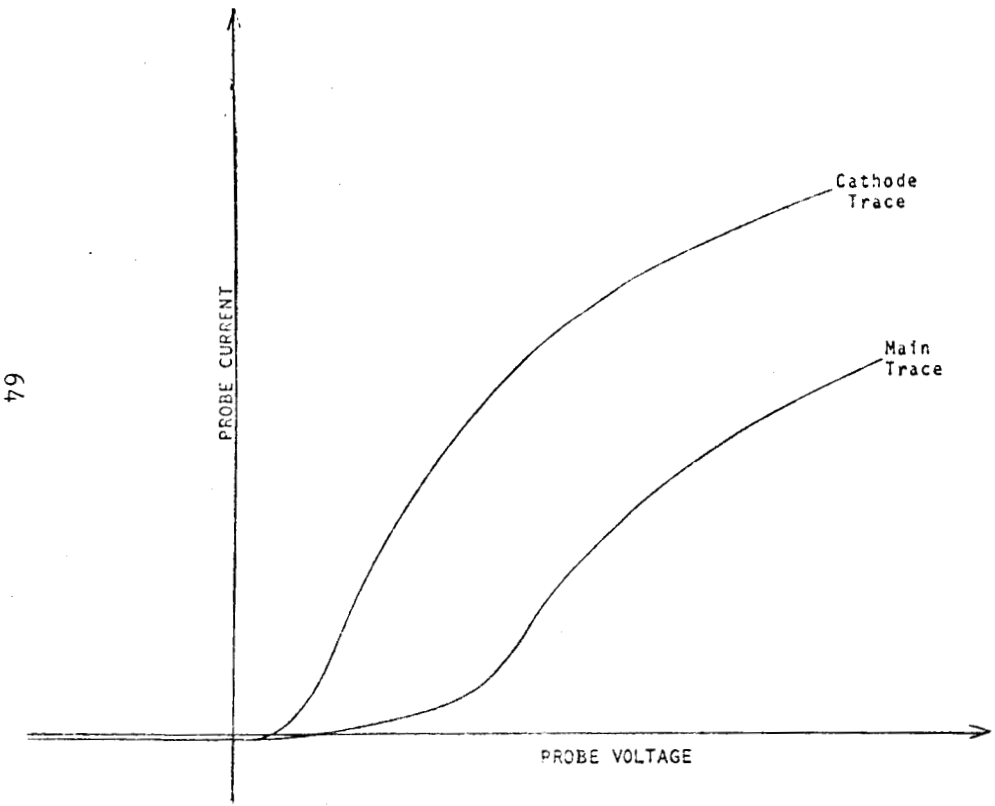

TYPICAL LANGMUIR PROBE DATA

FIGURE A-1

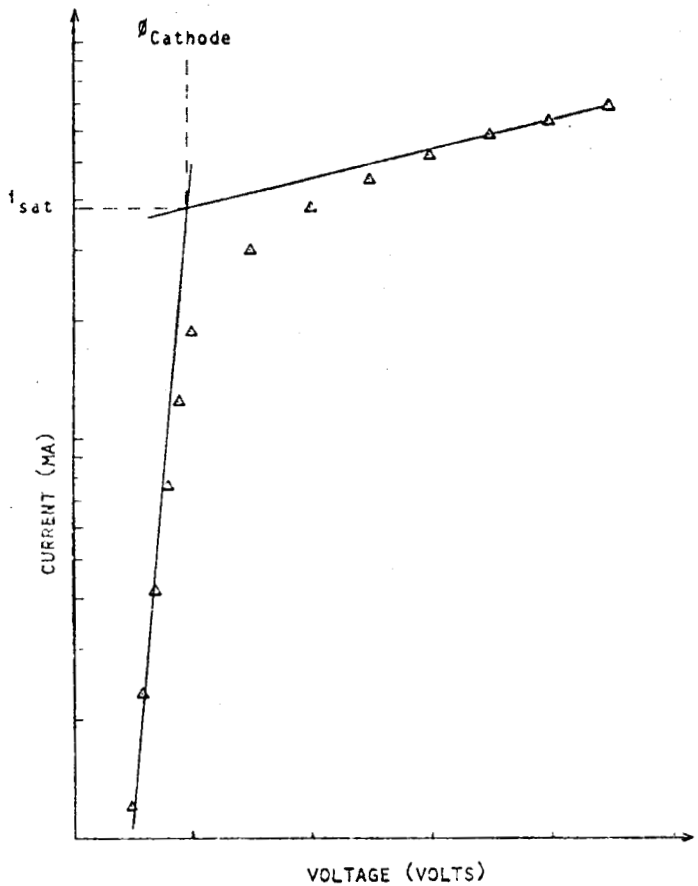

TYPICAL SEMI-LOG PLOT OF CATHODE DATA

FIGURE A-2

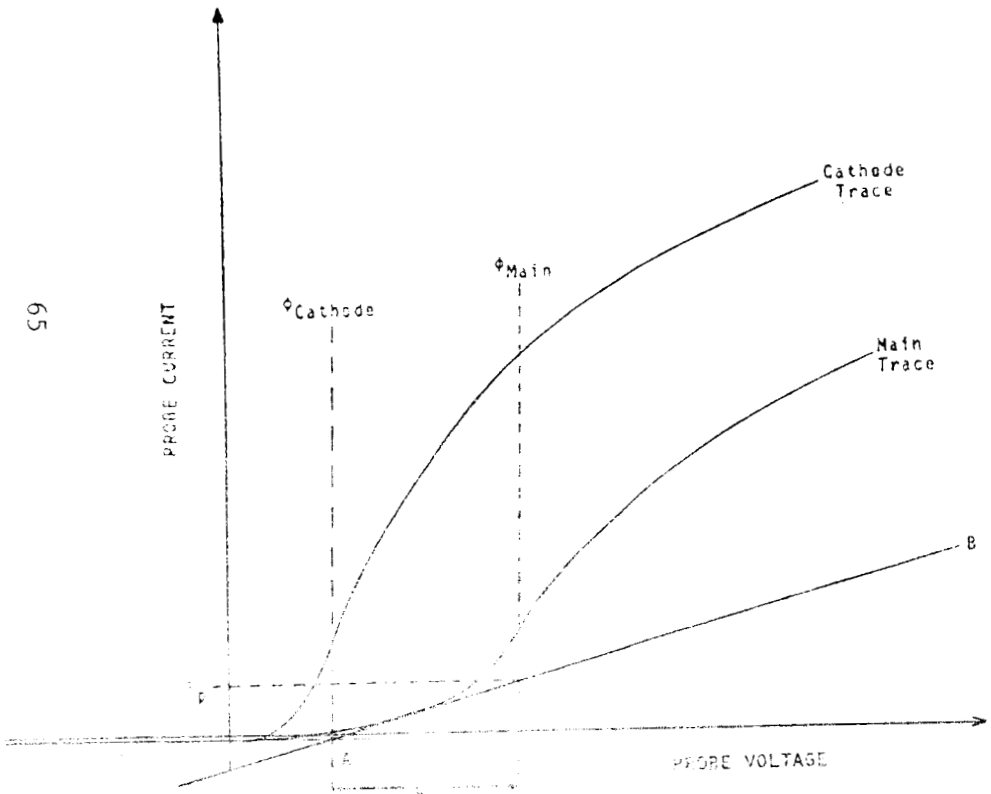

LANGMUIR PROBE TRACE IN ELECTRON

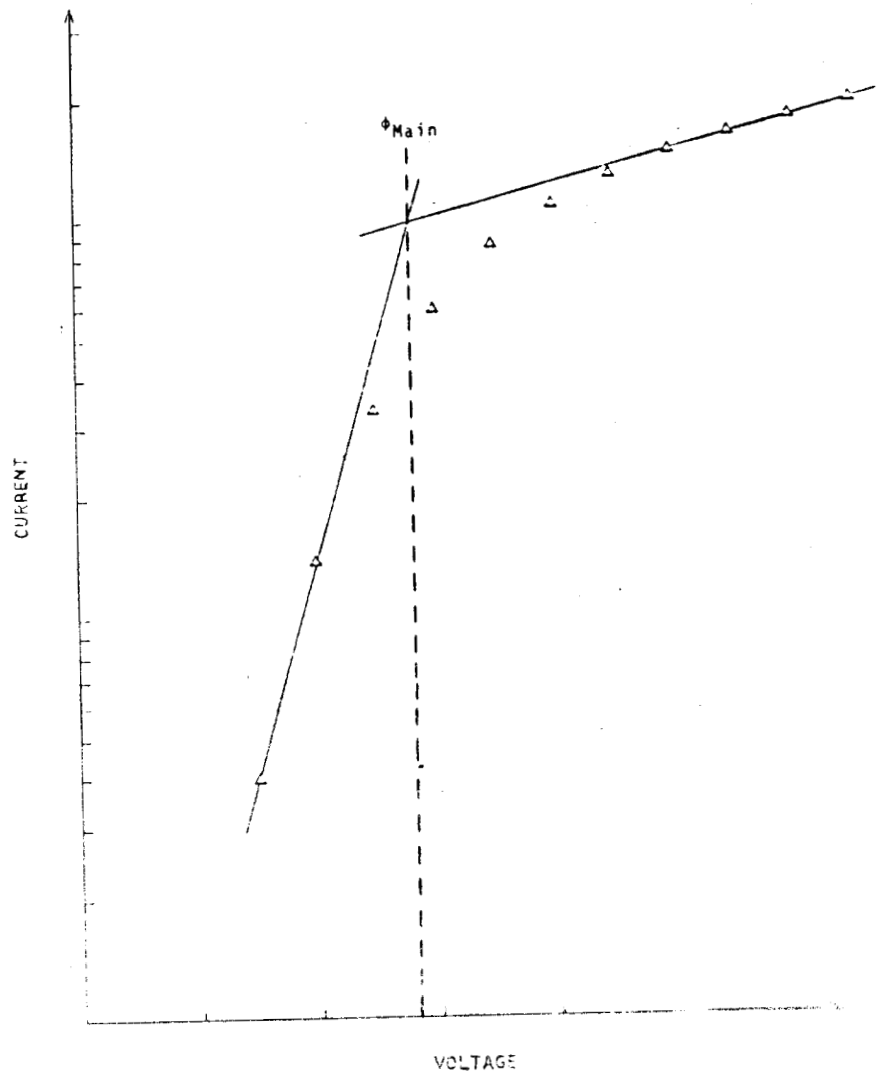

MAIN DISCHARGE MAXWELLIAN ELECTRON PLO

portion of the main trace). A line from A, tangent to the main trace would therefore be the best representation of the primary electron contribution, and the difference between A-B and the main trace is plotted as shown in Figure A-4 and analyzed in the same way as the cathode discharge to obtain the Maxwellian properties of the main discharge plasma. The primary electron energy (ζ_p in ev) is then given by the difference between the two plasma potentials and the primary electron density (n_p in cm^{-3}) is given by:

$$n_p = 1.25 \times 10^{10} \frac{i_p}{\sqrt{\zeta_p}}$$

where i_p is the primary electron current (in ma) at the main discharge plasma potential (ϕ_{main}) from the original probe trace (Figure A-3).

APPENDIX B

ION BEAM FLATNESS PARAMETER

In order to facilitate the comparison of several ion beam profiles particularly if they were obtained at different total beam currents, an ion beam flatness parameter ($\mathbb{F}$) has been devised. It is defined as the ratio of the average current density (j_{ave}) over the maximum current density in the beam (j_{max}).

$$\mathbb{F} = \frac{j_{ave}}{j_{max}}$$

For a cylindrical beam this becomes

$$\mathbb{F} = \int_{o}^{r_o} \frac{2\pi r\, j(r)\, dr}{\pi r_o^2\, j_{max}}$$

where r_o is the outer radius of the beam. This radius may exceed the radius of the beam at the accel grid because of beam spreading at the sensing location. This parameter takes on the value zero for a delta function profile and the value unity for a uniform profile.

The integration implied in the preceding expression is accomplished numerically by summing the current densities (j_i) at two diametrically opposed locations on the area centroid circles in each of a specified number (n) of equal area rings of the beam.

$$\mathbb{F} = \frac{\frac{1}{2n} \sum_{i=-n}^{n} j_i}{j_{max}}$$

where j_i's are the current densities at radii given by $r_i = \pm\sqrt{\frac{(2i-1)}{2n}}\, r_o$.

For ten equal area segments this becomes:

$$\mathbb{F} = \frac{\sum_{i=-10}^{10} j_i}{20 j_{max}}$$

and the j_i's are measured at or interpolated to the following radii:

$$r_1 = \pm 0.224\ r_o$$

$$r_2 = \pm 0.388\ r_o$$

$$r_3 = \pm 0.501\ r_o$$

$$r_4 = \pm 0.503\ r_o$$

$$r_5 = \pm 0.672\ r_o$$

$$r_6 = \pm 0.743\ r_o$$

$$r_7 = \pm 0.808\ r_o$$

$$r_8 = \pm 0.868\ r_o$$

$$r_9 = \pm 0.924\ r_o$$

$$r_{10} = \pm 0.975\ r_o$$

APPENDIX C

EFFECT OF CATHODE DISCHARGE SIZE ON ION LOSSES TO CATHODE REGION WALLS

Beam ion production costs are determined by the losses associated with both the main and cathode discharges. Masek[13] has suggested a method for determining these costs by calculating the ion currents to the walls confining each of the associated discharges. He further suggests that a reduction in the dimensions of the cathode discharge should reduce the beam ion production costs. Although a complete Langmuir probe survey has not been obtained in the cathode discharge region, data from the single probe used provides the information necessary to estimate the losses in this region.

Figure C-1 shows the variation of cathode region electron (and ion) density with cathode region dimensional changes for a fixed distribution of cathode and main flows obtained from the cathode Langmuir probe output. Figures 19 and 20 show similar data for variable cathode flow conditions. Unfortunately the data of Figure C-1 were obtained at variable propellant utilizations (values indicated on each curve). The data of both sets of figures show about the same magnitudes and a universal tendency for the cathode region electron density to drop off for short cathode region lengths. Calculation of the discharge power losses due to ion current to the cathode pole piece and baffle walls from the cathode discharge region has been accomplished using these data and the Bohm criterion to determine ion velocity in the manner suggested by Masek[13]. The ion current to confining walls J_i (amps) is given by:

$$J_i = 1.11 \times 10^{-14} \, A \, n_e \sqrt{T_e}$$

where A is the cathode discharge region interior area (cm^2), n_e is the electron density (cm^{-3}) and T_e is the electron temperature (ev). If one assigns an approximate ion production cost of 70 ev/plasma-ion based on Masek's results, the power loss due to ion wall currents to the interior of the cathode discharge region, P_c (ev/beam-ion) can be estimated:

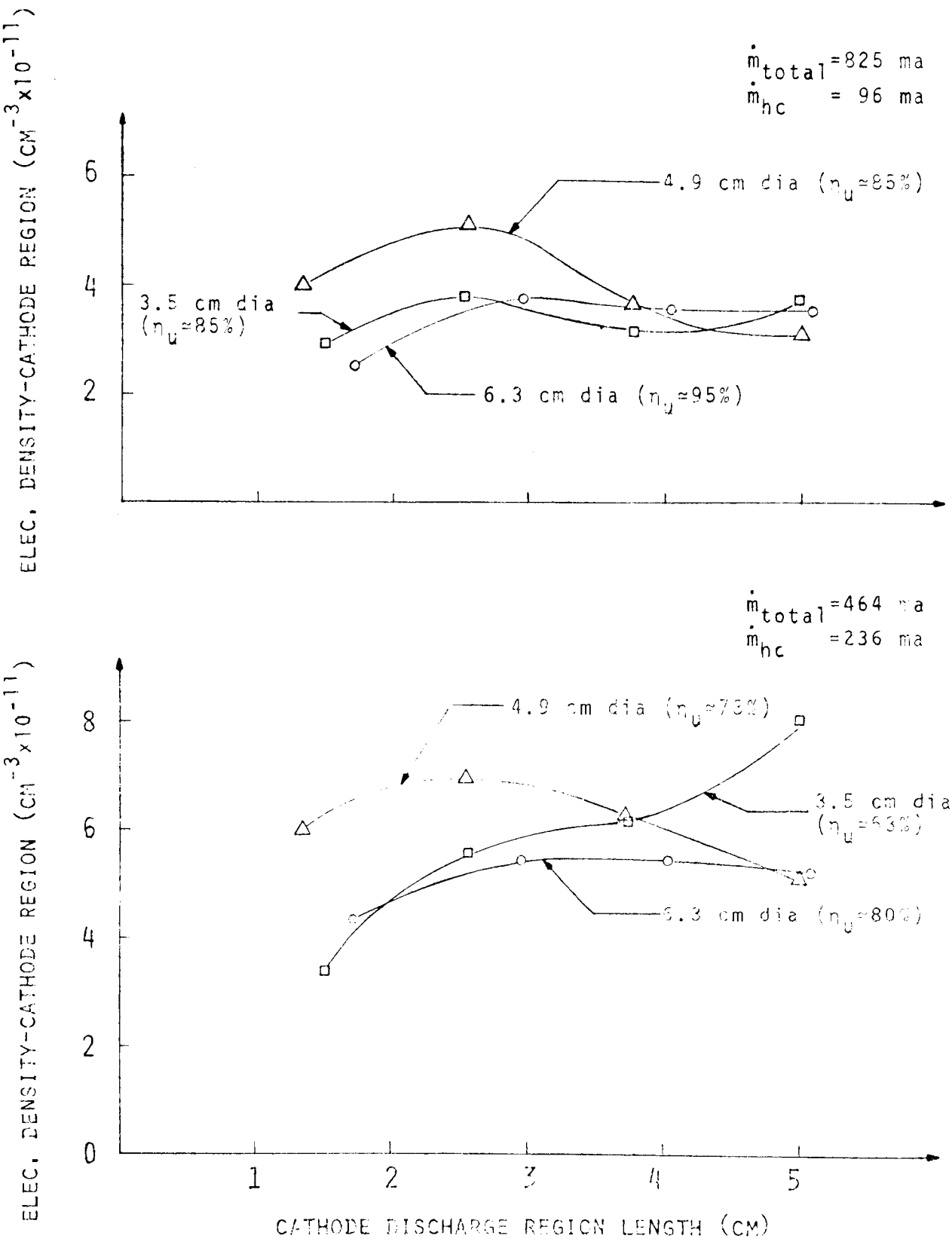

EFFECT OF CATHODE REGION DIMENSIONS ON ELECTRON DENSITY

FIGURE C-1

$$P_c = \frac{(70)\ J_i}{I_B}$$

I_B used in this equation is the beam current expressed in amperes.

The results of the above analysis are presented in Figures C-2 and C-3 where the power losses due to the ion current to the confining walls of the cathode discharge are presented as a function of the dimensions of the discharge. The two figures show data obtained for the fixed cathode flow (Figure C-2) and variable cathode flow (Figure C-3) cases which were discussed in the body of the report. These figures show a consistent tendency for reductions in cathode discharge length or diameter to reduce ion losses in the cathode discharge region. The fact that throttled flow cathode discharge losses are greater than those observed at the high flow rate and that dimensional changes have the greatest influence on these losses for throttled flow is of interest. This occurs primarily because cathode region ion losses are almost fixed and their effect on the beam ion cost is most significant at lower beam current conditions. The losses indicated for the low flow rate condition are considered somewhat high, probably because of the assumed plasma ion production cost, which will vary with cathode region ion and neutral density conditions. Ion wall losses in the cathode region show a universal tendency for reductions in cathode dimensions to reduce beam ion production costs. The fact that the performance data presented in Figures 10, 17, and 18 show both reductions and increases in discharge power with reductions in cathode dimensions means variations in losses in the main discharge mitigate against performance improvements achieved through reduction in ion wall losses in the cathode discharge region.

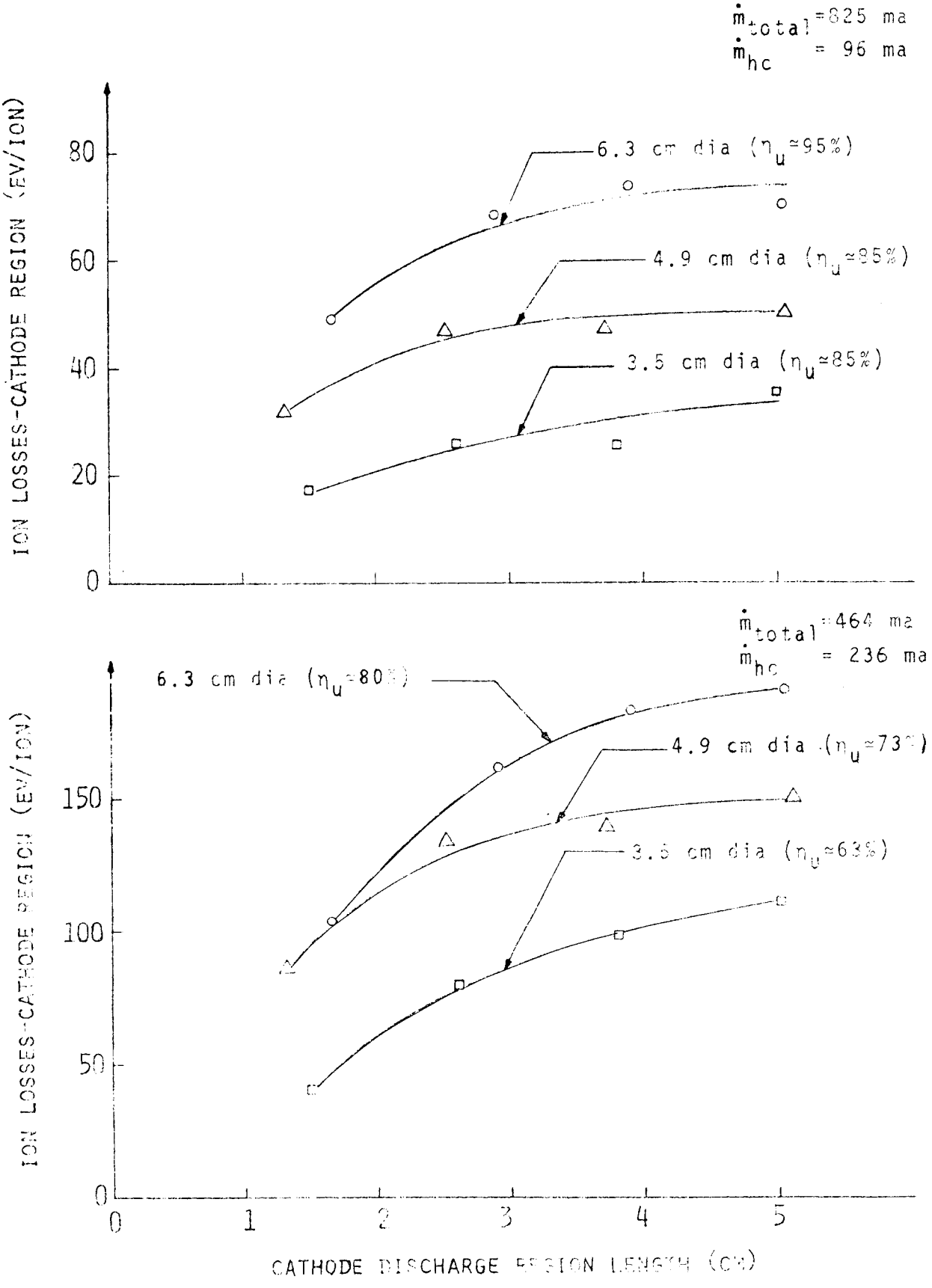

EFFECT OF CATHODE DISCHARGE SIZE ON DISCHARGE LOSSES DUE TO ION FLUX TO CONFINING WALLS
(FIXED CATHODE FLOW)

FIGURE C-2

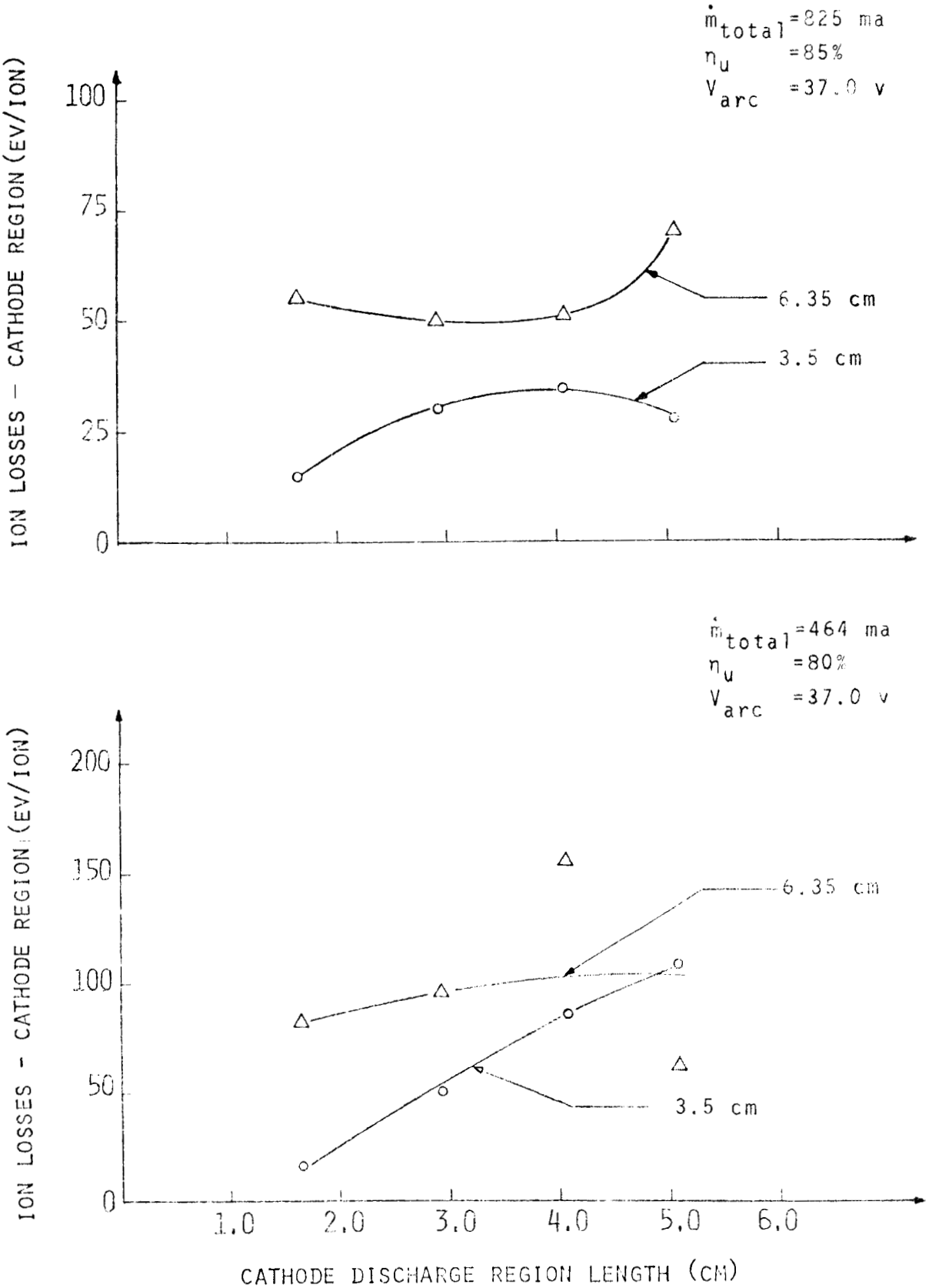

EFFECT OF CATHODE DISCHARGE SIZE ON DISCHARGE LOSSES DUE TO ION FLUX TO CONFINING WALLS (VARIABLE CATHODE FLOW)

FIGURE C-3

Distribution List

	Number of Copies
National Aeronautics and Space Administration Washington, D.C. 20546	
Attn: RPE/James Lazar	1
Jerome Mullin	1
National Aeronautics and Space Administration Lewis Research Center 21000 Brookpark Road Cleveland, Ohio 44135	
Attn: Research Support Procurement Section	
W.E. Park, MS 500-312	1
Technology Utilization Office, MS 3-19	1
Management Services Division, MS 5-5	1
Library, MS 60-3	2
Electromagnetic Propulsion Division, MS 301-1	
W. E. Moeckel	1
H. Kaufman	1
R. Finke	1
P. Reader	1
W. Kerslake	10
Spacecraft Technology Division, MS 54-1	
W. Plohr	1
E. Davison	1
S. Jones	1
Report Control Office, MS 5-5	1
National Aeronautics and Space Administration Marshall Space Flight Center Huntsville, Alabama 35812	
Attn: Ernst Stuhlinger (M-RP-DIR)	1
Research and Technology Division Wright-Patterson AFB, Ohio 45433	
Attn: (APIE-2) R. Johnson	1
National Aeronautics and Space Administration Scientific and Technical Information Facility P.O. Box 33 College Park, Maryland 20740	
Attention: NASA Representative RQT-2448	10

Jet Propulsion Laboratory
4800 Oak Grove Drive
Pasadena, California 91102
Attn: Mr. D. Kerrisk 1
Technical Library 1
E. Pawlik 1

Electro-Optical Systems, Inc.
300 North Halstead
Pasadena, California 91107
Attn: Mr. R. C. Speiser 1
Mr. R. Worlock 1

TRW Inc.
TRW Systems
One Space Park
Redondo Beach, California 90278
Attn: Mr. E. Cohen 1
Dr. H. Meissinger 1
Mr. D. Goldin 1

Westinghouse Astronuclear Laboratories
Electric Propulsion Laboratory
Pittsburgh, Pennsylvania 15234 1

National Aeronautics and Space Administration
Ames Research Center
Moffett Field, California 94035
Attn: Dr. F. Casal 1

National Aeronautics and Space Administration
Langley Research Center
Langley Field Station
Hampton, Virginia 23365
Attn: Technical Library 1

Hughes Research Laboratories
3011 Malibu Canyon Road
Malibu, California 90265
Attn: Mr. J. H. Molitor 1
Dr. H. J. King 1
Dr. R. L. Poeschel 1

United States Air Force
Office of Scientific Research
Washington, D. C. 20025
Attn: Mr. M. Slawsky 1

Case Institute of Technology
10900 Euclid Avenue
Cleveland, Ohio 44106
Attn: Mr. Eli Reshotko 1

Gruman Aircraft Engineering Corporation
Bethpage, Long Island, New York 11101
Attn: Mr. L. Tobias 1

Royal Aircraft Establishment
Space Department
Franborough, Hants, England
Attn: Dr. D. G. Fearn 1

United Kingdom Atomic Energy Authority
Culham Laboratory
Abingdon, Berkshire, England
Attn: Dr. A. A. Wells 1
Dr. M. F. Harrison 1

National Aeronautics and Space Administration
Goddard Space Flight Center
Greenbelt, Maryland 20771
Attn: Mr. W. Isley, Code 734 1
Mr. R. Hunter 1

SAMSO (SYAX/Capt. C. A. Baer) 1
Air Force Unit Post Office
Los Angeles, California 90045

Comsat Laboratories
P. O. Box 115
Clarksburg, Maryland 20734
Attn: B. Free 1

Rocket Propulsion Laboratory
Edwards AFB, California 93523
Attn: LKDA/Lt. S. Rosen 1

DFVLR
33 Braunschweig
Bienroder Weg 53
West Germany
Attn: Dr. G. F. Au 1

Giessen University
1st Institute of Physics
Giessen, West Germany
Attn: Professor H. W. Loeb 1